I. Run-up of Ocean Waves on Beaches

II. Nonlinear Waves in a Fluid-filled Elastic Tube

Thesis by

Jin E. Zhang

In Partial Fulfillment of the Requirements

for the Degree of

Doctor of Philosophy

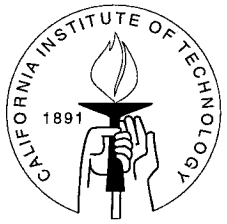

California Institute of Technology

Pasadena, California

1996

(Submitted April 23, 1996)

Acknowledgements

Thank you:

Professor Theodore Yao-tsu Wu, my advisor, for your intellectual inspiration and great guidance. Your philosophy and ways of learning have set a model for my life long emulation.

Dr. Chinhua S. Wu, for your affectionate care for our family.

Professor Thomas Yizhao Hou, for your valuable guidance in the numerical computation part of the work.

Professor Christopher E. Brennen, Andrew P. Ingersoll and Fredric Raichlen for your valuable discussion.

Professor Donald S. Cohen and Roberto Camassa, for a highly fruitful summer session at Center for Nonlinear Studies in Los Alamos National Laboratory in 1994.

Dr. George T. Yates, Michelle Hsiao-tsing Teng, Gary S. Guthart, Wooyoung Choi, Duo-min Lin, John Kao and Sunao Murashige, for sharing stimulating times in our weekly group research conferences.

Susan Nakashima, Holly Domingo and Raul Relles, for your assistance.

Ming Peng Zhang and Ju Zhen Huang, my parents, for your constant love and support.

Feng Zhou, my wife. Unlike my enthusiasm, your love and constant care never flagged.

I appreciate having musical background from my infant son Victor during my evening working hours.

Financial support from Caltech and C. L. Powell Fellowship is greatly appreciated.

This study has been partly supported by NSF Grant CMS-9503620, which is acknowledged with great appreciation.

Abstract

Part I

This study considers the three-dimensional run-up of long waves on a horizontally uniform beach of vertically constant or variable slope which is connected to an open ocean of uniform depth. An inviscid linear long-wave theory is first applied to obtain the fundamental solution for a uniform train of sinusoidal waves obliquely incident upon a uniform beach of variable downward slope without wave breaking. The linearly superposable solutions provide a basis for subsequent comparative studies when the nonlinear and dispersive effects are taken into account, both separately and jointly, thus providing a comprehensive prospect of the extents of influences due to these physical effects. These comparative results seem to be new.

By linear theory for waves at nearly grazing incidence, run-up is significant only for the waves in a set of eigenmodes being trapped within the beach at resonance with the exterior ocean waves. Fourier synthesis is employed to analyze a solitary wave and a train of cnoidal waves obliquely incident upon a sloping beach, with the nonlinear and dispersive effects neglected at this stage. Comparison is made between the present theory and the ray theory to ascertain a criterion of validity for the classical ray theory. The wave-induced longshore current is evaluated by finding the Stokes drift of the fluid particles carried by the momentum of the waves obliquely incident upon a sloping beach. Currents of significant velocities are produced by waves at incidence angles about 45° and by grazing waves trapped on the beach. Also explored are the effects of the variable downward slope and curvature of a uniform beach on three-dimensional run-up and reflection of long waves.

When the nonlinear effects are taken into account, the exact governing equations for determining a moving inviscid waterline are introduced here based on the local Lagrangian coordinates. A special numerical scheme has been developed for efficient evaluation of these governing equations. The scheme is shown to have a very high accuracy by comparison with some exact solutions of the shallow water equations. The maximum run-up of a solitary wave predicted by the shallow water equations depends on the initial location of the solitary wave and is *not unique* in value because the wave becomes increasingly more steepened given longer time to travel in the absence of the dispersive effects; it is in general larger than that predicted by the linear long-wave theory. The farther the initial solitary wave of the KdV form is imposed from the beach, the larger the maximum run-up it will reach.

The dispersive effects are also very important in two-dimensional run-ups in its role of keeping the nonlinear effects balanced at equilibrium, so that the run-ups predicted by the generalized Boussinesq model (Wu 1979) always yield *unique* values for run-up of a given initial solitary wave, regardless of its initial position. The result for the gB model is slightly larger than the wave run-up predicted by linear long-wave

theory. The dispersive effects tend to reduce the wave run-up either for linear system or for nonlinear system.

A three-dimensional process of wave run-up upon a vertical wall has also been studied.

Part II

This part is a study of nonlinear waves in a fluid-filled elastic tube, whose wall material satisfies the stress-strain law given by the kinetic theory of rubber. The results of this study have extended the scope of this subject, which has been limited to dealing with unidirectional solitary waves only (Olsen & Shapiro 1967), by establishing an *exact* theory for bidirectional solitons of arbitrary shape. This class of solitons has several remarkable characteristics. These solitons may have arbitrary shape and arbitrary polarity (upward or downward), and all propagate with the same phase velocity. The last feature of wave velocity renders the interactions impossible between unidirectional waves. However, the present new theory shows that bidirectional waves can have head-on collision through which our *exact* solution leaves each wave a specific phase shift as a permanent mark of the waves having made the nonlinear encounter. The system is at least tri-Hamiltonian and integrable. An iteration scheme has been developed to integrate the system. The system is distinguished by the fact that any local initial disturbance released from a state of rest will become two solitons traveling to the opposite direction, and shocks do not form if initial value is continuous.

Contents

List of Figures

List of Tables

List of Symbols

x	Space variable
t	Time variable
ζ	Wave elevation above the undisturbed water surface at $z = 0$
$\boldsymbol{u}$	Depth-averaged horizontal flow velocity, $\boldsymbol{u} = (u, v, 0)$
h	Unperturbed water depth measured from $z = 0$ to the bottom
l	Beach length measured from unperturbed waterline location to the junction between beach and ocean of the uniform depth
α	Beach slope, $\alpha = 1/l$
$\boldsymbol{k}$	Wave number vector, $\boldsymbol{k} = (k_1, k_2)$
κ	Wave number measured with beach length, $\kappa = kl$
β	Oblique angle of incident wave measured in the ocean
$M,\ U$	Confluent hypergeometric functions
R	Run-up of ocean waves on beaches, $R = R(t)$
Δ	The phase shift between the incident wave and the reflected wave
a	Amplitude of a solitary wave
c	Speed of a solitary wave
s	Area of the tube cross-section
u	Velocity averaged over the tube cross-section
$\mathcal{D}$	Hamiltonian operator
$\mathcal{H}$	Hamiltonian functional
$\delta\mathcal{H}$	Variational derivative

Part I

Run-up of ocean waves on beaches

Chapter 1 Linear nondispersive theory

1.1 Introduction

Gravity waves and circulatory currents are of fundamental importance in coastal dynamics. Surface gravity waves, either wind generated locally or arriving as long-wave swells from distant storm and interacting with local beach topographies, can give rise to a surf zone and drive the waves to run up on the beach. At oblique incidence, the excess momentum of the incoming waves can generate strong longshore currents which can induce local sediment suspension and transport to form sand bars. This natural phenomenon is quite complex and intricate, involving a number of key physical parameters dominating its appearance in various forms in different parametric domains. These problems have been investigated for simple cases, mostly in plane flows, with differing hypothesis. The state of the art, reflecting the underlying difficulties involved, has led Galvin in his review (1967) to conclude, rightfully, that, "A proven prediction of longshore current velocity is not available." This situation has not been much advanced in the intervening years.

Some plane problems of run-up and reflection of waves incident normally on a sloping beach have been investigated by Carrier & Greenspan (1958), Carrier (1966), and Tuck & Hwang (1972) based on Airy's model. Numerical calculations have been given by Pedersen and Gjevik (1983) using the nonlinear dispersive long-wave model and Kim et al. (1983) based on the Euler model. For the case of three-dimensional coastal dynamics, Carrier & Noiseux (1983) evaluated the oblique run-up and reflection of long waves on a plane beach connected to an open ocean based on linear long-wave theory, assuming the nonlinear and dispersive effects negligible. With this approach, one gains the advantage in providing a modal description of the resulting motion and in deriving a spectral distribution of wave energy and its dependence on the key parameters involved.

The present study is a series of investigations of the coastal physics related to the air-sea-land interactions. Here, linear nondispersive theory is adopted to evaluate oblique run-up, refraction and reflection of long waves incident from an open ocean, obliquely upon a uniform beach having an arbitrary variable downward slope, with the sloping plane beach as a special case. The main objective is to have the first principles of coastal physics well comprehended for this ideal case before the additional effects of nonlinearity, dispersion, and dissipation (including wave breaking, bottom friction, wind stresses, etc., as energy sources and sinks) are to be taken into account in subsequent studies.

In this chapter, the fundamental solution is first sought in §1.2 for modelling three-dimensional refraction, reflection and run-up of a train of sinusoidal waves obliquely incident upon a uniform beach of variable slope. From this solution, the run-up of the waterline and its phase lag behind that of the incident wave are deduced, in §1.2, to yield specific functions of the two key parameters, namely the wave incidence angle and the wave number scaled to the seaward length of the beach. For the case of grazing incidence upon a plane beach discussed in §1.4, i.e., when the incident wave propagates nearly parallel to the uniform beach, we obtain for the beach response a set of eigenmodes of low-frequency coastal waves trapped on the beach. In §1.5, the solution for the oblique run-up and reflection of solitary wave is obtained by making Fourier synthesis of the fundamental solution, and similarly in §1.6, for the oblique run-up of a train of cnoidal waves. These numerical results afford a quantitative comparison with the ray theory, as given in §1.7, where the criterion of their validity is sought. The longshore current induced by the balance of the mass-momentum transport of obliquely incident waves is evaluated and predicted in §1.8. These results are further discussed and concluded in §1.9. The effects of variable vertical curvature (i.e., in the vertical plane) of a uniform beach are compared with some sloping plane beaches concerning the run-up and reflection of obliquely incident waves; the result demonstrates existence of analogous beaches in the two categories that exhibit equivalent effects in regard to wave run-up and reflection.

1.2 Oblique run-up of sinusoidal waves upon a uniform sloping beach

We consider the specific case of three-dimensional run-up of long waves obliquely incident upon a uniform beach of variable downward slope, which is connected to an open ocean of uniform depth h_0 (figure 1.1), with the unperturbed water depth distribution

$$h = \begin{cases} h(x) & (0 \le x \le l,\ -\infty < y < \infty) \\ h_0 & (x > l,\ h_0 = \text{const.}), \end{cases} \tag{1.1}$$

$$h(0) = 0, \quad h'(0) \neq 0, \quad \text{and} \quad h(l) = h_0, \tag{1.2}$$

where the depth $z = -h(x)$ is a smooth, slowly varying function, but is otherwise arbitrary. A train of waves is obliquely incoming from the ocean and incident on the beach, interacting with the sloping beach, and is reflected back to the ocean. The waves are assumed to be sufficiently small and long compared to h_0, and the beach slope $h'(x)$ not exceedingly gradual so that the process can be assumed to go on without wave breaking or having any other energy sinks, such as bottom friction, to affect wave reflection. (For a review on the criteria separating the regimes with and without wave breaking, see e.g., Mei 1983.) The problem is to determine accordingly the wave motion in the flow field and the run-up on the beach.

For this class of problems, an appropriate theoretical model is the generalized Boussinesq equations (Wu, 1979):

$$\zeta_t + \nabla \cdot [(h+\zeta)\mathbf{u}] = 0\ , \tag{1.3}$$

$$\mathbf{u}_t + \mathbf{u} \cdot \nabla \mathbf{u} + \nabla \zeta = \frac{h}{2} \nabla [\nabla \cdot (h \mathbf{u}_t)] - \frac{h^2}{6} \nabla^2 \mathbf{u}_t\ , \tag{1.4}$$

where ζ is the wave elevation above the undisturbed water surface at $z = 0$, the time t in subscript denotes differentiation, $\mathbf{u} = (u, v, 0)$ is the depth-averaged horizontal flow velocity, $\nabla = (\partial_x, \partial_y, 0)$ is the horizontal vector operator. Here, the length is scaled by h_0 and the time by $(h_0/g)^{1/2}$, g being the gravitational acceleration. Its

validity is based on the assumptions that

$$\tilde{a} = a/h_0 \ll 1, \qquad \epsilon = (h_0/\lambda)^2 = O(\tilde{a}) \ , \tag{1.5}$$

for waves of typical amplitude a, length λ on water of depth $h(x)$ (see, e.g., Peregrine 1967; Whitham 1974; Miles 1977, 1979; Wu 1981, 1994; Teng & Wu 1992, 1994). It is on these scales that the effects of nonlinearity and dispersion are accounted for in equation (1.3) and (1.4), jointly with the net linear effects for this family of wave motion. These effects are thought to be of importance especially in a neighborhood of the moving waterline where these effects are of comparable significance.

In this chapter, however, the two parameters $\tilde{a}$ and ϵ are assumed to be so small that the nonlinear and dispersive effects may be neglected and the motion may be described by the linear, nondispersive long-wave model:

$$\zeta_t + \nabla \cdot (h\mathbf{u}) = 0 \ , \tag{1.6}$$

$$\mathbf{u}_t + \nabla\zeta = 0 \ , \tag{1.7}$$

which are the linearized version of equation (1.3) and (1.4). The effects of nonlinearity, dispersion and dissipation are left to be examined in a subsequent work.

Upon eliminating $\mathbf{u}$, equation (1.6) and (1.7) can be combined to give

$$(h(x)\zeta_x)_x + h(x)\zeta_{yy} - \zeta_{tt} = 0, \qquad (0 < x < l) \ , \tag{1.8}$$

$$\zeta_{xx} + \zeta_{yy} - \zeta_{tt} = 0 \qquad (x > l). \tag{1.9}$$

To assure continuity and smoothness of solutions, we require that

$$[\zeta] = 0 \quad \text{and} \quad [\zeta_x] = 0 \qquad (x = l), \tag{1.10}$$

where $[f]$ denotes the jump of f across $x = l$. In addition, we further require ζ to be

bounded at the waterline,

$$|\zeta(0, y, t)| < \infty. \tag{1.11}$$

In the open ocean, we have the incident and reflected waves as

$$\zeta = A(k)e^{i(k_2 y + k_1(x-l) - kt)} + B(k)e^{i(k_2 y - k_1(x-l) - kt)}, \tag{1.12}$$

$$k_1 = -k\cos\beta, \qquad k_2 = k\sin\beta\ , \tag{1.13}$$

where β is the wave incidence angle between the incoming wave vector $\mathbf{k} = (k_1, k_2)$ and the $-x$-axis (see figure 1.1), A is the given amplitude of the incident wave, B is an unknown (complex) amplitude of the reflected wave, and the real component of the complex expression is meant for physical interpretation. Here, A can, of course, be normalized to unity, but will be retained for clarity.

For the region within the sloping beach ($0 < x < l$), the wave resulting from the incident wave under interaction with the beach will assume the form

$$\zeta(x, y, t) = \eta(x)e^{iks} \qquad (s = y\sin\beta - t,\ 0 < x < l)\ , \tag{1.14}$$

where $\eta(x)$, by equation (1.8), satisfies the following equation:

$$(h(x)\eta_x)_x + k^2(1 - h(x)\sin^2\beta)\eta = 0\ . \tag{1.15}$$

1.2.1 Sloping plane beach

A special case of basic interest is the sloping plane beach,

$$h(x) = \alpha x \qquad (0 < x < l,\ \alpha l = h_0 = 1). \tag{1.16}$$

We recall that $h_0 = 1$ is taken for the length scale so that $l = 1/\alpha$. For this case equation (1.15) becomes:

$$x\eta_{xx} + \eta_x + k^2(\alpha^{-1} - x\sin^2\beta)\eta = 0 \qquad (0 < x < l). \tag{1.17}$$

This is the model equation adopted by Eckart (1951) and Carrier & Noiseux (1983). Using the transformation (here the variable z is not to be confused with the vertical coordinate)

$$\eta(x) = e^{-z/2}f(z), \qquad z = 2kx\sin\beta\ , \tag{1.18}$$

we obtain for $f(z)$ the Kummer equation:

$$zf'' + (b - z)f' - af = 0\ , \tag{1.19}$$

where $f'(z) = df/dz$,

$$b = 1, \quad a = \frac{1}{2}(1 - \kappa\csc\beta), \quad \kappa = kl\ . \tag{1.20}$$

We note that in terms of $\kappa = kl$ and $x_* = x/l$, the beach slope α (or the beach width l) is scaled out, leaving κ and β as the only two parameters. Equation (1.19) has the general solution

$$f(z) = C_1M(a;b;z) + C_2U(a;b;z)\ , \tag{1.21}$$

where C_1 and C_2 are coefficients, $M(a;b;z)$ and $U(a;b;z)$ are the confluent hypergeometric functions (Abramowitz & Stegun 1964),

$$M(a;b;z) = \sum_{n=0}^{\infty}\frac{a_nz^n}{b_nn!} = 1 + \frac{a}{b}z + \frac{a_2}{b_2}\frac{z^2}{2!} + \cdots\ , \tag{1.22}$$

$$U(a;b;z) = \frac{\pi}{\sin b\pi}\left\{\frac{M(a;b;z)}{\Gamma(1+a-b)\Gamma(b)} - z^{1-b}\frac{M(1+a-b;2-b;z)}{\Gamma(a)\Gamma(2-b)}\right\}, \tag{1.23}$$

$$a_n = \prod_{j=1}^{n}(a+j-1) = a(a+1)(a+2)\cdots(a+n-1)\ , \qquad (1.24)$$

and likewise for b_n. Since U is logrithmically singular at $z = 0$, we must have $C_2 = 0$. Thus, from equation (1.14), (1.18) and (1.21) we have for $0 < x < l$ the solution

$$\zeta(x,s) = C(k)e^{-k_2x+iks}M(a;1;2k_2x)\ , \qquad (1.25)$$

which has the derivative

$$\zeta_x = C(k)k_2e^{-k_2x+iks}[M(a;1;z) - (1+\kappa\csc\beta)M(a;2;z)]\ , \qquad (1.26)$$

where $k_2 = k\sin\beta$ and $z = 2k_2x$, as before.

Now, application of the matching conditions (1.10) yields

$$B(k) = A(k)e^{2i\Delta}, \qquad C(k) = A(k)R(\kappa,\beta)e^{i\Delta}, \qquad (1.27)$$

$$R(\kappa,\beta) = 2(M_0^2+N_0^2)^{-1/2}, \qquad \Delta(\kappa,\beta) = \arg(M_0+iN_0), \qquad (1.28)$$

$$M_0(\kappa,\beta) = e^{-\kappa\sin\beta}M(a;1;2k_2l) \qquad (k_2l = \kappa\sin\beta)\ , \qquad (1.29)$$

$$N_0(\kappa,\beta) = e^{-\kappa\sin\beta}\ [(1+\kappa\csc\beta)M(a;2;2k_2l) - M(a;1;2k_2l)]\tan\beta. \qquad (1.30)$$

This result shows that the incident waves are totally reflected, with the coefficient $|B/A| = 1$, as should be expected since the present solution has no wave energy sinks, such as wave breaking, in the flow field. However, the reflected wave has a phase lag $2\Delta(\kappa,\beta)$ due to the wave interaction with the beach bathymetry. In the beach region, the resulting wave propagates along shore with a phase lag $\Delta(\kappa,\beta)$, which is the algebraic mean of the incident and reflected wave phases, and has the *relative run-up* $R(\kappa,\beta)$ on the beach. Here, the run-up $R(\kappa,\beta)$ on the beach is taken, after Keller (1961), as the wave height at the waterline which is extrapolated horizontally to intercept the sloping beach. In this manner, Keller found, for the two-dimensional case of plane waves running up a uniform sloping beach, the somewhat surprising result that the nonlinear theory yields the same wave amplification as the

linear theory.

To exemplify the coastal dynamics for this simple beach-ocean configuration, let us take $\beta = 60^o$ for the wave incidence angle, and $\mathbf{k} = (-1/l, \sqrt{3}/l)$, $(\kappa = 2)$ to obtain $a = -0.6547, M_0 = -0.4622, N_0 = 0.2889$, and hence the run-up and the phase lag as

$$R = 3.670, \qquad \text{and} \qquad \Delta = 2.583 \text{ rad} . \tag{1.31}$$

As shown in figure 1.2, the perspective wave profile exhibits a superposed pattern of the incident and reflected waves which induce a quite pronounced run-up on the sloping beach, with an amplitude about 3.670 times that of the incident wave.

1.2.2 Uniform beach with variable downward slope

Returning to the general case of uniform beach of variable slope, (1.15) can be written as:

$$\eta'' + \frac{1}{x}p(x)\eta' + \frac{1}{x^2}q(x)\eta = 0 , \tag{1.32}$$

where the prime denotes differentiation with respect to x, and

$$p(x) = x\, h'(x)/h(x) , \tag{1.33}$$

$$q(x) = k^2 \left[\frac{1}{h(x)} - \sin^2\beta\right] x^2 . \tag{1.34}$$

We shall assume that $p(x)$ and $q(x)$ are analytic, regular in $0 \le x \le l$, hence

$$p(x) = \sum_{n=0}^{\infty} p_n (x/l)^n, \qquad q(x) = \sum_{n=0}^{\infty} q_n (x/l)^n . \tag{1.35}$$

Then $x = 0$ is a regular singular point. By Frobenius' theory, (1.32) has a solution of the form

$$\eta(x) = \sum_{n=0}^{\infty} b_n (x/l)^{n+\nu} , \tag{1.36}$$

where ν satisfies the indicial equation

$$\nu^2 + (p_0 - 1)\nu + q_0 = 0 \ , \tag{1.37}$$

which has two roots, ν_1 and ν_2 say, with $\nu_1 + \nu_2 = 1 - p_0$, $\nu_1\nu_2 = q_0$. For the run-up problem at hand, we are interested in those beach slopes of $h(x)$ that make $\nu_1 = 0$, for otherwise, if $\nu_1 < 0$, the run-up of (1.36) is singular at $x = 0$, and if $\nu_1 > 0$, the run-up is always zero, a case of no physical interest. The root of $\nu_1 = 0$ requires that

$$q_0 = 0 \ , \tag{1.38}$$

which we shall assume to hold, as for beaches of constant slope discussed above. Under this condition, the other root of (1.37) is

$$\nu_2 = 1 - p_0 \ . \tag{1.39}$$

For beaches of the class (1.2), $p_0 = 1$, so the indicial equation (1.37) has a double root $\nu_1 = 0, \nu_2 = 0$, inferring that the other solution is logarithmically singular at $x = 0$, as is the case of the confluent hypergeometric function $U(a, b, z)$ given in (1.23). This general property of $\nu_1 = \nu_2 = 0$ is seen to hold for beaches whose slope at the waterline does not vanish, as assumed. Accordingly, it follows that the solution for the case of regular run-up is of the form

$$\eta(x) = C_1(k)F(x; \kappa, \beta) = C_1(k) \sum_{n=0}^{\infty} b_n (x/l)^n \ , \tag{1.40}$$

where $b_0 = 1$ by normalization, so that $F(0; \kappa, \beta) = 1$, and b_n are determined by the recurrence formula,

$$n^2 \ b_n = -\sum_{r=0}^{n-1} (r p_{n-r} + q_{n-r}) b_r, \qquad (n = 1, 2, \cdots). \tag{1.41}$$

Here, we observe that $p_0 = 1$ and $q_0 = 0$, as explained above. Now, application of the matching conditions (1.10) determines the coefficients $B(k)$ and $C(k)$ as

$$B(k) = e^{2i\Delta_1(\kappa,\beta)} A(k) \ , \tag{1.42}$$

$$C_1(k) = R_1(\kappa,\beta) e^{i\Delta_1(\kappa,\beta)} A(k) \ , \tag{1.43}$$

where

$$R_1(\kappa,\beta) = 2(M_1^2 + N_1^2)^{-1/2}, \qquad \Delta_1(\kappa,\beta) = \arg(M_1 + iN_1), \tag{1.44}$$

$$M_1(\kappa,\beta) = F(l;\kappa,\beta) = \sum_{n=0}^{\infty} b_n \ , \tag{1.45}$$

$$N_1(\kappa,\beta) = -\frac{1}{k\cos\beta} F_x(l;\kappa,\beta) = -\frac{1}{\kappa\cos\beta} \sum_{n=0}^{\infty} n b_n \ . \tag{1.46}$$

The run-up function $R_1(\kappa,\beta)$ gives the relative run-up and the phase function $\Delta_1(\kappa,\beta)$, the phase lag of the waves in the beach region and the phase lag $2\Delta_1$ for the waves reflected.

This series solution therefore provides the result to the general family of uniform beach with arbitrary, variable downward slope. In particular, for the beach of constant slope, the function $F(x;\kappa,\beta)$ in (1.40) agrees with the previous solution $M(a;b;2k_2x)$ $\exp(-k_2x)$.

Figure 1.3a shows the variation of the run-up function, $R(\kappa,\beta)$, versus $\kappa = kl$ for waves incident upon the parabolic beach $h(x) = 2x/l - (x/l)^2$ and plane beach $h(x) = x/l$ for a set of different incidence angles β. Figure 1.3b shows the variation of run-up function, $R(\kappa,\beta = 0)$, at incidence angle $\beta = 0$, for different parabolic beaches, $h(x) = mx/l + (1-m)(x/l)^2$, $m = 0.6,\ 0.8,\ 1.0,\ 1.5,\ 2.0$. The beach becomes a plane for $m = 1.0$. These numerical results show that for the incidence angle up to about $\beta = 60^\circ$, the run-up on a parabolic beach is increased, or decreased, relative to the plane beach, as m is decreased ($m < 1$, more concave downward), or increased ($m > 1$, more concave upward) from $m = 1$. Within this range of β, the run-up appears to be heavily weighted by the beach slope *near* the waterline such

that, roughly, as a rule, the parabolic beach run-up can be estimated by that on a plane beach tangential to the parabola at the waterline. For greater values of β, especially near the grazing angle of $\beta = 90^o$, the run-up function R remains small except near a set of 'eigenvalues of κ', as exemplified by the case of $\beta = 89^o$ shown here and as will be discussed in detail in §4. These eigenvalues are shown to depend on the beach slope and curvature.

1.3 Normal wave incidence

For waves at normal incidence upon a uniform plane beach, $\beta = 0$, we make use of the following limit (Abramowitz & Stegun 1964 (13.3.2)) ,

$$\lim_{|a|\to\infty} M(a;b;-z/a) = \Gamma(b)\ z^{(1-b)/2}\ J_{b-1}(2\sqrt{z})\ , \tag{1.47}$$

where $J_\nu(z)$ is the Bessel function of the first kind, obtaining

$$\lim_{\beta\to 0} M((1-\kappa\csc\beta)/2;1;2k_2x) = J_0(2k\sqrt{lx}), \tag{1.48}$$

$$\lim_{\beta\to 0} M((1-\kappa\csc\beta)/2;2;2k_2x) = J_1(2k\sqrt{lx})/(k^2lx)^{1/2}\ . \tag{1.49}$$

Thereby we have

$$M_0 = J_0(2\kappa), \quad N_0 = J_1(2\kappa) \qquad (\kappa = kl)\ , \tag{1.50}$$

and hence with $s = y\sin\beta - t = -t$, the wave system has the pattern:

$$\zeta(x,t) = \begin{cases} A[e^{-ik(x-l+t)} + e^{ik(x-l-t)+i2\Delta_0}] & (x > l) \\ AR_0(\kappa)e^{-ikt+i\Delta_0}J_0(2k\sqrt{lx}) & (0 < x < l), \end{cases} \tag{1.51}$$

where

$$R_0(\kappa) = 2[J_0^2(2\kappa) + J_1^2(2\kappa)]^{-1/2}\ , \tag{1.52}$$

$$\Delta_0(\kappa) = \arg(J_0(2\kappa) + iJ_1(2\kappa))\ , \tag{1.53}$$

which are the run-up and phase-lag functions of the two-dimensional waves at normal incidence on the sloping beach.

As a numerical example, we take $\kappa = 2$ and $A(k) = 1$, then

$$R_0(\kappa) = 4.968, \qquad \Delta_0(\kappa) = 3.306 \text{ rad.} \tag{1.54}$$

The corresponding wave profile, as shown in figure 1.4, displays a pattern with the specified phase lag and a run-up which is somewhat greater than in the previous case of $\beta = 60^\circ$, by a margin of about 35%.

1.4 Grazing incidence; edge waves

As the incidence angle β tends to $\pi/2$ (or $-\pi/2$), the incoming waves become nearly along shore. This limit turns out to be of particular significance which we now consider for the case of sloping plane beach. In this limit, the general solution becomes

$$\zeta(x,s) = \begin{cases} A[1 + e^{2i\Delta_g}]e^{iks} & (x > l) \\ AR_g(\kappa)e^{-kx+i(ks+\Delta_g)}M(a;1;2kx) & (0 < x < l)\ , \end{cases} \tag{1.55}$$

where the run-up coefficient $R_g(\kappa)$ and phase lag $\Delta_g(\kappa)$ are given by the limit of (1.27-1.30) as $\beta \to \pi/2$, $k_2 \to k$. In this limit, we see from (1.30) that $\tan\beta \to \infty$, with N_0 either becoming unbounded for arbitrary k or vanishing like $(\pi/2 - \beta)$ for certain *eigenvalues* of k, since, as is easily seen, there are no values of k for which N_0 has a finite, nonzero limit as $\beta \to \pi/2$. In the first case, i.e., with κ arbitrary, we find that $\zeta \to 0$ for all $x > 0$ (because $N_0 \to \infty$) which is of no interest. The only nontrivial case is therefore for certain $k = k_n, \kappa = \kappa_n = k_n l$, such that

$$N_0(\kappa_n, \beta \to \pi/2) = 0 \qquad (n = 1, 2, \cdots). \tag{1.56}$$

This condition further implies by (1.28) that $\Delta(\kappa, \beta) = 0$, signifying that the reflected wave and the edge-wave on beach are both in phase with the incident wave. Under

this condition, the first several κ_n's have been calculated by applying the code of Mathematica to give

$$\kappa_n = k_n l = 2.5337,\ 4.5788,\ 6.5986,\ 8.6101,\ 10.6177,\ 12.6232,\ 14.6274, \cdots \quad (1.57)$$

which seems to suggest the relation that

$$\lim_{n\to\infty}(\kappa_{n+1} - \kappa_n) = 2\ . \quad (1.58)$$

Indeed, if we let $l \to \infty$ for fixed $h = \alpha x$, our problem becomes that of edge waves on an infinite sloping plane, for which case we obtain the eigenvalues for the trapped wave modes

$$\kappa_n = 2n + \frac{1}{2} \quad (1.59)$$

from the limit of $N_0(\kappa_n, \beta)$, as $\beta \to \pi/2$, given later by (1.88) asymptotically for $\kappa \gg 1$ while satisfying (1.56), so that $\kappa_{n+1} - \kappa_n = 2$ for all n. With $\kappa = \kappa_n$ given by (1.57), the solution may be written as

$$\zeta(x,s) = \begin{cases} 2Ae^{i\kappa_n s/l} & (x > l) \\ AR_g(\kappa_n)e^{-\kappa_n(x-is)/l}M(\frac{1-\kappa_n}{2}; 1; 2\kappa_n\frac{x}{l}) & (0 < x < l)\ , \end{cases} \quad (1.60)$$

$$R_g(\kappa_n) = 2e^{\kappa_n}/|M(\frac{1-\kappa_n}{2}; 1; 2\kappa_n)|\ . \quad (1.61)$$

In this case, the wave pattern in the open ocean is that of the simple harmonic waves propagating along the shore and is connected to a *longshore edge-wave* along the inclined beach with no phase lag. The run-up of the κ_n- mode wave is just $R_g(\kappa_n)$ of (1.61). As an example, if we take $\kappa_1 = 2.5337$ and $A = 1$, then $a = 0.7668$, giving a quite pronounced run-up of

$$R_g(\kappa_1) = 4.061. \quad (1.62)$$

The corresponding wave profile is shown in figure 1.5.

We note that on this linear theory, new solutions can be constructed by linear superposition of the above solutions corresponding to different eigenmodes of $\kappa_n's, n = 1, 2, \cdots$.

In general, the run-up function $R(\kappa, \beta)$ and the phase lag $\Delta(\kappa, \beta)$ are functions of κ and the incidence angle β. In figure 1.6, R is shown versus κ for eight values of β as listed. For β not too close to the grazing angle, $\beta < 60^\circ$ say, R increases with increasing κ from the value of $R(0, \beta) = 2$ at $\kappa = 0$, with some slight undulations as shown in figure 1.6. Within the grazing incidence range, $\beta > 80^\circ$, we find the remarkable feature that R remains small except in a narrow band of κ centered about the eigenvalues $\kappa = \kappa_n, n = 1, 2, \cdots$ as illustrated in figure 1.6. These eigenvalues also mark the narrow band in which the phase angle $\Delta(\kappa, \beta)$ jumps by π, as shown in figure 1.7.

It is of basic interest to examine the mechanism underlying the phenomenon of rapid rise-and-fall of the run-up function R as κ varies across the eigenvalue κ_n within the grazing incidence range. The underlying mechanism is discovered by observing that from (1.26) and (1.30), the condition of $N_0(\kappa_n) = 0$ with $\beta = \pi/2$ implies $\zeta_x = 0$ at $x = l$, which further infers, on account of (1.7), that the beach-ocean interface at $x = l$ will remain as a fixed vertical plane as long as κ is kept at $\kappa = \kappa_n$, since by (1.7), the normal velocity $u = 0$ at $x = l$ for all t. Physically, this indicates that the waves within the beach region bounded by $x = 0$ and $x = l$ planes may be regarded as being trapped, and being held at resonance by the exterior pressure field of the waves at grazing incidence.

1.5 Oblique reflection of solitary waves from a sloping beach

To simulate approximately the reflection of a solitary wave obliquely incident on a sloping beach, we shall adopt the present linear theory and utilize Fourier synthesis

to construct the desired solution. In other words, we shall take into account solitary waves only to satisfy the linear long-wave equations (1.8,1.9), leaving the effects of nonlinearity and dispersion on oblique wave run-up and reflection for further studies. For simplicity, we shall confine the present analysis to the case of sloping plane beach and give some discussion on the general case of beaches with arbitrary slope.

Suppose we have in the open ocean a solitary wave

$$\zeta_0(x,s) = a_0 \operatorname{sech}^2 \sqrt{\frac{3a_0}{4}}\,[s-(x-l)\cos\beta] \qquad (x>l)\ , \tag{1.63}$$

which is incoming at incidence angle β toward the inclined beach of uniform slope α. With the time properly rescaled in (1.8) and (1.63), this wave is a well-known solution of the Korteweg-de Vries (KdV) equation

$$\zeta_t + \zeta_x + \frac{3}{2}\zeta\zeta_x + \frac{1}{6}\zeta_{xxx} = 0 \tag{1.64}$$

when the nonlinear and dispersive effects are operating in accordence with (1.5). But with the nonlinear and dispersive effects both neglected at this stage, the solitary wave (1.63) also satisfies (1.9) in the open ocean where it can assume the Fourier integral form as

$$\zeta_0(x,s) = \mathrm{Re}\int_0^\infty A_0(k)e^{ik[s-(x-l)\cos\beta]}\,dk \qquad (x>l)\ , \tag{1.65}$$

$$A_0(k) = \frac{4}{3}k\ \mathrm{csch}(\frac{\pi k}{\sqrt{3a_0}}), \tag{1.66}$$

where Re denotes "the real part of". Therefore, by Fourier synthesis of the simple harmonic wave solutions (1.25)-(1.30), we obtain for the reflected solitary wave the solution

$$\zeta_r(x,s) = \mathrm{Re}\int_0^\infty A_0(k)e^{ik[s+(x-l)\cos\beta]+2i\Delta}dk \qquad (x>l)\ , \tag{1.67}$$

so that

$$\zeta(x,s) = \zeta_0(x,s) + \zeta_r(x,s) \qquad (x > l)\ . \tag{1.68}$$

And for the longshore wave we have the integral expression, for $0 < x < l$,

$$\zeta(x,s) = \mathrm{Re}\int_0^\infty A_0(k)R(\kappa,\beta)e^{-k_2x+i(ks+\Delta)}M(a;b;2k_2x)dk, \tag{1.69}$$

where $k_2 = k\sin\beta$ as before, $R(\kappa,\beta)$ and $\Delta(\kappa,\beta)$ are given by (1.28).

For the case of normal incidence, $\beta = 0$, we have

$$\zeta_0(x,t) = \mathrm{Re}\int_0^\infty A_0(k)e^{-ik(x-l+t)}dk \qquad (x > l)\ , \tag{1.70}$$

$$\zeta_r(x,t) = \mathrm{Re}\int_0^\infty A_0(k)e^{i[k(x-l-t)+2\Delta_0]}dk \qquad (x > l)\ , \tag{1.71}$$

$$\zeta(x,t) = \mathrm{Re}\int_0^\infty A_0(k)R_0(\kappa)e^{-ikt+i\Delta_0}J_1(2k\sqrt{lx})dk \quad (0 < x < l), \tag{1.72}$$

where $A_0(k)$ is again given by (1.66), $R_0(\kappa)$ and $\Delta_0(\kappa)$ by (1.52,1.53).

For this case of normal incidence, we present the following numerical results with $\beta = 0$, $a_0 = 0.1$, and $\alpha^{-1} = 1,2,3,4,5,6$ for increasingly smaller slopes of the beach. The wave profiles are numerically integrated from (1.70-1.72) and shown in figure 1.8 for $\zeta(0,t)$ at $x = 0$ and in figure 1.9 for the reflected wave $\zeta_r(l,t)$ at $x = l$, both versus time t. It is of interest to note that at the waterline, the run-up increases monotonically with decreasing $\alpha(< 1)$ (see table 1.1) and there appears, after reaching the maximum run-up, a negative run-down on the beach whose magnitude also increases with decreasing α. The increasing run-down is evidently playing an active role in resulting in an increasing departure from the fore-and-aft symmetry for the reflected wave, as depicted in figure 1.9, while giving rise to a dipped tail with its magnitude increasing with decreasing α.

For oblique incidence of a (linear) solitary wave, we take $\alpha = 1/5$ for the beach slope, $a_0 = 0.1$ for the incoming wave amplitude and obtain the numerical results of the wave elevation $\zeta(0,0,t)$ at $x = 0, y = 0$ as shown in figure 1.10 for incidence

angle $\beta = 0^o, 45^o, 60^o, 75^o$ and 85^o. Here we note that the variation of the waterline position with decreasing β and fixed α has a similar feature as that shown in figure 1.8 for ζ with decreasing α and fixed $\beta(=0)$.

1.6 Oblique reflection of cnoidal waves from a sloping beach

Another solution of the KdV equation (1.64) is the cnoidal wave (Whitham 1974)

$$\zeta = \alpha_1 \quad \mathrm{cn}^2(u|m), \tag{1.73}$$

$$u = k(x - ct), \qquad k = \sqrt{\frac{3\alpha_1}{4mh_0^2}}, \tag{1.74}$$

$$c = c_0(1 + \alpha_1 - \frac{\alpha_1}{2m}), \qquad (c_0 = \sqrt{gh_0}), \tag{1.75}$$

which is a periodic nonlinear wave for $\alpha_1 > 0$ and $0 \leq m \leq 1$, of wavelength

$$\lambda = \frac{2}{k}\,\mathrm{K}(m) = \frac{2}{k}\int_0^1 [(1-t^2)(1-mt^2)]^{-1/2}dt, \tag{1.76}$$

where m is a free parameter, $\mathrm{K}(m)$ is the complete elliptic integral of the first kind.

To evaluate the reflection of an infinite train of cnoidal waves obliquely incident upon the uniform sloping beach on linear theory, we again adopt (1.8,1.9), with proper rescaling of t, and make use of the Fourier synthesis (Abramowitz & Stegun 1964, p575):

$$\mathrm{cn}(u_0|m) = \sum_{n=0}^{\infty} a_n \cos nv, \tag{1.77}$$

$$v = \frac{\pi u_0}{2\mathrm{K}(m)}, \quad u_0 = k_0(s - (x-l)\cos\beta), \quad k_0 = \sqrt{\frac{3\alpha_1}{4m}}, \tag{1.78}$$

$$a_n = \frac{\pi(1-(-1)^n)}{2\sqrt{m}\mathrm{K}(m)}\mathrm{sech}(nb), \quad b = \frac{\pi}{2}\frac{\mathrm{K}'(m)}{\mathrm{K}(m)}, \quad \mathrm{K}'(m) = \mathrm{K}(1-m). \tag{1.79}$$

With this Fourier expansion, (1.73 - 1.75) gives

$$\zeta_0(x,s) = \alpha_1 \sum_{n=0}^{\infty} b_n \cos 2nv = \mathrm{Re} \sum_{n=0}^{\infty} \alpha_1 b_n e^{ink[s-(x-l)\cos\beta]}, \tag{1.80}$$

where

$$b_n = \frac{1}{2} \sum_{j=-\infty}^{\infty} a_{n+j} a_{n-j}, \qquad k = \frac{\pi}{\mathrm{K}(m)} \sqrt{\frac{3\alpha_1}{4m}}. \tag{1.81}$$

Thus, by Fourier synthesis, we have the reflected waves as

$$\zeta_r(x,s) = \mathrm{Re} \sum_{n=0}^{\infty} \alpha_1 b_n e^{ink[s+(x-l)\cos\beta]+2i\Delta}, \tag{1.82}$$

so that

$$\zeta(x,s) = \zeta_0(x,s) + \zeta_r(x,s) \qquad (x > l). \tag{1.83}$$

And for the longshore wave we obtain, for $0 < x < l$,

$$\zeta(x,s) = \mathrm{Re} \sum_{n=0}^{\infty} \alpha_1 b_n R(nkl,\beta) e^{-nk_2 x + i(nks+\Delta)} M(a;1;2nk_2 x), \tag{1.84}$$

where the phase lag Δ has the arguments $\Delta = \Delta(nkl,\beta)$.

As a numerical example, figure 1.11 shows the main features of the incident wave, ζ_0, and the reflected wave, ζ_r, in the open ocean $(x > l)$ for the case of uniform plane beach of length $l = 5$, with the wave-incident angle of $\beta = \pi/4$, for an incident cnoidal wave of amplitude $\alpha_1 = 0.1$ and characterized by the parameter $m = 0.99$. The run-up $\zeta(0,0,t)$ at $x = 0$ and $y = 0$ is also shown in figure 1.11; it increases to a height of 0.32 and falls, slightly faster than in rising, to a negative level of about -0.1, describing the run-down along the beach. Both the reflected and longshore waves exhibit marked skewness over the wave period. These main features are seen to resemble those of a solitary wave obliquely incident upon the beach for nearly equal wave amplitude and incidence angle, as can be seen by comparison with figure 1.10.

1.7 Beach of mild slope — comparison with the ray theory

It is of fundamental interest to compare the present beach wave theory with the classical ray theory. The premise common to both is based on the *geometric wave approximation* assuming slow variations of water depth and wavelength based on the wave scale, which is supposed to be very small by the beach scale, i.e.,

$$|d(\log kh)/dx| \ll 1, \qquad \kappa = kl \gg 1. \tag{1.85}$$

Accordingly, we seek the asymptotic expansion of $M(a;b;z)$ for $|a|$ and z both large so that with $2b-4a > z \gg 1$ and $\cos^2\theta = z/(2b-4a)$ (Abramowitz & Stegun (1964), after the misprints are corrected in the formula 13.5.21),

$$\begin{aligned} M(a;b;z) &= \Gamma(b)\ \exp[(b-2a)\cos^2\theta]\ [(b-2a)\cos\theta]^{1-b}\ [\pi(\frac{1}{2}b-a)\sin 2\theta]^{-\frac{1}{2}} \\ &\quad \{\sin[a\pi + (\frac{1}{2}b-a)(2\theta-\sin 2\theta) + \frac{1}{4}\pi] + O(|\frac{1}{2}b-a|^{-1})\}. \end{aligned} \tag{1.86}$$

For a train of sinusoidal waves obliquely incident on a plane beach of very mild slope (see (1.85)), we proceed with using asymptotic formula (1.86) and some algebra to obtain

$$\begin{aligned} M_0(\kappa,\beta) &= e^{-\kappa\sin\beta} M(a;1;2\kappa\sin\beta), \qquad a = \frac{1}{2}(1-\kappa\csc\beta) \\ &= (\pi\kappa\cos\beta)^{-\frac{1}{2}}\ \cos[(\beta\csc\beta+\cos\beta)\kappa - \frac{\pi}{4}] + O(\kappa^{-1}), \qquad (1.87) \\ N_0(\kappa,\beta) &= e^{-\kappa\sin\beta}\ [(1+\kappa\csc\beta)M(a;2;2\kappa\sin\beta) - M(a;1;2\kappa\sin\beta)]\tan\beta \\ &= (\pi\kappa\cos\beta)^{-\frac{1}{2}}\ \sin[(\beta\csc\beta+\cos\beta)\kappa - \frac{\pi}{4}] + O(\kappa^{-1}), \qquad (1.88) \\ R(\kappa,\beta) &= 2(M_0^2+N_0^2)^{-1/2} = 2(\pi\kappa\cos\beta)^{\frac{1}{2}} + O(\kappa^{-1}), \qquad (1.89) \\ \Delta(\kappa,\beta) &= \arg(M_0+iN_0) = (\beta\csc\beta+\cos\beta)\kappa - \frac{\pi}{4} + O(\kappa^{-1}). \qquad (1.90) \end{aligned}$$

With these asymptotic formulas of oblique run-up and phase lag for sinusoidal waves, incident on a plane beach with mild slope, the wave elevation becomes

$$\begin{aligned}
\zeta(x,s) &= \eta(x)\ \cos(ks+\Delta), \qquad s = y\sin\beta - t, && (1.91)\\
\eta(x) &= 2\ A_0\ \cos[kx\cos\beta - \kappa\cos\beta + \Delta(\kappa,\beta)] \\
&= 2\ A_0\ \cos[kx\cos\beta + \kappa\beta\csc\beta - \frac{\pi}{4}] + O(\kappa^{-1}) \quad (x > l); && (1.92)\\
\eta(x) &= A_0\ R(\kappa,\beta)e^{-kx\sin\beta}M(a;1;2kx\sin\beta) \\
&= 2\ A(x)\ \cos(\theta(x) - \frac{\pi}{4}) + O(\kappa^{-1}) \quad (0 < x < l), && (1.93)\\
A(x) &= A_0\ (\cos^{\frac{1}{2}}\beta)\ [\frac{x}{l}(1 - \frac{x}{l}\sin^2\beta)]^{-\frac{1}{4}}, && (1.94)\\
\theta(x) &= \kappa\csc\beta\arcsin(\sqrt{\frac{x}{l}}\sin\beta) + \kappa\sqrt{\frac{x}{l}(1-\frac{x}{l}\sin^2\beta)}. && (1.95)
\end{aligned}$$

On the beach, $0 < x < l$, $\zeta(x,y,t)$ can be written as

$$\begin{aligned}
\zeta(x,y,t) &= A(x)\ \cos(S_i(x,y,t)) + A(x)\ \cos(S_r(x,y,t)), && (1.96)\\
S_i(x,y,t) &= -\theta(x) + ky\sin\beta - kt + \kappa(\beta\csc\beta + \cos\beta), && (1.97)\\
S_r(x,y,t) &= \theta(x) + ky\sin\beta - kt + \kappa(\beta\csc\beta + \cos\beta) - \frac{\pi}{2}, && (1.98)
\end{aligned}$$

where S_i and S_r are the phase functions of the incident and reflected waves, respectively.

From the *ray theory* (e.g., Whitham 1974), the incident wave assumes on the beach the form $\zeta_i(x,y,t) = A(x)\ \exp[iS(x,y,t)]$, with

$$k_1 = \frac{\partial S}{\partial x} = -\sqrt{k_b^2 - k_2^2}, \qquad k_2 = \frac{\partial S}{\partial y} = \text{const.}, \qquad \omega = -\frac{\partial S}{\partial t}, \tag{1.99}$$

where the circular frequency $\omega = k_b\sqrt{h(x)} = k_b\sqrt{x/l} = \text{const.}(= k)$, $k_b = k\sqrt{l/x} = \sqrt{k_1^2 + k_2^2}$ is the wave number on the beach, and k_2 =const. by virtue of $\partial\omega/\partial y = 0$. After integrating the equations in (1.99), we obtain the phase function $S = S(x,y,t)$ to be exactly the same as $S_i(x,y,t)$ in equation (1.97). After integrating the equation

$dy/dx = k_2/k_1$, we obtain the ray trajectory of the incident waves as

$$y - y_0 = \frac{l}{\sin^2\beta}\left[\sin\beta\sqrt{\frac{x}{l}(1-\frac{x}{l}\sin^2\beta)} - \arcsin(\sqrt{\frac{x}{l}}\sin\beta) - \sin\beta\cos\beta + \beta\right] \quad (1.100)$$

where $y = y_0$ at $x = l$. Following the ray, we can compute the wave amplitude by the formula:

$$\frac{A(x)}{A_0} = \left[\frac{(c_g)_0}{c_g}\frac{d\sigma_0}{d\sigma}\right]^{\frac{1}{2}} = \left[\frac{1}{\sqrt{x/l}}\frac{\cos\beta}{k_1/k_b(x)}\right]^{\frac{1}{2}}, \quad (1.101)$$

where $d\sigma$ is the width of a ray filament and $d\sigma_0$ its value at $x = l$. For our linear nondispersive model, $c_g = c = \sqrt{x/l}$ on the beach. One can easily find that $A(x)$ given by (1.101) is the same as that of equation (1.94). Thus the ray theory gives the incident wave on the beach as

$$\zeta_i(x, y, t) = A(x)\ \cos(S_i(x, y, t)). \quad (1.102)$$

This result of ray theory is based on the "geometric wave approximation" (1.85), and is supposed to hold for all angles of incidence. However, it only covers the incident wave since the ray theory by itself is incapable of predicting the reflected wave. The reason is because the ray theory does not possess the detailed structures in the solution required for satisfying the boundary condition at the seabed effecting the refraction *and* reflection of the waves. In contrast, the present linear theory in its comprehensive form (without further expansion) predicts the resultant motion, which is finite up to the waterline but is not explicit in separating the incoming and relfected waves. Only when the asymptotic ray expansion is acquired from the linear solution do we have the incoming and reflected waves separated. But we should note that the expanasion is not uniformly valid since the wave amplitude diverges like $x^{-1/4}$ as $x \to 0$. It is in this asymptotic expansion of the linear solution that the ray theory is found in complete agreement with the *incident wave component* of the expansion, as indicated by (1.102) and (1.91)-(1.96). We further note that the ray theory cannot

predict the runup since it is singular at waterline.

Figure 1.12 shows η as a function of x/l for $A_0 = 1$, $\beta = 45^\circ$ and $\kappa = 0.5,\ 2,\ 5,\ 10$; and figure 1.13 is for $\kappa = 10$ and $\beta = 0^\circ,\ 70^\circ,\ 80^\circ,\ 89^\circ$. The results of this comparative study show that under condition (1.85), the asymptotic expansion is in excellent agreement with the linear theory for $\kappa > 2$ and $\beta < 60^o$ except in a small neighborhood of waterline with $0 < x/l < 0.02$, and becomes poorer for smaller κ and larger β. The first of figures 1.12 demonstrates the margin of departure of the asymptotic expansion from the linear theory at a κ as small as $\kappa = 0.5$. The discrepancy between the linear theory and its ray expansion becomes greater, the closer the incidence angle β approaches the grazing limit of 90°, this being apparently due to the singular behavior of the trapped modes of waves at resonance. These comparative results therefore imply that *the criteria of validity for the ray theory will be the same as that of the asymptotic expansion because of the complete agreement between the two on the incident component of the wave system.* These are the new conspicuous features that now qualify the ray theory.

Figure 1.14 shows the phase lines of incident and reflected waves for $S_i = -2\pi$, $0,\ 2\pi,\ 4\pi,\ 6\pi, 8\pi$, $S_r = 4\pi,\ 6\pi,\ 8\pi,\ 10\pi,\ 12\pi,\ 14\pi$, and the incident and reflected rays for $\kappa = 10,\ \beta = 60^\circ$. It is of interest to note that at the waterline, the reflected wave actually has a phase lead given by (1.96) as

$$S_r(0, y, t) - S_i(0, y, t) = -\pi/2, \tag{1.103}$$

as shown in the inset of figure 1.14. Physically, this phase lead indicates that the incoming wave, being long, feels the bottom early and continues to undergo the reflection process before reaching the waterline.

1.8 Wave-induced longshore current

According to the present linear long-wave approximation, the horizontal projection of the pathline of a fluid particle is given by the integral

$$\mathbf{x}(\xi,t) = \xi + \int_0^t \mathbf{u}_L(\xi,\tau)d\tau, \tag{1.104}$$

where $\xi = \mathbf{x}(\xi, t = 0)$ is the initial position of the fluid particle at $\mathbf{x} = (x, y, t)$ at time t, and $\mathbf{u}_L(\xi, t) = (u_L, v_L, 0)$ is the Lagrangian particle velocity, projected onto a horizontal plane, of the particle designated by $\xi = (\xi_1, \xi_2, 0)$. The Lagrangian drift velocity is related to the Eulerian field velocity, $\mathbf{u}(\mathbf{x}, t)$, for small $\Delta\xi = \mathbf{x} - \xi$, by

$$\mathbf{u}_L(\xi,t) = \mathbf{u}(\mathbf{x},t) = \mathbf{u}(\xi,t) + (\int_0^t \mathbf{u}(\xi,\tau)d\tau)\cdot\nabla\mathbf{u}(\xi,t) + O(\Delta\xi)^2. \tag{1.105}$$

For the case of a uniform beach, with ζ expressed as in (1.14), integration of (1.7) yields

$$\mathbf{u} = (u, v, 0) = (\frac{1}{ik}\zeta_x, \zeta\sin\beta, 0), \quad (0 < x < \infty). \tag{1.106}$$

To obtain the time average of $\mathbf{u}_L$, use may be made of the theorem that if $f = ae^{i\omega t}$ and $g = be^{i\omega t}$, a and b being complex constant, then

$$\overline{(\mathrm{Re}f)(\mathrm{Re}g)} = \frac{1}{2}\mathrm{Re}(f\ g^*). \tag{1.107}$$

where the overhead bar denotes the time average and $*$ indicates the complex conjugate. The mean current velocity is thus found from (1.104)-(1.107) to have the x-component as

$$\overline{u_L}(x) = \frac{1}{2}\mathrm{Re}\{u_x(\frac{1}{ik}u^*) + u_y(\frac{1}{ik}v^*)\} = \frac{1}{2k}\mathrm{Im}\{\frac{1}{k^2}\eta_{xx}\eta_x^* + \eta_x\eta^*\sin^2\beta\} = 0, \tag{1.108}$$

which vanishes since the quantity in the bracket is purely real in view of using (1.12) for $x > l$ and (1.14) for $0 < x < l$. The longshore (y-component) current has the

mean

$$\overline{v_L}(x) = \frac{1}{2}\mathrm{Re}\{v_x(\frac{1}{ik}u^*) + v_y(\frac{1}{ik}v^*)\} = \frac{1}{2}(\frac{1}{k^2}|\eta_x|^2 + |\eta|^2\sin^2\beta)\sin\beta, \qquad (1.109)$$

which is positive definite for $0 < \beta < \pi/2$ unless $|\eta|^2 = 0$, and is symmetric about $\beta = 0$. This formula holds for the general case of uniform beach of arbitrary downward slope.

At waterline $x = 0$ of a sloping plane beach, use of (1.14), (1.27– 1.30), (1.89) and (1.109) yields the current velocity

$$\overline{v_L}(x = 0; \kappa, \beta)) = \frac{1}{2}A_0^2R^2(\kappa^2 + \sin^2\beta)\sin\beta. \qquad (1.110)$$

where $R = R(\kappa, \beta)$ is the relative run-up function as before. For large κ, substituting the expansion (1.89) for R in (1.110) yields

$$\overline{v_L}(0; \kappa, \beta)) = A_0^2\pi\kappa^3 \ \sin 2\beta + O(\kappa^{3/2}). \qquad (1.111)$$

This aymptotic limit shows that $\overline{v_L}(0)$ increases like κ^3 for κ large and reaches, for κ fixed, its maximum at $\beta = 45^o$. For the open ocean, $x > l$, use of (1.12) in (1.109) yields the result:

$$\overline{v_L} = A^2\sin\beta\ \{1 - \cos 2\beta\cos 2[k(x - l)\cos\beta + \Delta]\}, \qquad (1.112)$$

to which the incident and reflected waves each contributes one half of the total. For sloping plane beach, the mean drift velocity can be calculated from (1.109) with η given by (1.25) and η_x by (1.26).

As a typical example, figure 1.15a shows the variations of η, η_x, mean longshore current $\overline{v_L}$, and the longshore discharge flux $q = h\overline{v_L}$, with increasing shore distance x/l, for the case with $\beta = 30^o$, $A_0 = 1$ and $\kappa = 2$. The longshore current increases shoreward quite rapidly to 23.86 at the shoreline, whereas the longshore mass flux has a maximum of 1.867 at $x/l = 0.205$. Figure 1.15b shows the variations of mean

longshore current $\overline{v_L}$ with increasing shore distance x/l, for $A_0 = 1, \kappa = 2$, $\beta = 10^o$, 20^o, 45^o. Figure 1.16ab shows the variation of mean longshore current function $\overline{v_L}(x = 0; \kappa, \beta)$ at waterline with increasing κ for different β. From these results we see that the longshore current velocity on the beach, $\overline{v_L}$, increases with β, for fixed κ, up to about $\beta = 45^o$, and within this range of β, increases with κ like κ^3. In the range $45^o < \beta < 90^o$, the outstanding feature is that $\overline{v_L}$ is dominated by the eigenmodes of the trapped waves.

For a fluid particle, initially at $(x_0, -\Delta/k_2)$, its trajectory $(x(t), y(t))$ satisfies the following equations:

$$\frac{dx}{dt} = \frac{1}{k}\eta_x \sin[k(y\sin\beta - t) + \Delta], \tag{1.113}$$

$$\frac{dy}{dt} = \eta \sin\beta \cos[k(y\sin\beta - t) + \Delta], \tag{1.114}$$

$$x(0) = x_0, \quad y(0) = -\Delta/k_2. \tag{1.115}$$

Numerical results of pathlines are obtained by integrating (1.113,1.114) for $k = 0.5$, $\beta = 60^o$, $l = 4$ and $A = 0.05$, on the beach

$$h(x) = x, \quad \eta(x) = 0.1835\, e^{-\sqrt{3}x/4} M(-0.6547, 1, \sqrt{3}x/2), \quad 0 < x < l, \tag{1.116}$$

and in the sea, with

$$h(x) = 1, \quad \eta(x) = 0.1\cos(x + 2.583), \quad x > l. \tag{1.117}$$

Figure 1.17 shows the horizontal projection of several trajectories of water particles at different places on the beach and in the sea, for $\alpha = 1/4$, $\beta = 60^o$, $k = 0.5$, and $A = 0.05$. This figure shows clearly how the coiling of pathlines traversed by fluid particles becomes increasingly stretched out in both longshore and seaward directions as the longshore current is amplified toward the waterline. This varying pattern of pathlines is thought to play a basic role in the processes of sand suspension and sandbar formation.

1.9 Conclusion and discussion

In this study linear long-wave theory has been applied to obtain the fundamental solution for a uniform train of sinusoidal ocean waves obliquely incident upon a uniform beach of variable downward slope. This fundamental solution is applied with Fourier synthesis to obtain analytical solutions to several problems including oblique reflections of solitary waves and cnoidal waves by sloping beaches, bringing forth salient features of the wave field regarding the effects of wave incidence angle and variable slope and curvature of a uniform beach.

An outstanding feature of the solution is the trapping of waves over a sloping beach that arises when the incident wave becomes grazing to the coast and with the wave number falling in a spectrum of eigenvalues characterizing the system at resonance. This is a variation of the phenomenon previously found by Eckart (1951) for the edge waves on an infinite slope as the sea floor. The impact of this phenomenon upon coastal environmental quality is not yet in focus, but its effects should be of interest on coastal ocean circulation and long term interactions between ocean and land.

Under the asymptotic limit admitting ray theory, the same asymptotic expansion of the present solution based on beach wave theory provides a solution, in closed form, describing the refraction and amplification of both the obliquely incident wave on water of variable depth and the reflected wave as well as the phase shift of the latter upon reflection. By comparison, this result has established a criterion, given in §1.7, under which the classical ray theory is found in excellent agreement with the asymptotic linear theory in predicting the evolution of incident wave, and beyond which the ray theory becomes poor. Prediction of wave reflection and phase shift generally requires certain detailed structures of the solution for satisfying the specific boundary conditions, which the ray theory lacks.

The longshore current occurring in nature is a very complicated phenomenon. The present result is basically built on the Stokes drift of the water resulting from the waves obliquely incident on a uniform sloping beach, without wave breaking and dissipation. (For a review on the criteria separating the regimes with and without

wave breaking, see e.g., Mei 1983.) The remarkable magnitude of the longshore current predicted here for the incidence angles near the optimum obliquity and for the eigenmodes seem to have not been presented explicitly before. For the regime without wave breaking, these current speeds may be regarded as to give an upper limit which would be reduced when they are modified by the viscous effects involved. In the presence of wave breaking, various formulas for evaluating longshore currents have been proposed, e.g., by Longuet-Higgins & Stewart (1962) for predicting the current velocity across the surf zone based on the radiation stress concept, and by others proposing modifications of the model. It should be of interest to extend the present theory to cover these general cases.

Improvement of the present theory can be attained by including the effects of nonlinearity, dispersion and dissipation so far neglected, since these effects become significant at least in a neighborhood of the moving waterline where the water depth vanishes. An estimate of the importance of these effects on run-up of waves can be inferred by the finding of J. B. Keller (1961) that for the case of normal incidence of periodic waves on a sloping beach, the nonlinear theory yields the same amplification as the linear theory. This lends a support to justifying that linear run-up theory has validity, even though it cannot predict, equally accurately as nonlinear theory, the transient wave profiles near the moving waterline and the time for reaching maximum run-up. It is of great interest to find if the same implications can be said about the general case with oblique incidence of waves upon such beaches horizontally curved in configuration as what is common in nature.

Table 1.1: Run-up predicted by linear nondispersive theory, for a solitary wave of amplitude $a/h = 0.1$, running up from an ocean of depth $h = 1$ to a plane beach of slope $\alpha = 1/l$.

Beach length l	The maximum run-up R
0.0	0.2000
1.0	0.2163
2.0	0.2561
3.0	0.2981
4.0	0.3366
5.0	0.3717
6.0	0.4039

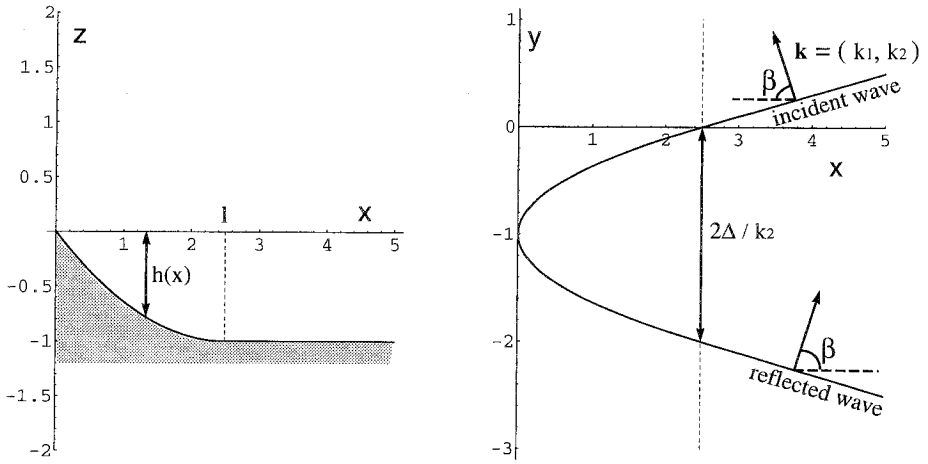

(a) Side view

(b) Top view

Figure 1.1: A sketch of the ocean bathymetry.

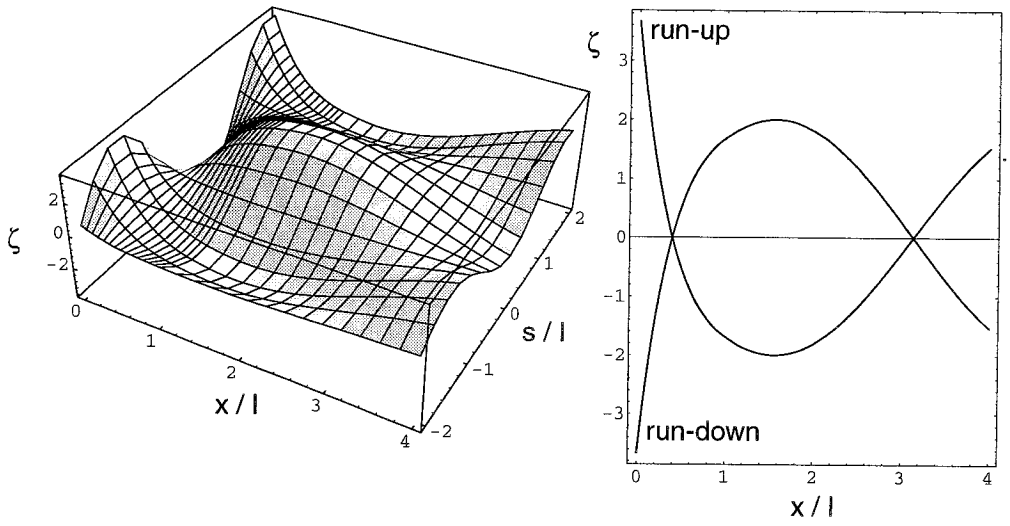

Figure 1.2: The wave profile on the beach ($0 < x/l < 1$) and sea ($x/l > 1$) for $\beta = 60°, \kappa = 2$.

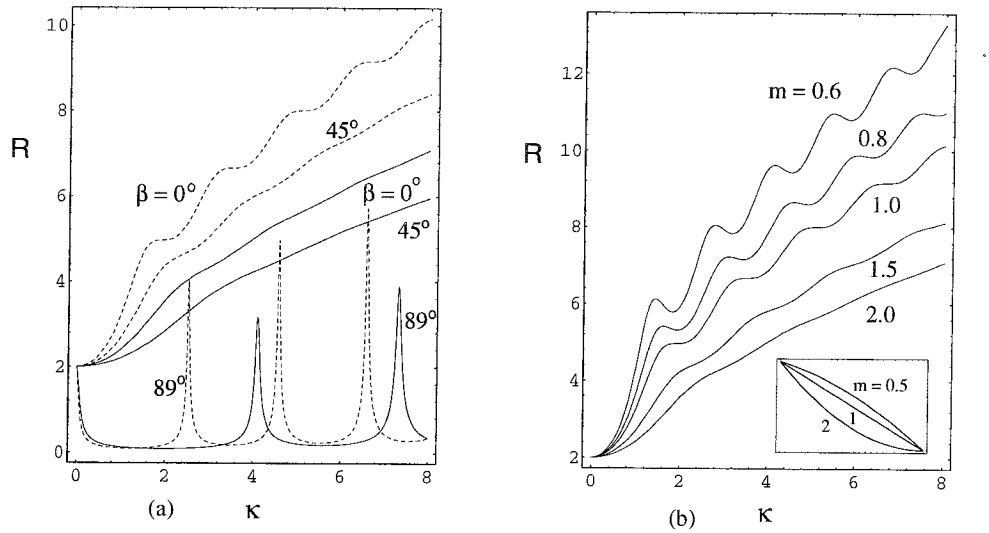

Figure 1.3: (a) Variation of run-up function, $R(\kappa, \beta)$, with increasing $\kappa = kl$, ——— for parabolic beach $h(x) = 2x/l - (x/l)^2$; – – – – for plane beach $h(x) = x/l$; at incidence angle $\beta = 0°$, 45°, 89°. (b) Variation of run-up function, $R(\kappa, \beta = 0)$, with increasing $\kappa = kl$ for parabolic beaches, $h(x) = mx/l + (1-m)(x/l)^2$, $m = 0.6,\ 0.8,\ 1.0,\ 1.5,\ 2.0$ (see the inset).

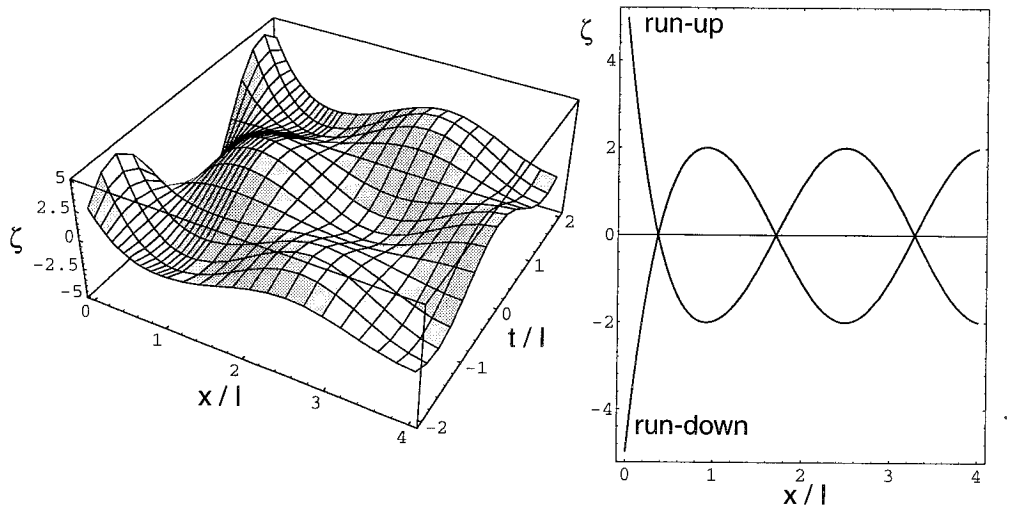

Figure 1.4: The perspective wave profile on the beach and in the ocean for normal incidence at $\beta = 0^o$ and wave number $\kappa = 2$.

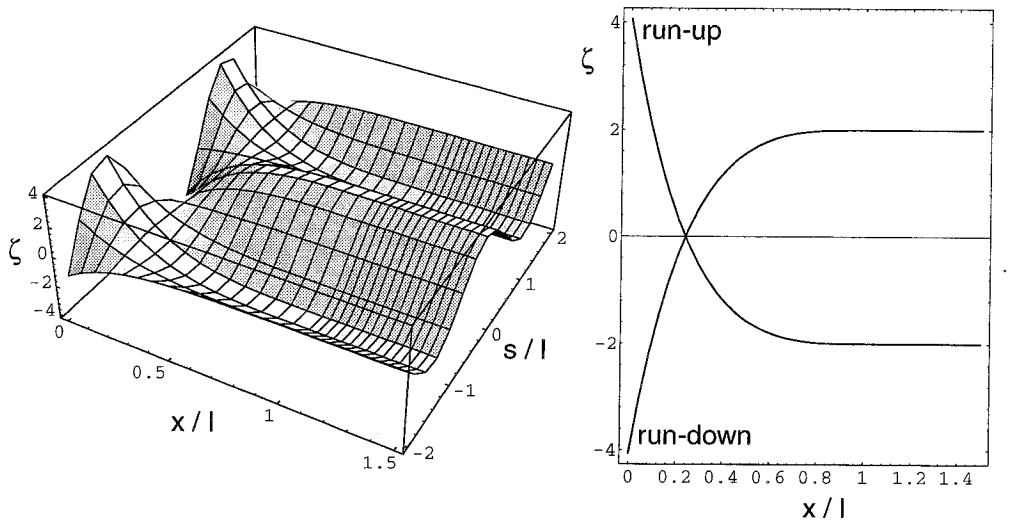

Figure 1.5: The perspective wave profile on the beach and sea for grazing incidence at $\beta = 90^o$ for $\kappa = 2.5337$.

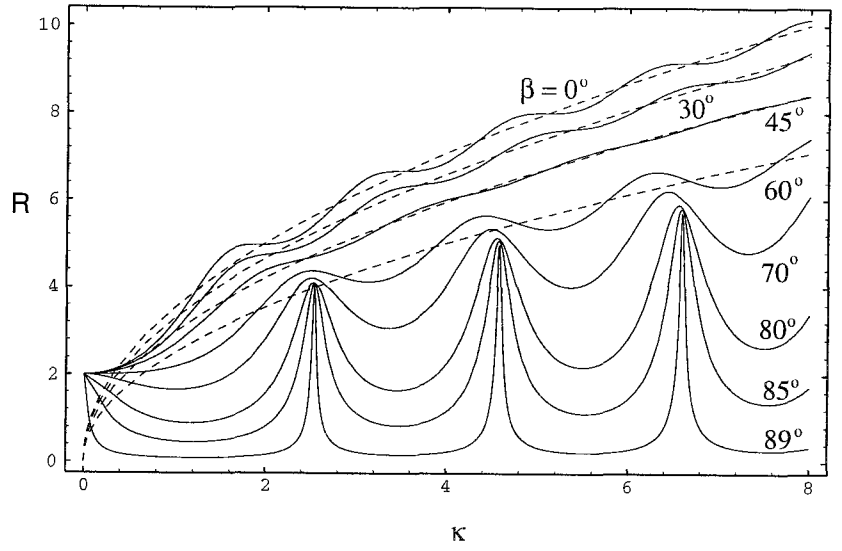

Figure 1.6: Variation of the run-up function $R(\kappa, \beta)$ with $\kappa = kl = kh_0/\alpha$, ——— for a list of β indicated; – – –– asymptotic formula (equation 1.89).

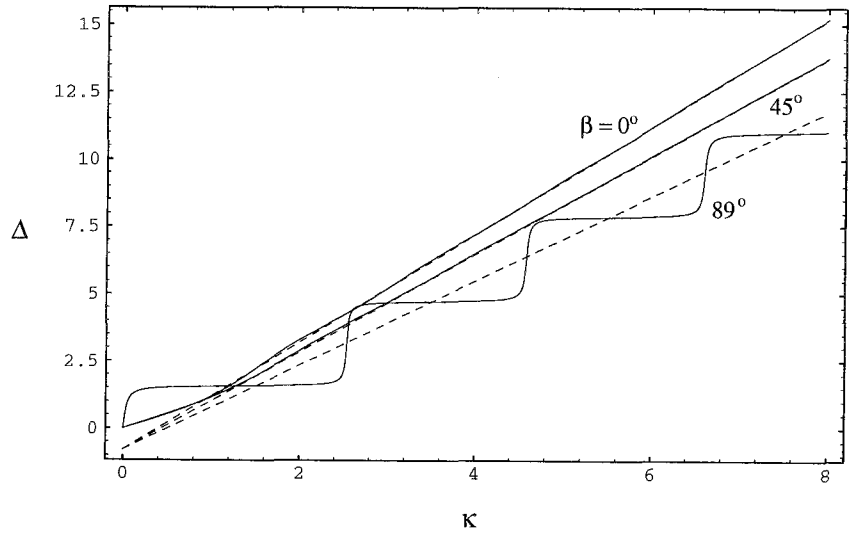

Figure 1.7: Variation of the phase lag function $\Delta(\kappa, \beta)$ with $\kappa = kl = kh_0/\alpha$,——— for $\beta = 0°$, $45°$, and $89°$; – – –– asymptotic formula (equation 1.90).

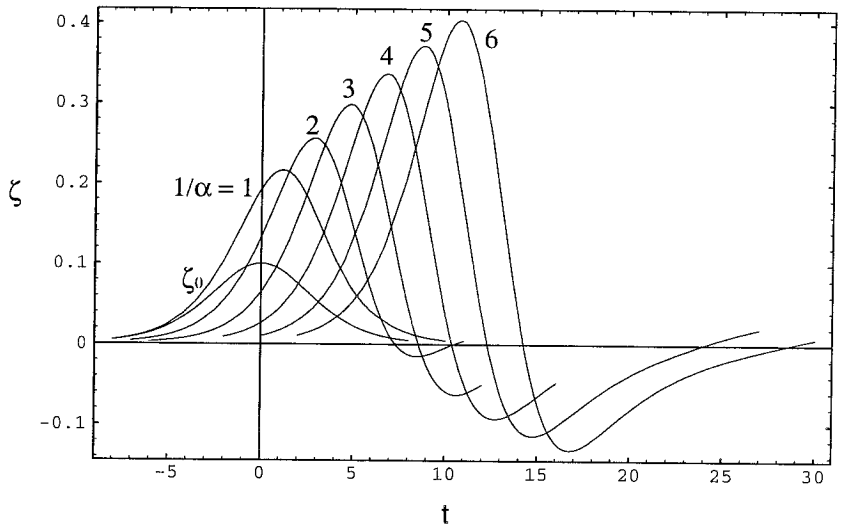

Figure 1.8: Time records of run-up, at $x = 0$, of a solitary wave with $a_0 = 0.1$ at normal incidence ($\beta = 0°$) on a sloping beach for $1/\alpha = 1, 2, 3, 4, 5, 6$.

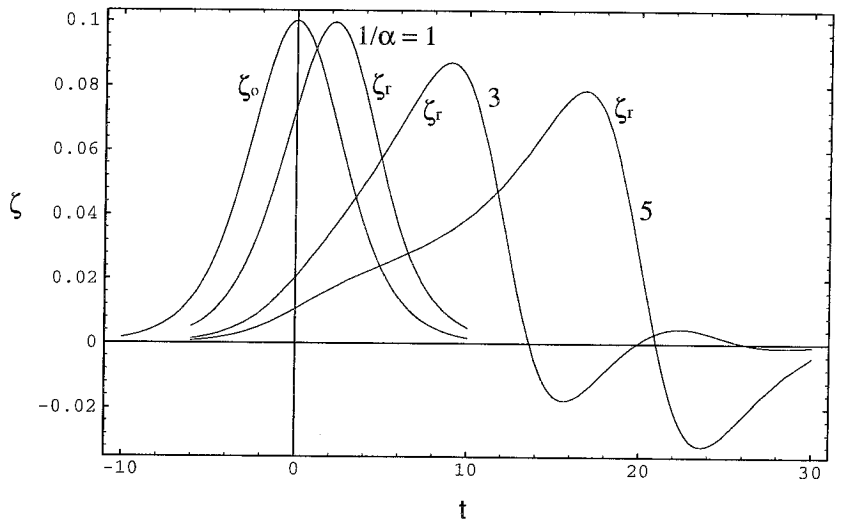

Figure 1.9: Time records of reflected wave ζ_r at $x = l$, from an incoming solitary wave with $a_0 = 0.1$ at normal incidence ($\beta = 0°$) on a sloping beach for $1/\alpha = 1,\ 3,\ 5$.

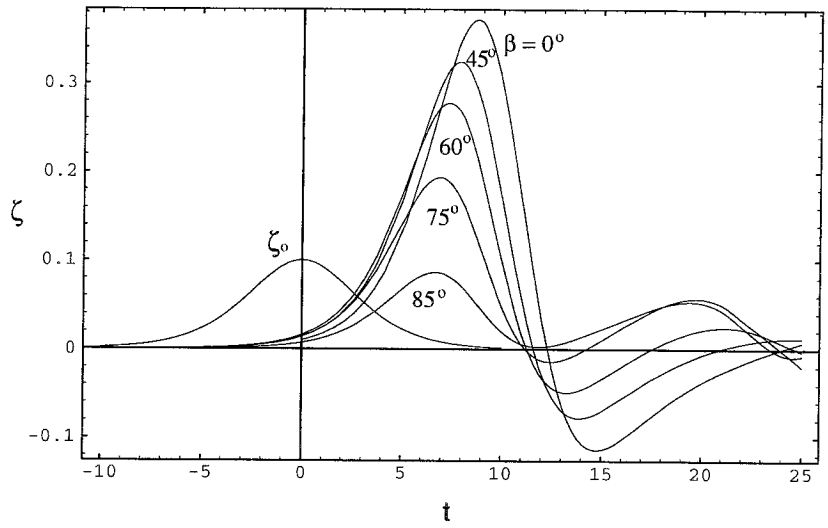

Figure 1.10: Time records of oblique run-up, taken at $x = 0$ and $y = 0$, of a solitary wave with $a_0 = 0.1$ on a beach with slope $\alpha = 1/5$ at incidence angle $\beta = 0^\circ$, 45°, 60°, 75°, 85°.

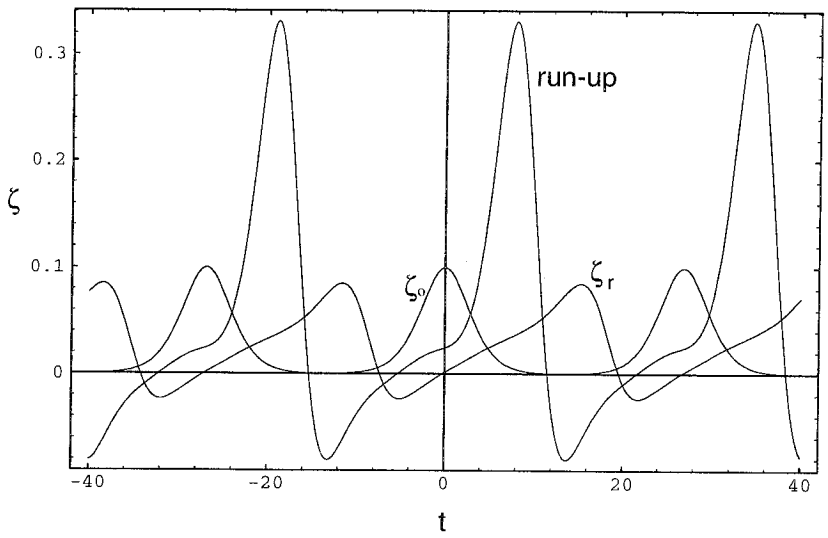

Figure 1.11: The incident wave ζ_0, the reflected wave ζ_r at $x = l$, and run-up at $x = 0$, $y = 0$ of a train of cnoidal waves with $\alpha_1 = 0.1$, $m = 0.99$ at incidence angle $\beta = 45^\circ$ upon a beach of slope $\alpha = 1/5$.

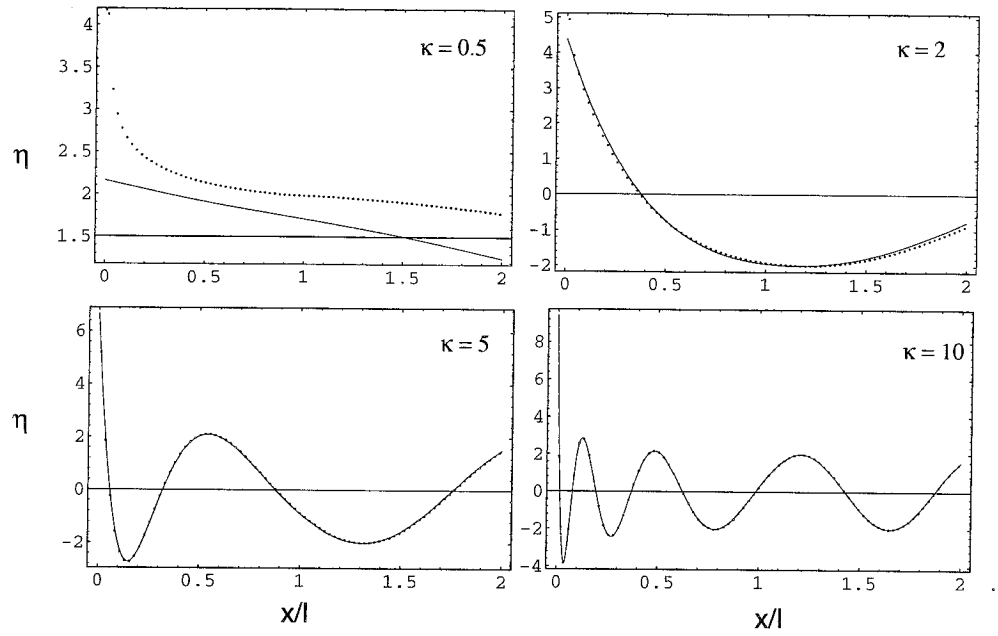

Figure 1.12: Variations of the wave elevation η over a range of x/l for $A = 1$, $\beta = 45°$, $\kappa = 0.5,\ 2,\ 5,\ 10$, ——— present theory; $- - - -$ asymptotic formula (1.93).

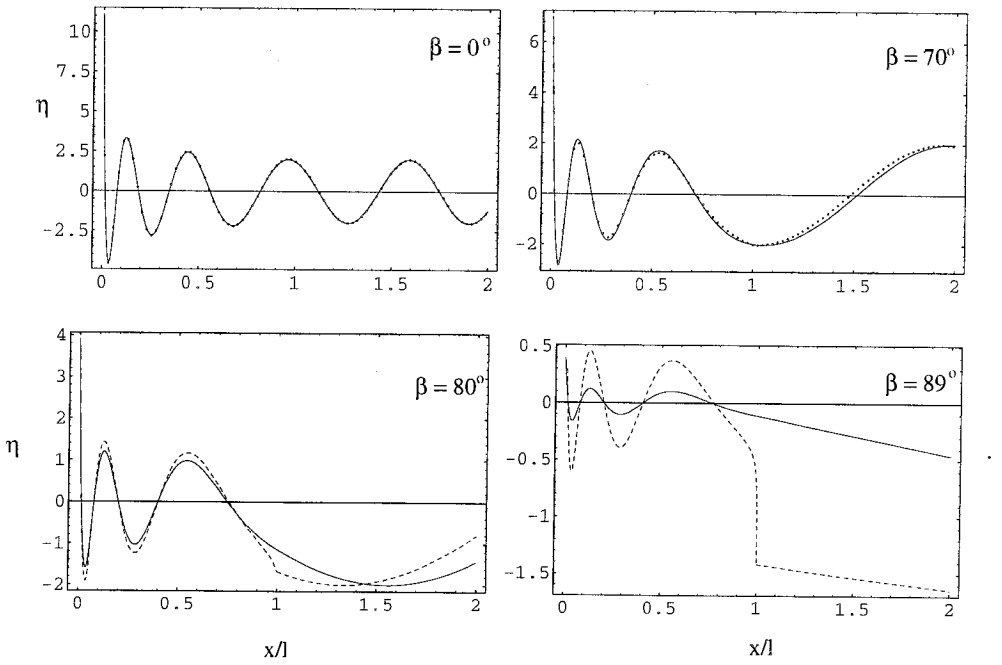

Figure 1.13: Variations of the wave elevation η over a range of x/l for $A = 1$, $\kappa = 10$, $\beta = 0°,\ 70°,\ 80°, 89°$, ——— present theory; $- - - -$ asymptotic formula (1.93).

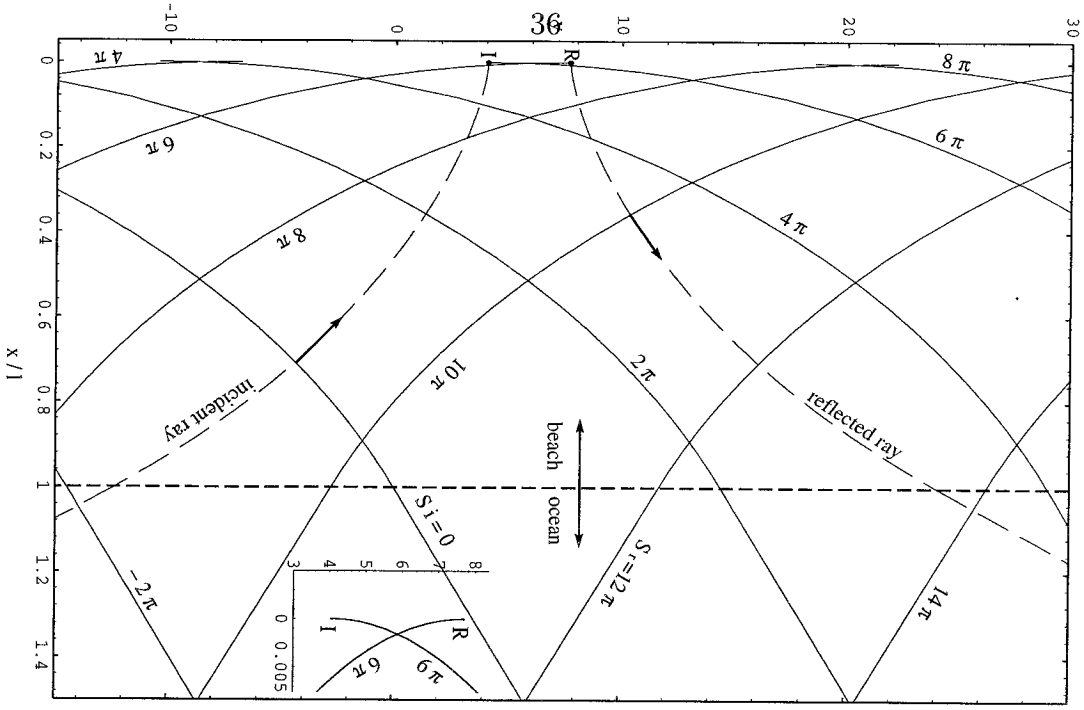

Figure 1.14: ——, phase lines of incident and reflected waves for $S_i = -2\pi,\ 0,\ 2\pi,\ 4\pi,\ 6\pi,\ 8\pi,\ S_r = 4\pi,\ 6\pi,\ 8\pi,\ 10\pi,\ 12\pi,\ 14\pi$; – – ––, incident and reflected ray tracks for $\kappa = 10,\ \beta = 60°$. The phase lag between the incident wave (point I) and reflected wave (point R) at $x = 0$ is $\pi/2$ (see equation 1.103), i.e., $y_R - y_I = \pi/(2k_2)$.

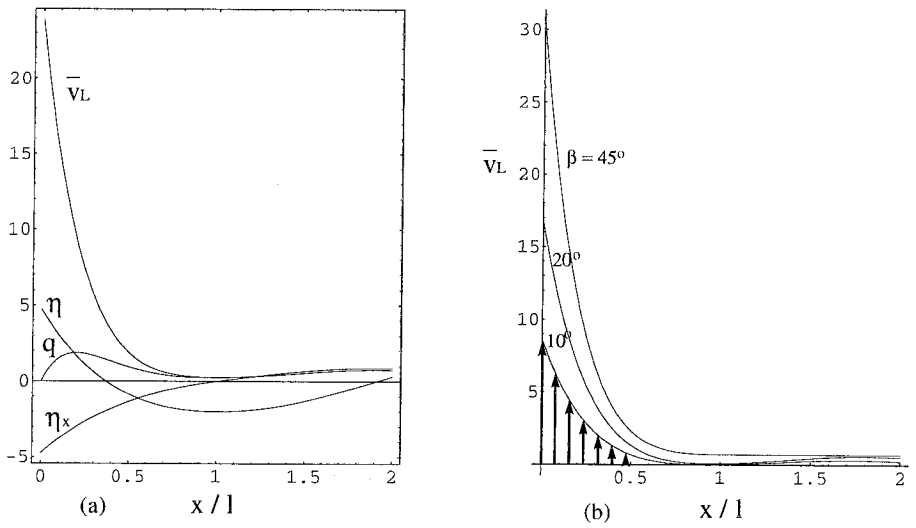

Figure 1.15: a. Variations of η, η_x, mean longshore current $\overline{v_L}$ and longshore discharge flux $q = h\overline{v_L}$, with shore distance x/l, for $\beta = 30°$, $A_0 = 1$ and $\kappa = 2$. b. Distributions of mean longshore current $\overline{v_L}$ over shore distance x/l, for $A_0 = 1$ and $\kappa = 2$ and $\beta = 10°,\ 20°, 45°$.

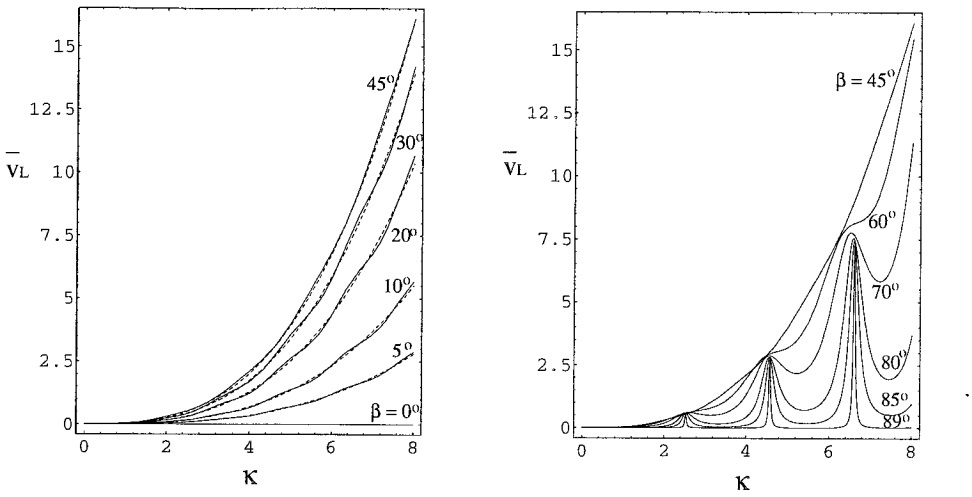

Figure 1.16: Variations of the mean longshore current $\overline{v_L}$ at waterline with increasing κ for different β, – – –– asymptotic formula (equation 1.111).

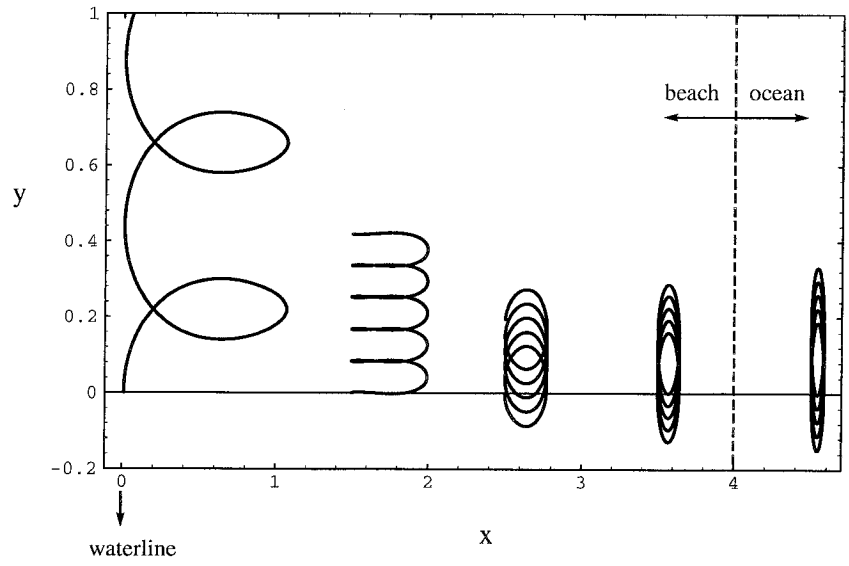

Figure 1.17: Horizontal projections of pathlines of water particles at different places on the beach and in the ocean, for $\alpha = 1/4$, $\beta = 60^{\circ}$, $k = 0.5$, and $A = 0.05$. These tracks are the pathlines traversed by the water particles in five time periods except for the one at the waterline which covers only about two periods.

Chapter 2 The nonlinear effects in run-up of waves on beach

The linear theory presented in Chapter 1 is based on the following assumptions

$$(h+\zeta) \simeq h, \text{ and } \quad u \ll 1. \tag{2.1}$$

They require that the wave amplitude be everywhere small compared with the water depth. But this can *not* be true around waterline where h and $(h+\zeta)$ are close to zero, so linear theory is not a good approximation around waterline. Actually, it is beyond linear theory to indicate how waves go across initial waterline point ($x = 0$, and $h = 0$ in figure 1.1). This is because the wave speed from linear theory is $\sqrt{h}$, which approaches to zero when wave propagates from ocean to the waterline $h = 0$. Finally the wave gets reflected at the point $h = 0$. There is no run-up and run-down process on beach for linear theory. This is not a physical reality. The reason for this nonphysical result is that we neglect the nonlinear effects. If we include the nonlinear terms, the wave speed will be $\sqrt{h+\zeta}$; it never reaches zero until at the real waterline point $h + \zeta = 0$. So we should be able to see wave running up and running down on the beach, instead of stopping at $x = 0$.

There is a big difference between linear theory and nonlinear theory in regard to run-up of waves. In linear theory, we may define (see, e.g., Keller 1961) the run-up as the wave elevation reached at $h = 0$ (i.e., $x = 0$),

$$R = \zeta|_{h=0}. \tag{2.2}$$

In nonlinear theory, we now define the run-up, on physical ground neglecting only

the viscous effects, by the wave elevation at $h + \zeta = 0$,

$$R = \zeta|_{h+\zeta=0}. \tag{2.3}$$

It is thus clear that when we compare the run-ups predicted by linear and nonlinear theories, we actually compare wave elevations at two different points, $h = 0$ and $h + \zeta = 0$.

A few technical terms are often used in this thesis, for which we define as following:

1. *Linear run-up*: run-up predicted by linear theory according to (2.2).

2. *Nonlinear run-up*: run-up predicted by nonlinear theory using (2.3).

3. *Two-dimensional run-up*: run-up of waves normally incident upon beaches. The physical picture for this phenomenon is two-dimensional, x and z. The governing equations for this case have one space x and one time t. Some people call it $1 + 1$ dimensional.

4. *Three-dimensional run-up*: run-up of waves obliquely incident upon (uniform or nonuniform) beaches. The physical picture for this phenomenon is three-dimensional x, y and z. The governing equations for this case have two space x, y and one time t. Some people call it $2 + 1$ dimensional.

The case of *two-dimensional nonlinear run-up* is studied in this chapter. A brief review of literature on nonlinear theories is given in §2.1. In §2.2 we present a new numerical scheme for computing wave run-up on beaches, which is shown to have a very high accuracy by comparison with some exact solutions of nonlinear theories. In §2.3 we apply the scheme to compute a few cases for the run-up of solitary waves, for which case we only have an approximate solution known in literature. Our numerical results, with its error estimate assessed, therefore provide a criterion to evaluate the accuracy of this approximate theory.

2.1 Nonlinear theories

Due to the difficulties of this nonlinear problem, only very few theoretical studies have been presented over the last half century, of which Carrier-Greenspan's theory (1958) is classic. Other theories are more or less extensions of Carrier-Greenspan's theory.

2.1.1 The Carrier-Greenspan theory

Carrier and Greenspan (1958) presented a theory for wave run-up on a sloping plane beach based on the shallow water equations, also known as Airy's model,

$$\zeta_t + [(-\alpha x + \zeta)u]_x = 0, \tag{2.4}$$

$$u_t + uu_x + \zeta_x = 0, \tag{2.5}$$

with $h = -\alpha x$ (see figure 2.1). Rescaling x, t, ζ, and u

$$x' = x, \quad t' = \sqrt{\alpha}t, \quad \zeta' = \zeta/\alpha, \quad u' = u/\sqrt{\alpha}, \tag{2.6}$$

converts (2.4, 2.5) into the following equations in terms of x', t', ζ', and u' (with primes dropped) as

$$\zeta_t + [(-x + \zeta)u]_x = 0, \tag{2.7}$$

$$u_t + uu_x + \zeta_x = 0, \tag{2.8}$$

which means that we only need to study the case with beach slope $\alpha = 1$. Solutions for arbitrary slope α can then be constructed by similarity variables (2.6).

It is interesting to note that another rescalling can also transform equation (2.4, 2.5) to (2.7, 2.8)

$$x' = \alpha x, \quad t' = \alpha t, \quad \zeta' = \zeta, \quad u' = u, \tag{2.9}$$

which is due to the group structure underlying the shallow water equations (2.4, 2.5) (Olver 1986).

Introduce a new variable c

$$c = \sqrt{-x + \zeta}, \tag{2.10}$$

which is local wave speed. Substituting $\zeta = c^2 + x$ into (2.7, 2.8) yields the equations

$$2c_t + 2uc_x + cu_x = 0, \tag{2.11}$$

$$u_t + uu_x + 2cc_x = -1. \tag{2.12}$$

Next we introduce two new variables σ and λ:

$$\sigma = 4c, \qquad \lambda = 2u + 2t, \tag{2.13}$$

in terms of which (2.11, 2.12) become

$$\sigma_t + u\sigma_x + c\lambda_x = 0, \tag{2.14}$$

$$\lambda_t + u\lambda_x + c\sigma_x = 0. \tag{2.15}$$

We then use the hodographic transformation

$$x_\sigma = \lambda_t/J, \qquad x_\lambda = -\sigma_t/J, \qquad t_\sigma = -\lambda_x/J, \qquad t_\lambda = \sigma_x/J, \tag{2.16}$$

where

$$J = \frac{\partial(\sigma, \lambda)}{\partial(x, t)} = \begin{vmatrix} \sigma_x & \sigma_t \\ \lambda_x & \lambda_t \end{vmatrix} = \sigma_x\lambda_t - \sigma_t\lambda_x \tag{2.17}$$

is the Jacobian of the transformation, to interchange the dependent and independent

variables, by which equations (2.14, 2.15) become

$$x_\lambda - ut_\lambda + ct_\sigma = 0, \tag{2.18}$$

$$x_\sigma - ut_\sigma + ct_\lambda = 0. \tag{2.19}$$

x and t are dependent variables in these equations. Substituting $t = \lambda/2 - u$ into these equations, after some algebra, we have

$$(x + \frac{1}{2}u^2)_\lambda - \frac{\sigma}{4}u_\sigma - \frac{1}{2}u = 0, \tag{2.20}$$

$$(x + \frac{1}{2}u^2 + \frac{1}{16}\sigma^2)_\sigma - (\frac{\sigma}{4}u)_\lambda = 0. \tag{2.21}$$

Here, equation (2.21) is automatically satisfied by a new 'potential' variable $\phi(\sigma, \lambda)$ such that

$$x + \frac{1}{2}u^2 + \frac{1}{16}\sigma^2 = \frac{1}{4}\phi_\lambda, \quad \frac{\sigma}{4}u = \frac{1}{4}\phi_\sigma. \tag{2.22}$$

Substituting (2.22) into (2.20), we finally have a linear equation for $\phi(\sigma, \lambda)$

$$(\sigma\phi_\sigma)_\sigma - \sigma\phi_{\lambda\lambda} = 0. \tag{2.23}$$

Based on this equation Carrier and Greenspan find an exact solution for $\zeta(x, t)$ and $u(x, t)$, which is written in parametric form in terms of σ and λ as

$$\phi = AJ_0(\sigma)\cos\lambda, \tag{2.24}$$

$$\zeta = \frac{1}{4}\phi_\lambda - \frac{1}{2}u^2 = -\frac{A}{4}J_0(\sigma)\sin\lambda - \frac{A^2}{2\sigma^2}J_1^2(\sigma)\cos^2\lambda, \tag{2.25}$$

$$u = \frac{1}{\sigma}\phi_\sigma = -\frac{A}{\sigma}J_1(\sigma)\cos\lambda, \tag{2.26}$$

$$x = -\frac{\sigma^2}{16} + \frac{1}{4}\phi_\lambda - \frac{1}{2}u^2 = -\frac{\sigma^2}{16} - \frac{A}{4}J_0(\sigma)\sin\lambda - \frac{A^2}{2\sigma^2}J_1^2(\sigma)\cos^2\lambda, \tag{2.27}$$

$$t = \frac{1}{2}\lambda - u = \frac{1}{2}\lambda + \frac{A}{\sigma}J_1(\sigma)\cos\lambda. \tag{2.28}$$

This solution is a time-periodic wave on a sloping beach for $0 < A \leq 1$ (as shown

in figure 2.1). Each curve in figure 2.1 is for a fixed time instant, $t = 4\pi/16$, $5\pi/16$, $6\pi/16$, $7\pi/16$, $8\pi/16$, $9\pi/16$, $10\pi/16$, $11\pi/16$, $12\pi/16$. For fixed time t, given a σ, λ can be solved numerically with iteration from (2.28). Substituting σ and λ into (2.25, 2.26, 2.27) gives the solution for ζ, u and x. Changing σ we can get another set of λ, ζ, u, x, and so on. Thus we find for $t = t_n$, $n = 1, 2, \cdots$,

$$\zeta = \zeta(x, t = t_n), \qquad u = u(x, t = t_n), \tag{2.29}$$

which are the curves shown in figure 2.1. The wave is supposed to break when it reaches its maximum slope of infinity at a position of the moving waterline during the run-down period with $A = 1$. For $A > 1$, $\zeta(x, t)$ is multivalued.

2.1.2 The Tuck-Hwang theory

For a beach with constant slope, Tuck and Hwang introduce the following transformation

$$\zeta^* = \zeta + \tfrac{1}{2}u^2, \qquad u^* = u, \tag{2.30}$$

$$-x^* = -x + \zeta, \qquad t^* = t + u, \tag{2.31}$$

and convert the nonlinear equations (2.7, 2.8) into their linearized version

$$\zeta^*_{t^*} + (-x^* u^*)_{x^*} = 0, \tag{2.32}$$

$$u^*_{t^*} + \zeta^*_{x^*} = 0. \tag{2.33}$$

This set of equations has a solution given by

$$\zeta^* = A(k) J_0(2k\sqrt{-x^*}) \cos(kt^*), \tag{2.34}$$

$$u^* = -\frac{A(k)}{\sqrt{-x^*}} J_1(2k\sqrt{-x^*}) \sin(kt^*). \tag{2.35}$$

The solution for ζ and u is given by (2.30, 2.31).

We notice that the Tuck-Hwang and the Carrier-Greenspan transformations are related by

$$\zeta^* = \zeta + \tfrac{1}{2}u^2, \qquad u^* = u \tag{2.36}$$

$$-x^* = \tfrac{\sigma^2}{16}, \qquad t^* = \tfrac{1}{2}\lambda. \tag{2.37}$$

With the new linear equations (2.32, 2.33) Tuck and Hwang (1972) studied a particular problem of releasing an initial excess mass of water supported underneath by a sloping plane seabed.

For this problem, the initial velocity is zero everywhere, while the initial wave elevation ζ is an implict function of x, given by

$$x = b\log(\zeta/a) + \zeta, \tag{2.38}$$

corresponding to which the initial condition in the star variables is

$$\zeta^*(x^*, 0) = ae^{x^*/b} = \int_0^\infty 2ab\kappa e^{-b\kappa^2} J_0(2\kappa\sqrt{-x^*})d\kappa, \qquad u^*(x^*, 0) = 0, \tag{2.39}$$

for $x^* < 0$. In the star coordinate, they use the Hankel transformation to obtain the following solution for ζ^* and u^*

$$\zeta^*(x^*, t^*) = 2ab\int_0^\infty \kappa e^{-b\kappa^2} J_0(2\kappa\sqrt{-x^*})\cos(\kappa t^*)d\kappa, \tag{2.40}$$

$$u^*(x^*, t^*) = -\frac{2ab}{\sqrt{-x^*}}\int_0^\infty \kappa e^{-b\kappa^2} J_1(2\kappa\sqrt{-x^*})\sin(\kappa t^*)d\kappa. \tag{2.41}$$

In the original physical coordinates, the solution of this initial value problem is therefore given by the inversion:

$$u = u^*, \tag{2.42}$$

$$\zeta = \zeta^* - (u^*)^2/2, \tag{2.43}$$

$$x = x^* + \zeta^*, \tag{2.44}$$

$$t = t^* - u^*. \tag{2.45}$$

With the integrals evaluated numerically, Tuck and Hwang gave results for a few particular cases.

Spielvogel (1976) studied a similar problem of mass release based on a superposition of Carrier - Greenspan's periodic wave solutions.

2.1.3 Run-up of solitary wave

Synolakis (1987) developed an approximate nonlinear theory for the run-up of solitary waves. He introduced a matching condition at the junction of a sloping plane beach and an exterior uniform ocean, i.e., at $x = -1$,

$$\zeta = \zeta^* = \frac{1}{4}\phi_\lambda, \quad u = u^* = \frac{1}{\sigma}\phi_\sigma, \quad x = x^* = -\frac{\sigma^2}{16}, \quad t = t^* = \frac{1}{2}\lambda. \tag{2.46}$$

With these relations, one may see that $\zeta(x,t)$ and $u(x,t)$ satisfy the linearized equations (2.32, 2.33). These matching conditions are valid under assumptions

$$\zeta/h \ll 1, \quad u \ll 1, \tag{2.47}$$

i.e., small wave amplitude. Once we admit the matching relations (2.46), it is very straightforward to get solution for nonlinear equations. Simply changing (x,t,ζ,u) given by solution (1.72) to the linear equations (2.32, 2.33) for (x^*,t^*,ζ^*,u^*), we obtain the solution for run-up of a solitary wave from ocean of unform depth to a beach of constant slope,

$$\zeta^*(x^*,t^*) = \mathrm{Re}\int_0^\infty A_0(k)R_0(\kappa)e^{-ikt^*+i\Delta_0}J_1(2k\sqrt{x^*})dk \quad (-1 < x < 0), \tag{2.48}$$

where $A_0(k)$, R_0, and Δ_0 are given in Chapter 1. It is obvious that the maximum nonlinear run-up, R_n, is equal to maximum linear run-up, R_l, based on this solution,

since at the run-up point,

$$u = u^* = 0, \quad \text{and hence} \quad R_n = \zeta^* = \zeta + \frac{1}{2}u^2 = \zeta = R_l. \tag{2.49}$$

Actually, this is true for any shape of incident wave. This has to be true under the matching conditions (2.46) or small amplitude linear wave assumptions.

We recall that for solitary head-on collisions of a solitary wave of amplitude a with a vertical wall, the maximum nonlinear run-up on the wall is (Wu 1994)

$$R_n = 2a + \frac{1}{2}a^2 + O(a^3), \tag{2.50}$$

whereas the corresponding linear maximum run-up is

$$R_l = 2a. \tag{2.51}$$

This tells us that the linear run-up is the leading order approximation of the nonlinear run-up

$$R_n = R_l(1 + O(a)), \tag{2.52}$$

and the next order term is of order aR_l.

Run-up on a vertical wall is but a special case of run-up on a sloping beach, with an infinite beach slope. So we may conjecture that for run-ups on a sloping beach, equation (2.52) is also true. This is a reasonable conjecture, since it is true for the special case of run-ups on a vertical wall.

It should be noted that Synolakis' conclusion that "the maximum run-up predicted by the nonlinear theory is identical with the maximum run-up predicted by the linear theory" is made under (2.46), i.e., linear wave assumption. We will come back to this point later.

2.2 Numerical computation

In excecuting numerical computations of run-ups of waves on sloping beach based on the shallow water model equation, the most difficult part is reckoned to be related with how to handle the moving waterline, i.e., the place of zero total water depth in motion or the boundary between land, water and air.

2.2.1 Other treatments of waterline

Hibberd and Peregrine (1979) studied the run-up of a uniform bore on a beach by using the finite difference method to compute numerical solutions of the shallow water equations (2.7, 2.8). The total water depth $\eta = h + \zeta$ and momentum $m = \eta u$ (in our notation) were used as the dependent variables in order to keep the conservation laws of mass and momentum satisfied, which are very important to obtain correct wave speed in computation of the shock wave propagation. The operation involves dividing the momentum m by the total water depth η gives the velocity u. Consequently near the waterline, errors in determining the water velocity can be magnified due to the division of m by small values of total water depth η. To avoid these difficulties, Hibberd and Peregrine used the water velocity near waterline as a dependent variable, and a lower bound, δ say (usually taken as 10^{-4}), of the water depth is set, below which the water depth is considered to be zero. In general, the position of the waterline does not coincide with a grid point and it is therefore the last underwater point, denoted by subscript s, that requires special attention. In short, Hibberd and Peregrine's treatment of waterline for run-up is by assuming that all values are known at time level $n\Delta t$ and it is required to solve explicitly for $\eta_{s,n+1}$, $\eta_{s+1,n+1}$, $u_{s,n+1}$ and $u_{s+1,n+1}$ at the $(n+1)\Delta t$ time step. The following procedure is followed.

1. Obtain values of (η, u) at grid index $(s+1, n)$ by *linear extrapolation* from values at grid points (s, n) and $(s-1, n)$.

2. Use the Lax-Wendroff scheme to obtain values of (η, u) at $(s, n+1)$.

3. Calculate the provisional values at grid point $(s+1, n+1)$, denoted by $u^*_{s+1,n+1}$ and $\eta^*_{s+1,n+1}$ by *linear extrapolation* from values at $(s, n+1)$ and $(s-1, n+1)$. If $\eta^*_{s+1,n+1} > \delta$, final values at $(s+1, n+1)$ are calculated. If $\eta^*_{s+1,n+1} \leq \delta$, corrected values at $(s, n+1)$ are calculated.

In Hibberd & Peregrine's treatment, they often use *linear extrapolation* to get information around waterline. This technique is not physical. Since this linear extrapolation introduces some considerable error at the waterline point, making the run-up computation, especially the local velocity, to be inaccurate, as can be attested by their figure 5 for comparison of their numerical results with Carrier-Greenspan's exact solution.

Pedersen & Gjevik (1983), Zelt (1986) and Zelt & Raichlen (1990) used the Lagrangian description in order to avoid the moving waterline difficulty; however, this approach brings forth some new nonlinear terms and makes the governing equations very complicated.

Kim, Liu & Liggett (1983) studied the problem of two-dimensional run-up with the BIEM (Boundary integral equation method) based on potential flow theory, for which case the whole free surface becomes moving boundary. They used the Laplace equation for velocity potential, and the free-surface boundary conditions on $z = \zeta(x,t)$, including the waterline point. Therefore, their treatment of the waterline is very different from what we are using here.

Titov & Synolakis (1995) treated the waterline with the following relations:

$$
\begin{aligned}
& h + \zeta = 0, \\
& \frac{dx}{dt} = u, \\
& u_x = 0.
\end{aligned}
$$

The first two relations are correct, the same as our (2.53, 2.54). But the third one is an artificial treatment, not physical. It could introduce some considerable error in the computation of run-up.

2.2.2 The present treatment of the waterline

We develop a new treatment of calculating a moving waterline to compute the run-up problem in this section.

First we catch the waterline by employing a special scheme described below. At waterline $x = X(t)$, we have the following relations:

$$h(X(t)) + \zeta(X(t), t) = 0, \tag{2.53}$$

$$\frac{dX}{dt} = u(X(t), t) = U(t), \tag{2.54}$$

$$\frac{dU}{dt} = -\zeta_x. \tag{2.55}$$

These three relations are geometrical, in (2.53), kinematical, in (2.54), and dynamical conditions in (2.55), for any waterline, noting that (2.55) is identical to (2.8). They are the Lagrangian description of a waterline.

With these three conditions, we can compute position and velocity at waterline at the $(n+1)$-th time step by the information at the n-th time step. Subject to this step, we redefine the grid points with the new waterline position $X(t_{n+1})$ to constitute the same number of nodes. Then we compute the values of $\zeta(x, t_{n+1})$ and $u(x, t_{n+1})$ at each new node, followed by going to compute the next time step and so on. In this way we keep the waterline captured by satisfying its Lagrangian equations.

For calculating the values of (ζ, u) inside the domain, we still use the Euler description, since the Euler description is simpler than the full Lagrangian counterpart. The only thing we need to take care of is to observe that the grid points are changing with time. In this way, we actually compute the wave elevation and velocity at different places at different time instants. Of course we can alternatively compute the wave elevation and velocity at the same spatial locations first, then use interpolation to get the values at the new grid points in the next step. The interpolation has to be done every time step. However, this may introduce errors. Because of this, we prefer to use another approach, namely the following transformation approach.

Introduing the transformation

$$x = (1 + X/L)x' + X, \tag{2.56}$$

$$t = t', \tag{2.57}$$

where $X = X(t)$ is the waterline position as a function of t, and L is the total initial length of the computation domain. We can see that the waterline at $x = X(t)$ always corresponds to $x' = 0$, and the other boundary $x = -L$ corresponds to $x' = -L$. In the x', t' coordinates, the grid points therefore never change with t.

With this transformation, we transform the computation domain from a moving boundary problem to a fixed boundary problem. The cost is that we have to modify our equations. The partial derivatives in the two systems have the following relations:

$$\frac{\partial}{\partial t} = \frac{\partial}{\partial t'} + \frac{\partial x'}{\partial t}\frac{\partial}{\partial x'}, \tag{2.58}$$

$$\frac{\partial}{\partial x} = \frac{\partial x'}{\partial x}\frac{\partial}{\partial x'}. \tag{2.59}$$

Taking the partial derivatives with respect to x and t from equation (2.56) and (2.57) gives

$$\frac{\partial x'}{\partial x} = \frac{1}{1 + X/L}, \tag{2.60}$$

$$\frac{\partial x'}{\partial t} = \frac{1 + x'/L}{1 + X/L}U, \tag{2.61}$$

and substituting these relations into (2.58, 2.59) gives

$$\frac{\partial}{\partial t} = \frac{\partial}{\partial t'} - \frac{1 + x'/L}{1 + X/L}U\frac{\partial}{\partial x'}, \tag{2.62}$$

$$\frac{\partial}{\partial x} = \frac{1}{1 + X/L}\frac{\partial}{\partial x'}. \tag{2.63}$$

Substituting these relations between the two sets of partial derivatives into (2.7, 2.8), we obtain the governing equations in the new coordinate system(dropping the primes)

as

$$\zeta_t - c_1 U \zeta_x + c_2[(h+\zeta)u]_x = 0, \tag{2.64}$$

$$u_t - c_1 U u_x + c_2(u u_x + \zeta_x) = 0, \tag{2.65}$$

where

$$c_1 = c_1(x,t) = \frac{1+x/L}{1+X/L}, \qquad c_2 = c_2(t) = \frac{1}{1+X/L}, \tag{2.66}$$

are coefficients arising from the transformation. As we are not computing any shock wave, we can compute ζ and u from the above equations directly. If we should compute a flow field involving shock waves, we need to use $\eta = h + \zeta$ and $m = \eta u$ as our dependent variables.

2.2.3 The present scheme for the run-up computation

For numerical computation of the model equation

$$u_t + f_x(u) = 0, \tag{2.67}$$

the Richtmyer two-step Lax-Wendroff scheme reads

$$u_{i+\frac{1}{2}}^{n+\frac{1}{2}} = \frac{1}{2}(u_i^n + u_{i+1}^n) - \frac{\Delta t}{2\Delta x}[f(u_{i+1}^n) - f(u_i^n)], \tag{2.68}$$

$$u_i^{n+1} = u_i^n - \frac{\Delta t}{\Delta x}[f(u_{i+\frac{1}{2}}^{n+\frac{1}{2}}) - f(u_{i-\frac{1}{2}}^{n+\frac{1}{2}})]. \tag{2.69}$$

If we take

$$f(u) = Au, \tag{2.70}$$

the scheme will become

$$u_i^{n+1} = u_i^n - \frac{\Delta t}{2\Delta x} A(u_{i+1}^n - u_{i-1}^n) + \frac{(\Delta t)^2}{2(\Delta x)^2} A^2(u_{i+1}^n - 2u_i^n + u_{i-1}^n). \tag{2.71}$$

If we assume

$$u_i^n = \rho^n e^{ikx_i}, \tag{2.72}$$

then from (2.71) we have

$$\rho = 1 - iC\sin(k\Delta x) - 2C^2\sin^2(k\Delta x/2), \tag{2.73}$$

where $C = A\Delta t/\Delta x$. In order to make $|\rho| \leq 1$, we require that

$$C \leq 1. \tag{2.74}$$

This is the stability condition for the scheme.

Scheme (2.71) can be written as

$$u_i^{n+1} = u_i^n - \Delta t A(u_x + \frac{1}{6}(\Delta x)^2 u_{xxx}) + \frac{1}{2}(\Delta t)^2 A^2(u_{xx} + \frac{1}{12}(\Delta x)^2 u_{xxxx}) + \text{h.o.t} \tag{2.75}$$

where h.o.t. means higher order terms. By Taylor's expansion of u_i^{n+1}, we have

$$u_i^{n+1} = u_i^n + \Delta t u_t + \frac{1}{2}(\Delta t)^2 u_{tt} + \frac{1}{6}(\Delta t)^3 u_{ttt} + \text{h.o.t.} \tag{2.76}$$

Subtracting (2.76) from (2.75) and dividing the difference by Δt gives

$$[1 + \frac{1}{2}\Delta t(\partial_t - A\partial_x)](u_t + Au_x) = -\frac{1}{6}(\Delta t)^2 u_{ttt} - \frac{1}{6}(\Delta x)^2 A u_{xxx} + \text{h.o.t.} \tag{2.77}$$

or

$$u_t + Au_x = -\frac{1}{6}(\Delta t)^2 u_{ttt} - \frac{1}{6}(\Delta x)^2 A u_{xxx} + \text{h.o.t.} \tag{2.78}$$

This is the modified equation for the Richtmyer two-step Lax-Wendroff scheme. This scheme is second order in space and time.

For our problem, the first step of the Richtmyer two-step Lax-Wendroff scheme reads

$$\begin{aligned}
\zeta_{i+\frac{1}{2}}^{n+\frac{1}{2}} &= \frac{1}{2}(\zeta_i^n + \zeta_{i+1}^n) + \frac{\Delta t}{2\Delta x} c_1 U(\zeta_{i+1}^n - \zeta_i^n) \\
&\quad - \frac{\Delta t}{2\Delta x} c_2[(h_{i+1} + \zeta_{i+1}^n)u_{i+1}^n - (h_i + \zeta_i^n)u_i^n], \qquad (2.79) \\
u_{i+\frac{1}{2}}^{n+\frac{1}{2}} &= \frac{1}{2}(u_i^n + u_{i+1}^n) + \frac{\Delta t}{2\Delta x} c_1 U(u_{i+1}^n - u_i^n) \\
&\quad - \frac{\Delta t}{2\Delta x} c_2[\frac{1}{2}(u_{i+1}^n)^2 + \zeta_{i+1}^n - \frac{1}{2}(u_i^n)^2 - \zeta_i^n]; \qquad (2.80)
\end{aligned}$$

where $c_1 U$ and c_2 are evaluated at grid points $(i + \frac{1}{2}, n)$. The second step of the Richtmyer two-step Lax-Wendroff scheme reads

$$\begin{aligned}
\zeta_i^{n+1} &= \zeta_i^n + \frac{\Delta t}{\Delta x} c_1 U(\zeta_{i+\frac{1}{2}}^{n+\frac{1}{2}} - \zeta_{i-\frac{1}{2}}^{n+\frac{1}{2}}) \\
&\quad - \frac{\Delta t}{\Delta x} c_2[(h_{i+\frac{1}{2}} + \zeta_{i+\frac{1}{2}}^{n+\frac{1}{2}})u_{i+\frac{1}{2}}^{n+\frac{1}{2}} - (h_{i-\frac{1}{2}} + \zeta_{i-\frac{1}{2}}^{n+\frac{1}{2}})u_{i-\frac{1}{2}}^{n+\frac{1}{2}}], \qquad (2.81) \\
u_i^{n+1} &= u_i^n + \frac{\Delta t}{\Delta x} c_1 U(u_{i+\frac{1}{2}}^{n+\frac{1}{2}} - u_{i-\frac{1}{2}}^{n+\frac{1}{2}}) \\
&\quad - \frac{\Delta t}{\Delta x} c_2[\frac{1}{2}(u_{i+\frac{1}{2}}^{n+\frac{1}{2}})^2 + \zeta_{i+\frac{1}{2}}^{n+\frac{1}{2}} - \frac{1}{2}(u_{i-\frac{1}{2}}^{n+\frac{1}{2}})^2 - \zeta_{i-\frac{1}{2}}^{n+\frac{1}{2}}], \qquad (2.82)
\end{aligned}$$

where $c_1 U$ and c_2 are evaluated at the grid points (i, n).

At the waterline point $(I, n+1)$, we use the Beam-Warming scheme for the integration of velocity u,

$$u_I^{n+1} = u_I^n - \frac{\Delta t}{2\Delta x}(3\zeta_I^n - 4\zeta_{I-1}^n + \zeta_{I-2}^n) + \frac{(\Delta t)^2}{2(\Delta x)^2}(\zeta_I^n - 2\zeta_{I-1}^n + \zeta_{I-2}^n), \qquad (2.83)$$

and the trapezoidal integration for X,

$$X_I^{n+1} = X_I^n + \frac{1}{2}\Delta t(u_I^{n+1} + u_I^n). \qquad (2.84)$$

These schemes are second order in space and time.

2.2.4 Test on a few cases

The first test is for the case of run-up of periodic waves on a beach of constant slope. We take $A = 1.0$ and the initial condition as posed at $t = 3\pi/4$ by Carrier-Greenspan exact solution (2.24 - 2.28), which is

$$\zeta = \frac{1}{4} J_0(\sigma), \tag{2.85}$$

$$u = 0, \tag{2.86}$$

$$x = -\frac{\sigma^2}{16} - \frac{1}{4} J_0(\sigma). \tag{2.87}$$

For a given x, we can find the σ by solving (2.87) numerically with iteration, then compute ζ from (2.85). The initial condition for wave elevation is defined by (2.85, 2.87). For the boundary condition on the left side boundary, say at $x = x_0$, of the region of computation, we have two choices: one is to find $\zeta(x = x_0, t)$ and $u(x = x_0, t)$ numerically from the exact solution, and use these values as our boundary condition. The other way is to compute ζ and u over a larger domain, while the left boundary of this larger domain could be a solid wall, but make sure that any disturbance emanating from the left boundary does not reach the experimental domain within the time period of the numerical experiment. We chose the latter approach.

Figure 2.2 shows the comparison between our numerical results and Carrier-Greenspan's exact solution. At the beginning, counting from $t = 3\pi/4$, the waterline runs down slowly. It becomes faster and faster, then decelerates quickly, until it stops at $t = 5\pi/4$, while the velocity equals zero everywhere in the flow field at this time instant. Then it reverses the procedure described above. We notice that the flow described by the shallow water equations is reversible in time, since by changing t to $-t$, and u to $-u$, the equations remain invariant.

Our numerical results are thus found to agree with Carrier-Greenspan's theory very well. Typically, with $\Delta x = 1/500, \Delta t = \pi/500$, the relative error of the wave elevation is less than 10^{-3} if we use single precision. And it takes one to two minutes CPU on a sun station at the Caltech Campus Computer Organization for computation

over a period from maximum run-up to run-down.

The second test is on the problem of mass release statically from the initial shape

$$\alpha x = \frac{H}{\log(R/H)} \log(\zeta/R) + \zeta. \tag{2.88}$$

Since Tuck & Hwang's and Spielvogel's results were calculated numerically and presented with figures. It is not so straightforward to reproduce their results. Figure 2.3 shows our numerical results for $\alpha = 1/20$, $R = 0.1$ and $H = 0.05$, which corresponds to Spielvogel's figure 4 in his *JFM* paper. The time instant for the waterline to pass through the origin is $t = 4$ by Spielvogel's numerical results, $t = 3.94$ by the present scheme. The difference is less than 2%. They agree with each other very well.

2.3 Numerical solution to the run-up of a solitary wave on a beach of constant slope

We now consider a specific case of two-dimensional run-up of solitary waves normally incident on a uniform beach of constant slope α, which is connected to an open ocean of uniform depth $h = 1.0$ (figure 2.4). The shallow water equations are used to study the problem.

In our first numerical experiment, we take an incoming solitary wave of initial amplitude $a = 0.1$ in the open ocean and impinging on a beach of constant slope $\alpha = 1/4$. We pose the quiescent initial condition at $t = 0$ and for the boundary condition at $x_0 = -12$ by the following relation

$$\zeta = a \operatorname{sech}^2 \sqrt{\frac{3a}{4}}(x_0 - ct + 32), \qquad c = 1 + a/2 \tag{2.89}$$

for the wave elevation, which is an exact solution of the KdV equation (1.64), and

$$u = \frac{c\zeta}{1+\zeta} \tag{2.90}$$

for the velocity at $x_0 = -12$, which is the first integral of the mass conservation law for a solitary wave with speed c.

We carry out the computation with the scheme described in the previous section. Figure 2.5 shows wave elevation during run-up at time $t = 20$, 24, 27.28, 28.88, 30.48, 32.08, 33.68. The solitary wave reaches the maximum run-up $R = 0.3666$ at time $t = 33.68$. Figure 2.6 shows the velocity during run-up at the same time instant as listed in figure 2.5. The maximum speed during run-up is as high as 0.3706, which occurs at the waterline at $t = 30.36$.

Figure 2.7 shows the wave elevation during backwash at time $t = 33.68$, 35.28, 36.88, 38.48, and figure 2.8 shows the velocity during backwash at the same time instant as listed in figure 2.7. The maximum speed during backwash is as high as 0.6103, which occurs at the waterline at $t = 38.16$, and the velocity gradient u_x at this point is getting quite large. Based on this result, we may conjecture that it is somewhere during backwash that the solution may violate the assumption invoked on the shallow water model equations which requires

$$\frac{\partial}{\partial x} \ll 1, \tag{2.91}$$

i.e., a steep wave may most likely first break near the extreme of a run-down.

Figure 2.9 shows the wave elevation as a function of t at the waterline.

It is of importance to note that the shallow water equations do not have solutions for travelling wave of permanent form, even in water of uniform depth. Actually, a wave is always getting more and more steepened forward as time goes on, for lack of the dispersive effects to balance out the wave steepening according to this model. It followed that if we pose the boundary conditon (2.89) at different places for x_0, we should expect somewhat different run-up results.

In our second numerical experiment, we take the same $a = 0.1$ for the initial wave amplitude and $\alpha = 1/4$ for the beach slope as before, but pose boundary condition at different places $x_0 = -16$, -12, -10, -8, -6, -4. We compute the maximum run-up for each case. The results are shown in table 2.1. Figure 2.10 shows the maximum

Table 2.1: Run-up of a solitary wave of amplitude $a/h = 0.1$, predicted by the shallow water equations and linear theory (see Chapter 1), with the boundary condition posed at x_0 as (2.89), running up from an ocean of depth $h = 1$ to a plane beach of slope $\alpha = 1/4$.

	x_0	The maximum run-up R	Time to reach the maximum run-up	Time from beach foot to the maximum run-up
	-16	0.3816	33.44	
	-14	0.3743	33.56	
	-12	0.3666	33.68	
the shallow	-10	0.3594	33.80	
water equations	-8	0.3526	33.96	
	-6	0.3464	34.12	
	-4	0.3408	34.24	7.57
linear theory	-4	0.3366	33.43	6.76

run-up as a function of x_0. The maximum run-up decreases with decreasing x_0. Actually, if we stand at the point $x = -4$, we see different waves passing through this point in the different cases due to the nonlinear steepening effect inherent to the shallow water equations. The larger x_0 taken for imposing the same boundary condition, the more steepened the wave becomes at the beach foot and therefore the greater the maximum run-up.

We take $\Delta x = 1/20,\ \Delta t = 1/100$ in both numerical experiments. It takes one to two minutes CPU for a sun station to compute one run-up case.

We can now draw the following conclusion: *The maxmum run-up of a solitary wave predicted by the shallow water equations depends on the initial position of the solitary wave. It is not a fixed value. The farther the initial solitary wave of the KdV form is imposed from the beach, the larger the maximum run-up it will reach.* Of course it can not be too far from the beach, otherwise it may break before reaching the beach. Therefore, *nonlinear run-up is not identical with linear run-up*, i.e.,

$$R_n \neq R_l, \tag{2.92}$$

which disagrees with Synolakis' conclusion.

The reason for having this result is because we have neglected the dispersive effect in the governing equations. The solitary wave changes its shape when it propagates from the ocean of uniform depth to the beach, which is not entirely a physical reality. If we include the dispersive effect, i.e., by using the Boussinesq equations as our model, we should expect to obtain a different result that would correct this specific error. This is what we are going to study in the next chapter.

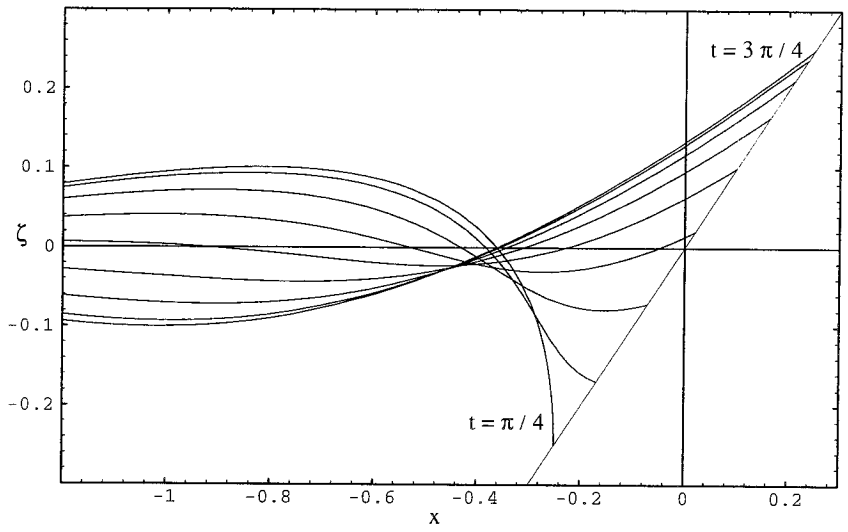

Figure 2.1: Carrier & Greenspan exact solution for run-up of periodic wave on a beach with constant slope, $A = 1.0$.

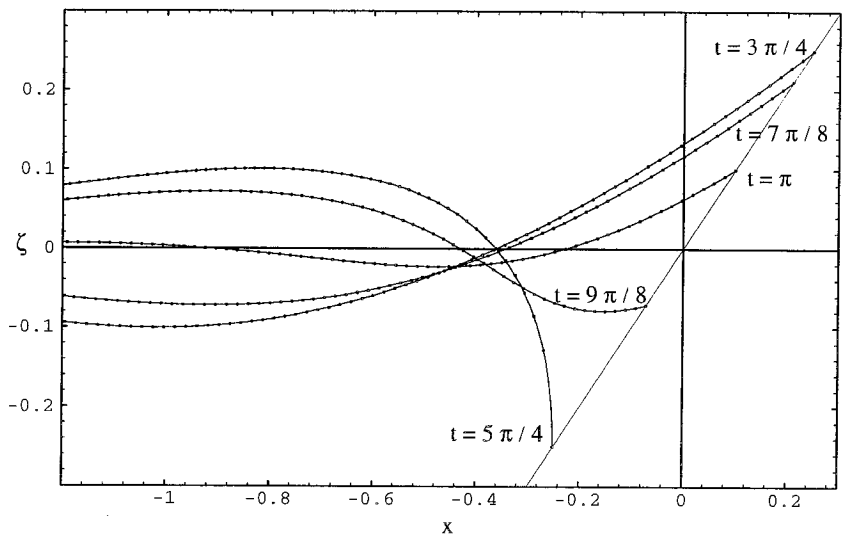

Figure 2.2: Comparison of our numerical results and Carrier- Greenspan exact solution for periodic wave on a sloping beach, $A = 1.0$, —— exact solution, ... present scheme.

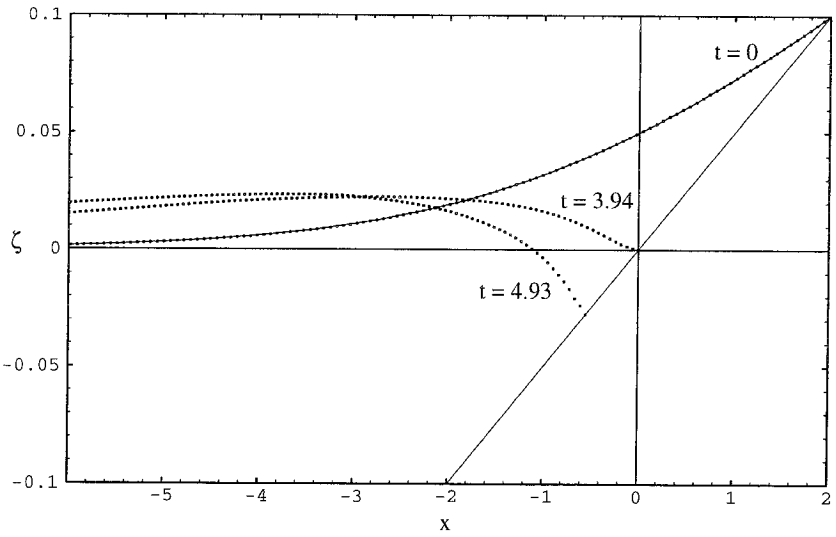

Figure 2.3: Our numerical results for water release problem, $\alpha = 1/20$, $R = 0.1$ and $H = 0.05$ (corresponding to figure 4 in Spielvogel's 1976 paper), —— initial shape, ... present scheme.

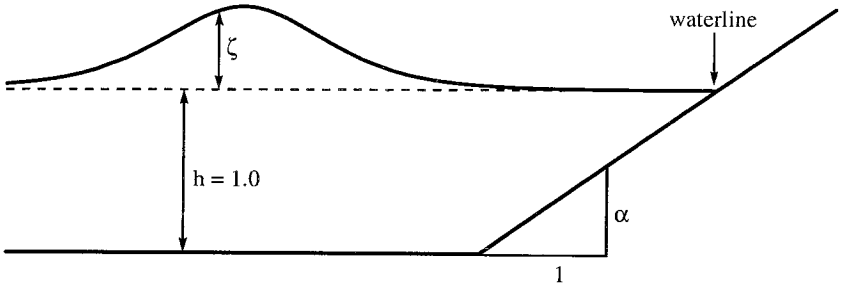

Figure 2.4: A sketch of the ocean bathymetry.

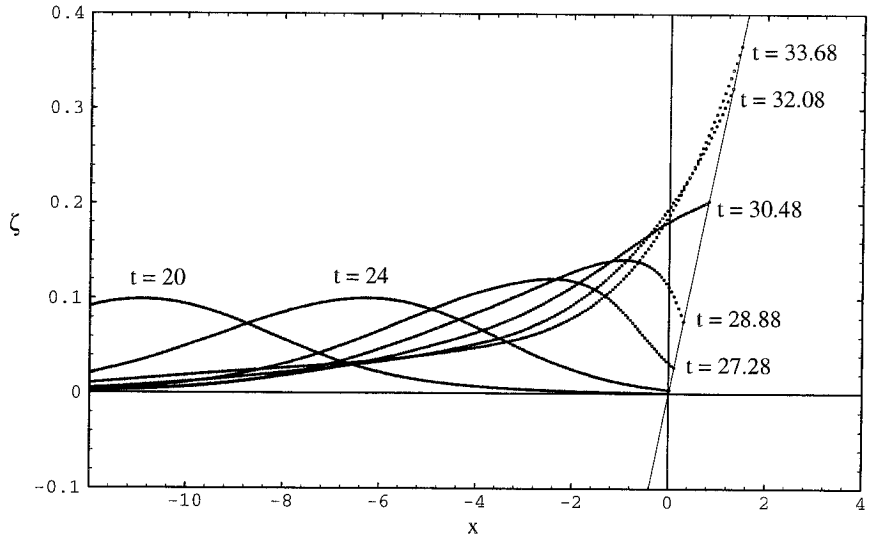

Figure 2.5: Wave elevation as a function of x at time $t = 20$, 24, 27.28, 28.88, 30.48, 32.08, 33.68, ... present scheme.

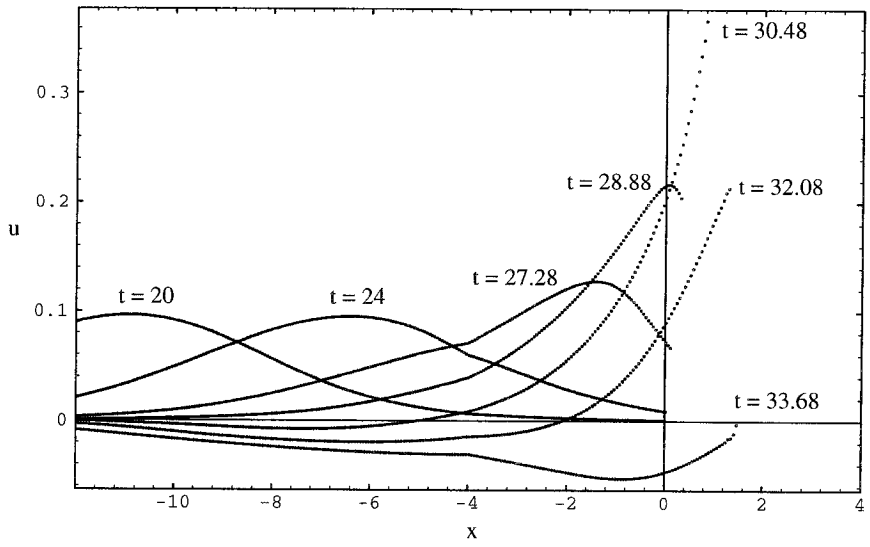

Figure 2.6: Velocity as a function of x at time $t = 20$, 24, 27.28, 28.88, 30.48, 32.08, 33.68, ... present scheme.

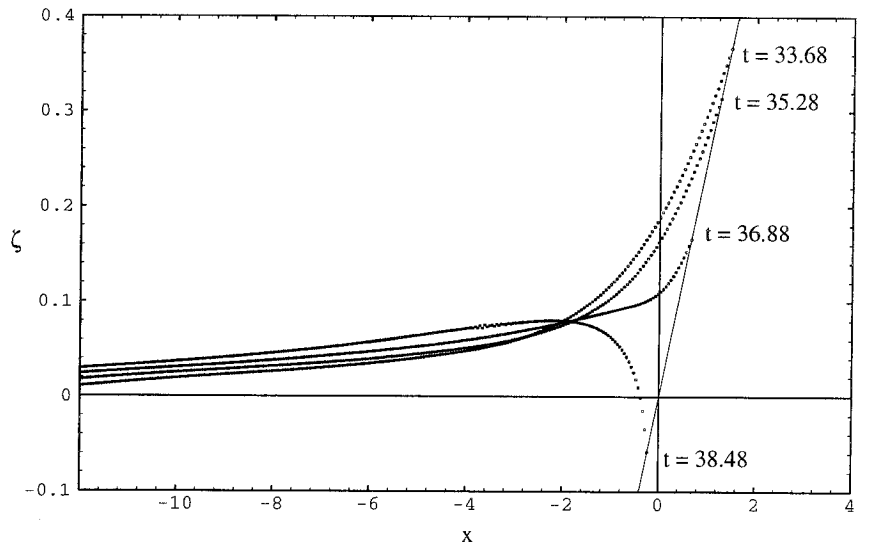

Figure 2.7: Wave elevation as a function of x at time $t = 33.68$, 35.28, 36.88, 38.48, ... present scheme.

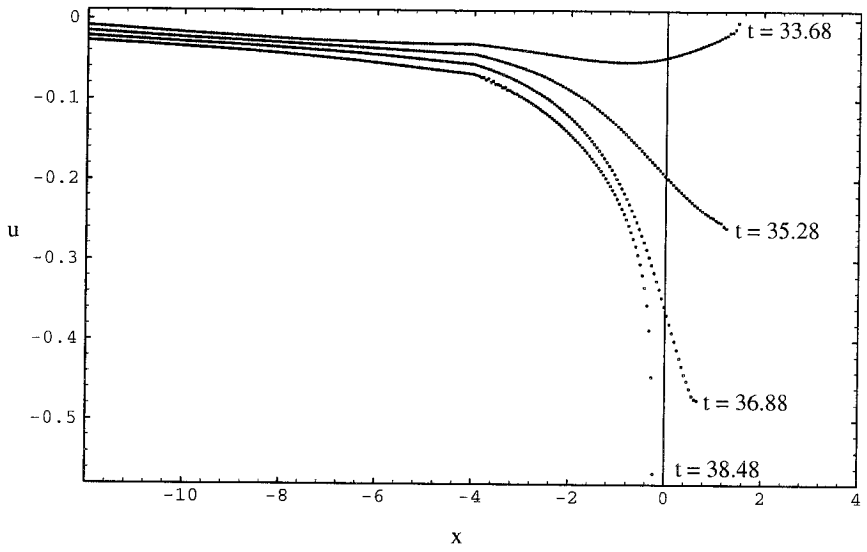

Figure 2.8: Velocity as a function of x at time t = 33.68, 35.28, 36.88, 38.48, ... present scheme.

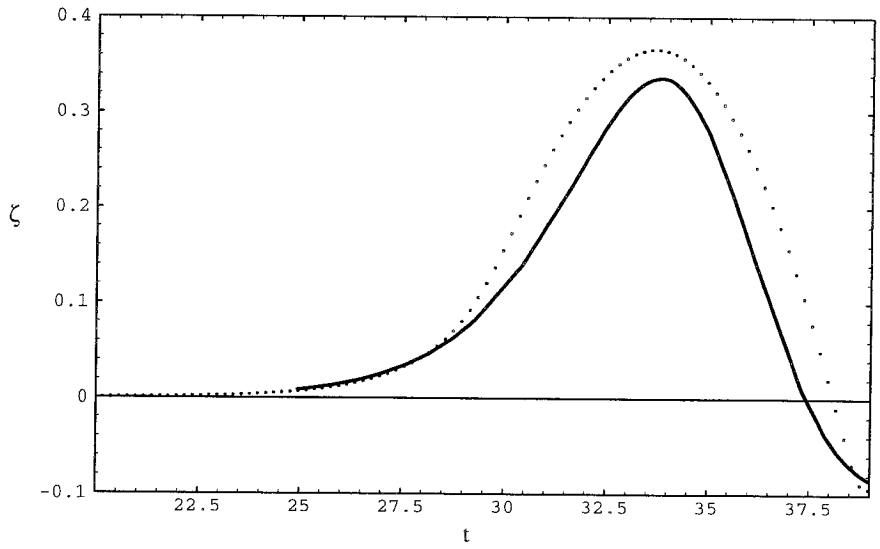

Figure 2.9: Wave elevation as a function of t at waterline, —— linear theory, ... present scheme.

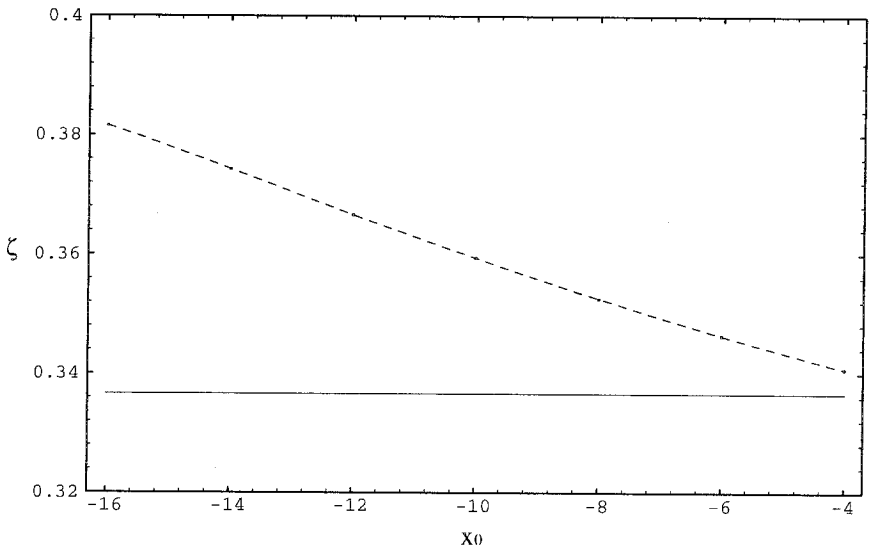

Figure 2.10: Maximum run-up as a function of x_0, the place at which we pose boundary condition of solitary wave.

Chapter 3 The dispersive effects in run-up of waves on beach

In Chapter 2, we find that the run-up of solitary wave predicted by the shallow water equations depends on the initial position of the solitary wave, which is not entirely a physical reality. This leads us to consider the dispersive effects for what they may change the entire run-up process.

In §3.1, we will study the dispersive effects in the linear system. We will then evaluate the importance of the dispersive effects in Carrier-Greenspan's exact solution for periodic waves on a sloping beach in §3.2. In §3.3 we will perform numerical experiments on two-dimensional run-ups of solitary wave with the generalized Boussinesq model and compare the results with that predicted by the shallow water equations. In §3.4, we will study the problem of two-dimensional run-ups of solitary wave on beach with variable downward slope.

3.1 Linear dispersive model

In Chapter 1, we have developed a theory for three-dimensional wave run-up on beach based on the linear nondispersive model

$$\zeta_t + \nabla \cdot (h\mathbf{u}) = 0 \ , \tag{1.6}$$

$$\mathbf{u}_t + \nabla\zeta = 0 \ , \tag{1.7}$$

which is valid for long waves of very small amplitude. If the wave amplitude is small but with the wavelength getting shorter (yet still long), we should consider the

underlying dispersive effects, i.e., we may use the linear dispersive model

$$\zeta_t + \nabla \cdot (h\mathbf{u}) = 0 \ , \tag{3.1}$$

$$\mathbf{u}_t + \nabla\zeta = \frac{h}{2}\nabla[\nabla \cdot (h\mathbf{u}_t)] - \frac{h^2}{6}\nabla^2\mathbf{u}_t \ , \tag{3.2}$$

which comes from the generalized Boussinesq model (Wu 1979) by neglecting the nonlinear effects.

We study the same problem as that in Chapter 1 by now using the linear dispersive model. The bathymetry of the ocean and beach is again

$$h = \begin{cases} h(x) & (0 \le x \le l, \ -\infty < y < \infty), \\ 1 & (x > l), \end{cases} \tag{3.3}$$

$$h(0) = 0, \quad h'(0) \neq 0. \tag{3.4}$$

For slowly varying $h(x)$, (3.2) can be written as

$$\mathbf{u}_t + \nabla\zeta = \frac{h}{3}\nabla[\nabla \cdot (h\mathbf{u}_t)] + \frac{1}{6}\nabla h\nabla \cdot (h\mathbf{u}_t) + \frac{1}{6}\nabla h \cdot \nabla(h\mathbf{u}_t), \tag{3.5}$$

and by eliminating $\mathbf{u}$ from (3.1) and (3.5) we obtain for ζ the equation:

$$\zeta_{tt} - (h\zeta_x)_x - h\zeta_{yy} - \frac{1}{3}h^2(\zeta_{xxtt} + \zeta_{yytt}) - hh_x\zeta_{xtt} = 0. \tag{3.6}$$

In the open ocean, $h(x) = 1$, equation (3.6) becomes

$$\zeta_{tt} - \zeta_{xx} - \zeta_{yy} - \frac{1}{3}(\zeta_{xxtt} + \zeta_{yytt}) = 0, \tag{3.7}$$

which has an incident and reflected sinusoidal wave solution in the following form

$$\zeta = A(k)e^{i(k_2y - k_1(x-l) - \omega t)} + B(k)e^{i(k_2y + k_1(x-l) - \omega t)}, \tag{3.8}$$

where (k_1, k_2) is the wave number vector, ω is the frequency,

$$k_1 = k\cos\beta, \qquad k_2 = k\sin\beta, \tag{3.9}$$

$$\omega = k/\sqrt{1+k^2/3}. \tag{3.10}$$

For the region along the inclined beach $(0 < x < l)$, solution is assumed to have the form

$$\zeta(x,y,t) = \eta(x)e^{iks} \quad (s = y\sin\beta - \omega t/k,\ 0 < x < l). \tag{3.11}$$

Substituting (3.11) into (3.6) gives for $\eta(x)$ the equation

$$(h\eta_x)_x - \frac{1}{3}h^2\omega^2\eta_{xx} - hh_x\omega^2\eta_x + (\omega^2 - hk^2\sin^2\beta + \frac{1}{3}\omega^2k^2h^2\sin^2\beta)\eta = 0, \tag{3.12}$$

which can be written as

$$\eta'' + \frac{1}{x}p(x)\eta' + \frac{1}{x^2}q(x)\eta = 0, \tag{3.13}$$

where

$$p(x) = x\,\frac{h_x(1-\omega^2h)}{h(1-\frac{1}{3}\omega^2h)}, \tag{3.14}$$

$$q(x) = x^2\frac{\omega^2 - hk^2\sin^2\beta + \frac{1}{3}\omega^2k^2h^2\sin^2\beta}{h(1-\frac{1}{3}\omega^2h)}. \tag{3.15}$$

For the present case, $h \leq 1$ over the whole field, so we have

$$1 - \frac{1}{3}\omega^2h \geq 1 - \frac{1}{3}\omega^2 = \frac{1}{1+\frac{1}{3}k^2} > 0, \tag{3.16}$$

for any wave number k. We shall further assume that $p(x)$ and $q(x)$ are analytic, regular in $0 \leq x \leq l$, hence

$$p(x) = \sum_{n=0}^{\infty} p_n(x/l)^n, \qquad q(x) = \sum_{n=0}^{\infty} q_n(x/l)^n. \tag{3.17}$$

Then $x = 0$ is a regular singular point. By Frobenius' theory, (3.13) has a solution

$$\eta(x) = \sum_{n=0}^{\infty} b_n (x/l)^{n+\nu}, \tag{3.18}$$

where ν satisfies the indicial equation

$$\nu^2 + (p_0 - 1)\nu + q_0 = 0. \tag{3.19}$$

Since $p_0 = 1$ and $q_0 = 0$, we have $\nu_1 = \nu_2 = 0$.

We can define a beach function $F(x; \omega, l, \beta)$ similar to that in Chapter 1 for the root $\nu_1 = 0$ and discard the logarithmically singular solution corresponding to the double root $\nu_2 = 0$, so that we have

$$\eta(x) = C_1(k) F(x; \omega, l, \beta) = C_1(k) \sum_{n=0}^{\infty} b_n (x/l)^n, \tag{3.20}$$

where $b_0 = 1$ by normalization, so that $F(0; \omega, l, \beta) = 1$, and b_n are determined by the recurrence formula,

$$n^2 \, b_n = -\sum_{r=0}^{n-1} (r p_{n-r} + q_{n-r}) b_r, \qquad (n = 1, 2, \cdots). \tag{3.21}$$

Here, we observe that $p_0 = 1$ and $q_0 = 0$, as explained above. We now have two parameters in ω and l in the case for dispersive waves, which is different from the nondispersive case treated in Chapter 1 for which we have only one parameter, $\kappa = kl = \omega l$. Now, application of the matching conditions (1.10) determines the coefficients $B(k)$ in (3.8) and $C_1(k)$ in (3.20) as

$$B(k) = e^{2i\Delta(\omega,l,\beta)} A(k) \ , \tag{3.22}$$

$$C_1(k) = R(\omega, l, \beta) e^{i\Delta(\omega,l,\beta)} A(k) \ , \tag{3.23}$$

where

$$R(\omega,l,\beta)=2(M^2+N^2)^{-1/2},\qquad \Delta(\omega,l,\beta)=\arg(M+iN), \tag{3.24}$$

$$M(\omega,l,\beta)=F(l;\omega,l,\beta)=\sum_{n=0}^{\infty}b_n\ , \tag{3.25}$$

$$N(\omega,l,\beta)=-\frac{1}{k\cos\beta}F_x(l;\omega,l,\beta)=-\frac{1}{kl\cos\beta}\sum_{n=0}^{\infty}nb_n\ . \tag{3.26}$$

The run-up function $R(\omega,l,\beta)$ gives the relative wave run-up on the beach and the phase function $\Delta(\omega,l,\beta)$ gives the phase lag of the waves in the beach region and the phase lag 2Δ for the waves reflected.

Figure 3.1 shows the variation of the run-up function, $R(\omega,l,\beta)$, versus ω for waves incident upon a plane beach $h(x)=x/l$, $l=10$ for a set of different incidence angles β.

We have a sinusoidal wave with a given frequency propagating from the open ocean of uniform depth $h=1$ to the sloping plane beach. The maximum run-up of this sinusoidal wave train predicted by the linear dispersive model is smaller than that predicted by the linear nondispersive model. *Dispersion reduces run-up.*

3.2 The dispersive effects on Carrier-Greenspan's exact solution for periodic waves

The basic object in this section is to directly evaluate the dispersive effects on Carrier-Greenspan's exact solution to the shallow water equations.

The Generalized Boussinesq model, referred to as the gB model (Wu 1979), is a weakly nonlinear and weakly dispersive model. For the two-dimensional case, gB model reads

$$\zeta_t+[(h+\zeta)u]_x = 0 \tag{3.27}$$

$$u_t+uu_x+\zeta_x = D \tag{3.28}$$

where

$$D = \frac{h}{2}(hu_t)_{xx} - \frac{h^2}{6}u_{xxt}, \tag{3.29}$$

with error of order $O(\alpha\epsilon^2, \epsilon^4)$. Its validity is based on the assumptions that

$$\epsilon = h_o/\lambda \ll 1, \qquad \alpha = a/h_o = O(\epsilon^2) \tag{3.30}$$

for waves of typical amplitude a, length λ on water of typical depth h_0.

In order to use the model about a waterline, the dispersive term is modified as

$$\begin{aligned} D &= \frac{1}{3}h^2u_{xxt} + hh_xu_{xt} + \frac{1}{2}hh_{xx}u_t \\ &= \frac{1}{3}(h+\zeta)^2u_{xxt} + (h+\zeta)h_xu_{xt} + \frac{1}{2}(h+\zeta)h_{xx}u_t \\ &= -\frac{1}{3}(h+\zeta)^2\zeta_{xxx} - (h+\zeta)h_x\zeta_{xx} - \frac{1}{2}(h+\zeta)h_{xx}\zeta_x, \end{aligned} \tag{3.31}$$

in which the modifications are made by using the lower order relations without changing the order of error estimate. We further assume the variation of $h(x)$ to be very small,

$$h_x = O(\epsilon^2), \qquad h_{xx} = O(\epsilon^3). \tag{3.32}$$

Accordingly, the dispersive term is reduced to

$$D = -\frac{1}{3}(h+\zeta)^2\zeta_{xxx}. \tag{3.33}$$

In §2.1 we have introduced Carrier-Greenspan's exact solution for a periodic train of standing waves run-up and run-down on an inclined plane beach of infinite extent. The solution is obtained from the shallow water equations, i.e., without the terms representing the dispersive effects. Now we are going to evaluate the dispersive effects D by using Carrier-Greenspan's periodic wave solution, and compare the dispersive effects D with the linear term $-\zeta_x$. Figure (3.2) and (3.3) show their values as a

function of x at time $t = 3\pi/4,\ \pi/4$, which correspond to the end of run-up and run-down time instants respectively. Slope of the beach is taken as $1/4$.

Compared with the linear term $-\zeta_x$, the dispersive term D is very small at $t = 3\pi/4$. This result seems natural since the wave is very flat during the run-up time, hence

$$\frac{\partial}{\partial x} \ll 1, \quad |\zeta_{xxx}| \ll |\zeta_x|. \tag{3.34}$$

But at $t = \pi/4$, i.e. the limit of run-down, the wave profile appears so much more curved that $\zeta_x \to \infty$ at $x = -1$, maximum run-down point, and $\zeta_{xxx} \to \infty$ faster than ζ_x. The dispersive effect thus becomes very important around the waterline at this time. It could be larger than the linear term $-\zeta_x$ originally retained. This result shows that dispersive effect is important in run-up, especially when wave becomes relatively short.

3.3 Numerical solution of wave run-up by the gB model

In this section, we use the gB model

$$\zeta_t + [(h+\zeta)u]_x = 0, \tag{3.35}$$

$$u_t + uu_x + \zeta_x = D = \frac{1}{3}(h+\zeta)^2 u_{xxt}, \tag{3.36}$$

to compute two-dimensional wave run-ups. Since

$$D|_{h+\zeta=0} = 0, \tag{3.37}$$

dispersive term vanishes at the waterline, we therefore have the same governing equations for waterline as that in equations (2.53 – 2.55). And we use the same scheme for numerical computation of waterline (2.83, 2.84). After waterline transformation

(2.56, 2.57), the governing equations for ζ and u in (x', t') becomes (after dropping the primes)

$$\begin{aligned} \zeta_t - c_1 U \zeta_x + c_2[(h+\zeta)u]_x &= 0, & (3.38) \\ u_t - c_1 U u_x + c_2(u u_x + \zeta_x) &= \frac{1}{3}(h+\zeta)^2 u_{xxt}, & (3.39) \end{aligned}$$

which are valid with an error of order $O(\alpha\epsilon^2, \epsilon^4)$, and where

$$c_1 = c_1(x,t) = \frac{1 + x/L}{1 + X/L}, \qquad c_2 = c_2(t) = \frac{1}{1 + X/L}, \tag{3.40}$$

are coefficients of the transformation.

The leapfrog scheme is used to perform the numerical computation

$$\zeta_i^{n+1} = \zeta_i^{n-1} + \frac{\Delta t}{\Delta x} c_1 U(\zeta_{i+1}^n - \zeta_{i-1}^n) - \frac{\Delta t}{\Delta x} c_2 \{[(h+\zeta)u]_{i+1}^n - [(h+\zeta)u]_{i-1}^n\}, \tag{3.41}$$

$$\begin{aligned} &-\frac{1}{3(\Delta x)^2} c_2^2 (h_i + \zeta_i^n)^2 u_{i-1}^{n+1} + \left[1 + \frac{2}{3(\Delta x)^2} c_2^2 (h_i + \zeta_i^n)^2\right] u_i^{n+1} \\ &-\frac{1}{3(\Delta x)^2} c_2^2 (h_i + \zeta_i^n)^2 u_{i+1}^{n+1} = u_i^{n-1} + \frac{\Delta t}{\Delta x} c_1 U(u_{i+1}^n - u_{i-1}^n) \\ &-\frac{\Delta t}{3\Delta x} c_2 (u_{i+1}^n + u_i^n + u_{i-1}^n)(u_{i+1}^n - u_{i-1}^n) - \frac{\Delta t}{\Delta x} c_2 (\zeta_{i+1}^n - \zeta_{i-1}^n) + \\ &\frac{1}{3(\Delta x)^2} c_2^2 (h_i + \zeta_i^n)^2 (u_{i+1}^{n-1} - 2u_i^{n-1} + u_{i-1}^{n-1}). \end{aligned} \tag{3.42}$$

The scheme is explicit for ζ, and is implicit for u. They are second order in space and time.

The first numerical experiment is to evaluate the propagation of a solitary wave on shallow water of uniform depth (Figure 3.4). The amplitude of the solitary wave is taken to be $a = 0.1$, scaled by the water depth, with the initial condition

$$\zeta(x, t=0) = a \operatorname{sech}^2 \sqrt{\frac{3a}{4}}(x + 24), \tag{3.43}$$

for wave elevation, and

$$u = \frac{c\zeta}{1+\zeta}, \qquad c = 1 + a/2 \tag{3.44}$$

for velocity. For the numerical computation, we take $\Delta t = 0.04$, $\Delta x = 0.05$, and use the leapfrog scheme. Figure 3.4 shows that the scheme works very well for solitary waves of permanent form. The amplitude of the solitary wave at time $t = 8.0$ is $a = 0.1001$, having increased only 0.1%, the speed of the solitary wave is $c \doteq (24 - 15.687)/8.0 = 1.039$ which is slightly smaller than the wave speed of the KdV solution, namely 1.05. The solitary wave speed for the gB model is known to be smaller than that for the KdV equation. This has been pointed out by Teng & Wu (1992). Computation here reconfirms their result.

The second numerical experiment is to compare the wave run-up predicted by the shallow water equations and the gB model, with an objective to investigate the role which the dispersive effect plays during wave run-ups. Figure 3.5 shows the run-up process of a solitary wave upon a sloping beach. Initial condition is the same as that adopted in the former experiment, except we center the solitary wave at $x = -16$, i.e.,

$$\zeta(x, t = 0) = a \operatorname{sech}^2 \sqrt{\frac{3a}{4}}(x + 16). \tag{3.45}$$

In order to deal with the dispersive term, which is a higher order derivative, we smoothen the connection point between the ocean and beach by using

$$h(x) = 1 - \frac{1}{10} \log(1 + e^{10(x/l+1)}) \tag{3.46}$$

as the depth function, where l is the beach length. We notice that

$$h(x \to \infty) = -\frac{x}{l}, \qquad h(x \to -\infty) = 1, \tag{3.47}$$

and $h(x)$ has a smooth corner about $x = -l$. We take $l = 4$ in our computation.

For the shallow water equations, the solitary wave is steepening as time goes on, and tends to have a higher run-up. But for the gB model, the solitary wave maintains its shape in the uniform depth region and has less run-up on a sloping beach than that predicted by the shallow water equation. The dispersive effect plays an important role in the evolution of solitary waves. One may notice that the wave starts to fluctuate at $t = 14.4$. We find that it will blow up at $t = 15.6$. The reason for it to blow up is the dispersive term. The wave becomes shorter around waterline at this time, while the dispersive term becomes larger and larger, somehow to become dominant in the run-up process. This is not a physical reality. Based on our assumption for the gB model, the dispersive term is always in the same order as the nonlinear term, and smaller than a single linear term. In order to make the numerical computation convergent, we multiply the following factor

$$f(x) = \tanh^4(10\ x/l) \tag{3.48}$$

to the dispersive term, where x is the new coordinate after waterline transformation. This factor is almost 1 when $x < -l$, i.e., in the ocean. The factor is 0.95 at $x = l/4$ (Figure 3.6). It suppresses the dispersive effect only near the region very close to waterline.

Figure 3.7 shows the run-up of the solitary wave predicted by the gB model without and with the suppression factor. We see that at $t = 15.6$ the wave does not blow up if we include the suppressing factor. In the following computation, we will always include the factor as understood.

Figure 3.8 shows the wave elevation during run-up at time $t = 13.04$, 14.64, 16.24, 17.84, 19.44. The solitary wave reaches the maximum run-up $R = 0.3400$ at time $t = 19.44$. Figure 3.9 shows the velocity during run-up at the same time instants as listed in figure 3.8. The maximum speed during this run-up is as high as 0.2697, which occurs at the waterline at $t = 15.88$.

Figure 3.10 shows the wave elevation during the backwash at time $t = 19.44$, 21.04, 22.64, 24.24, and figure 3.11 shows the velocity during the backwash at the same time

Table 3.1: Run-up of a solitary wave of amplitude $a/h = 0.1$, predicted by linear theory, the shallow water equations and the gB model, with the solitary wave centered at $x = -16$ initially (see equation 3.45), running up from an ocean of depth $h = 1$ to a plane beach of slope $\alpha = 1/4$.

Models	Maximum run-up R	Time to reach maximum run-up
Linear theory	0.3366	18.76
Shallow water equation	0.3816	18.20
gB model	0.3400	19.44

instants as listed in figure 3.10. The maximum speed reached during backwash is as high as 0.6972, which occurs at the waterline at $t = 24.40$.

For a solitary wave of amplitude $a = 0.1$, initially centered at $x = -16$, the maximum run-ups on a plane beach with slope 0.25, predicted by the linear theory, the shallow water equation and the gB model, are in table 3.1.

The results show that both nonlinear and dispersive effects are important during the wave run-up. Figure 3.12 shows the comparison of wave run-up predicted by the three models. Figure 3.13 shows both the results of linear theory and the gB model on run-up of a solitary wave of amplitude $a = 0.1$ on plane beaches with different slopes α, $1/\alpha = l$.

We have carried out a few more numerical experiments on the cases which have appeared in publication, and made comparison between these results. For more comparison, see Appendix A.

3.4 Run-up of solitary wave on arbitrary beaches

Here, the first experiment is to calculate the run-up of a solitary wave of amplitude $a = 0.1$, initially centered at $x = -16$, on a beach with following geometry

$$h(x) = 1 - 0.1 \log(1.0 + e^{10(1+x/l+0.3\sin^2(\pi x/l))}). \tag{3.49}$$

Table 3.2: Comparison between numerical results of the present scheme and other's results. HH: Heitner & Housner (1970); KKL: Kim et al. (1983); PG: Pedersen & Gjevik (1983). The laboratory experiments column shows results derived from the interpolation of Hall & Watts (1953) data set, when possible.

Source	Beach length l	a	Other's results	Results by present scheme	Laboratory experiments
HH	10	0.05	0.180	0.2428	na
KLL	3.732	0.05	0.135	0.1783	0.173
KLL	3.732	0.1	0.308	0.3408	0.281
KLL	3.732	0.2	0.766	0.7502	0.599
HH	3.333	0.1	0.310	0.3245	na
PG	2.747	0.098	0.275	0.2866	0.252
PG	2.747	0.193	0.599	0.6441	0.552
PG	2.747	0.294	0.958	1.0309	0.898
KLL	1.0	0.2	0.504	0.4991	0.454
KLL	1.0	0.480	1.610	1.2909	1.270

The corresponding run-up and run-down results are shown in figures 3.14 and 3.15. The maximum run-up $R = 0.3408$ occurs at time $t = 17.84$.

The second experiment is on the run-up of a solitary wave of amplitude $a = 0.1$, initially centered at $x = -16$, on a beach with following depth variation

$$h(x) = 1 - 0.1 \log(1.0 + e^{10(1+x/l-0.3\sin^2(\pi x/l))}). \tag{3.50}$$

The run-up results are shown in figure 3.16. The maximum run-up $R = 0.3735$ occurs at time $t = 19.84$.

The third experiment is on the run-up of a solitary wave of amplitude $a = 0.1$, initially centered at $x = -16$, on a step beach given by

$$h(x) = \begin{cases} 1 - 0.1 \log(1.0 + e^{10(1+x/l)}) & x < 0, \\ -0.1 \tanh(10x/l) & x > 0. \end{cases} \tag{3.51}$$

The resultant wave elevations during the wave run-up are shown in figure 3.17.

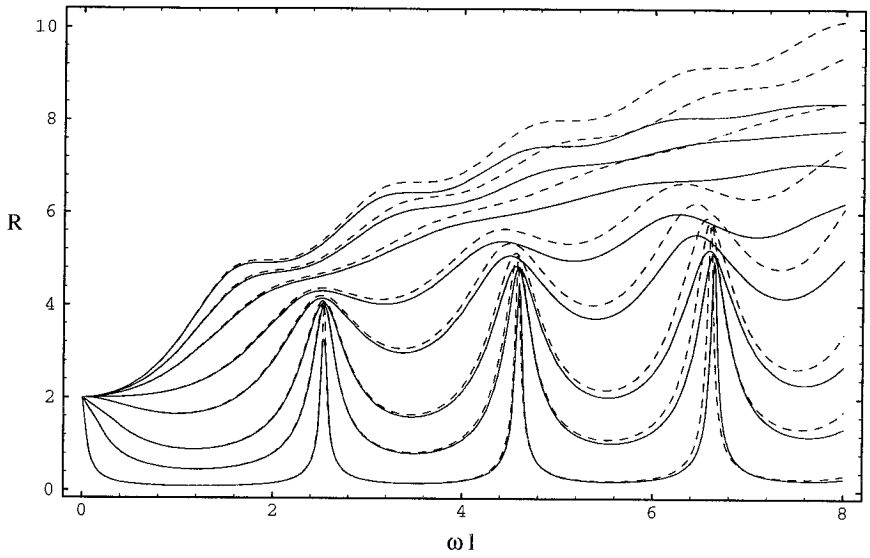

Figure 3.1: Variation of the run-up function, $R(\omega, l, \beta)$, versus ωl for waves incident upon a plane beach $h(x) = x/l$, $l = 10$ for a set of different incidence angles, β= 0°, 30°, 45°, 60°, 70°, 80°, 85°, 89°, from the top to the bottom. —— linear dispersive model, - - - linear nondispersive model.

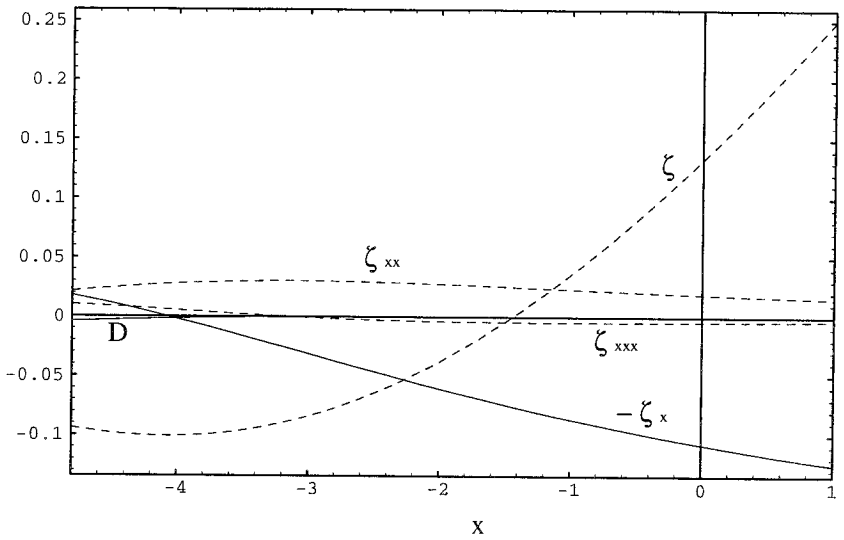

Figure 3.2: Wave elevation ζ, its derivatives $-\zeta_x$, ζ_{xx}, ζ_{xxx} and the value of dispersive term $D = -\frac{1}{3}(h+\zeta)^2\zeta_{xxx}$ of Carrier - Greenspan exact solution at the maximum run-up time $t = 3\pi/4$ for $A = 1.0,\ l = 4$.

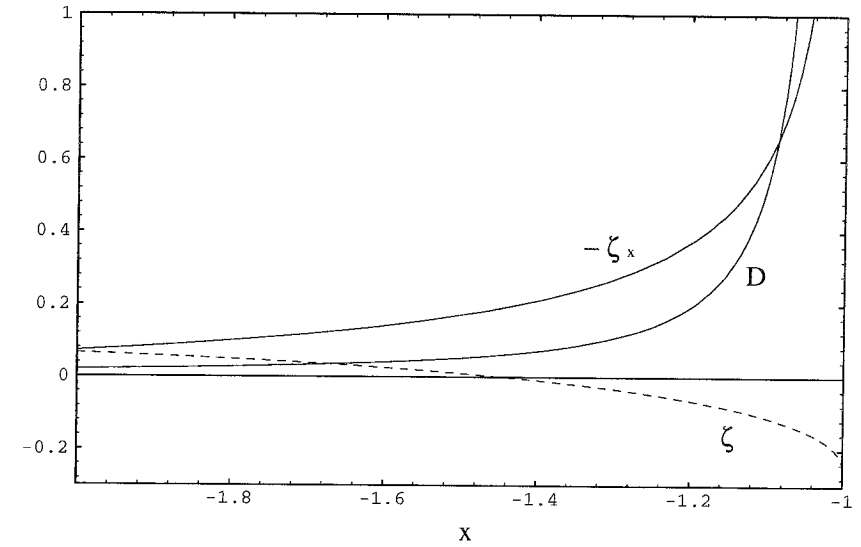

Figure 3.3: Wave elevation ζ, its derivatives $-\zeta_x$ and the value of dispersive term $D = -\frac{1}{3}(h+\zeta)^2\zeta_{xxx}$ of Carrier - Greenspan exact solution at the maximum run-down time $t = \pi/4$ for $A = 1.0,\ l = 4$.

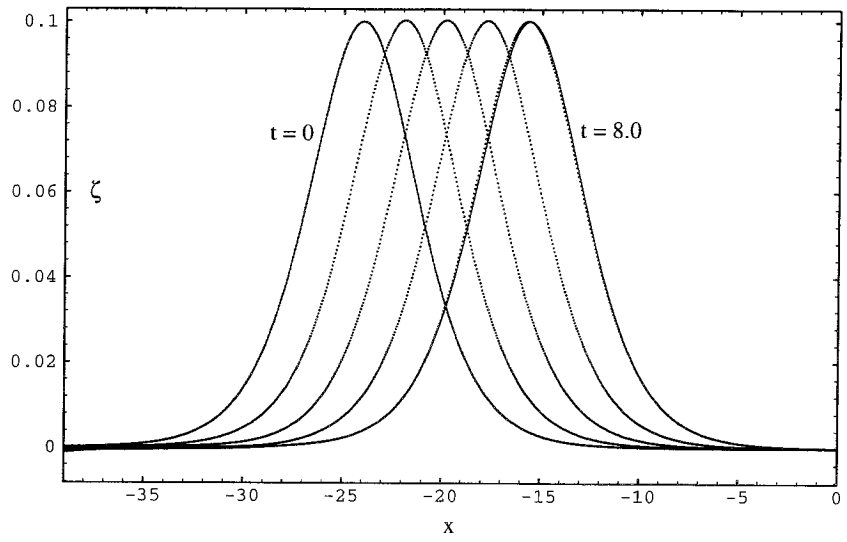

Figure 3.4: Propagation of a solitary wave with amplitude $a = 0.1$ on shallow water $h = 1$, —— exact solution of KdV equation, ... numerical solution by present scheme, $\Delta x = 0.05$, $\Delta t = 0.04$.

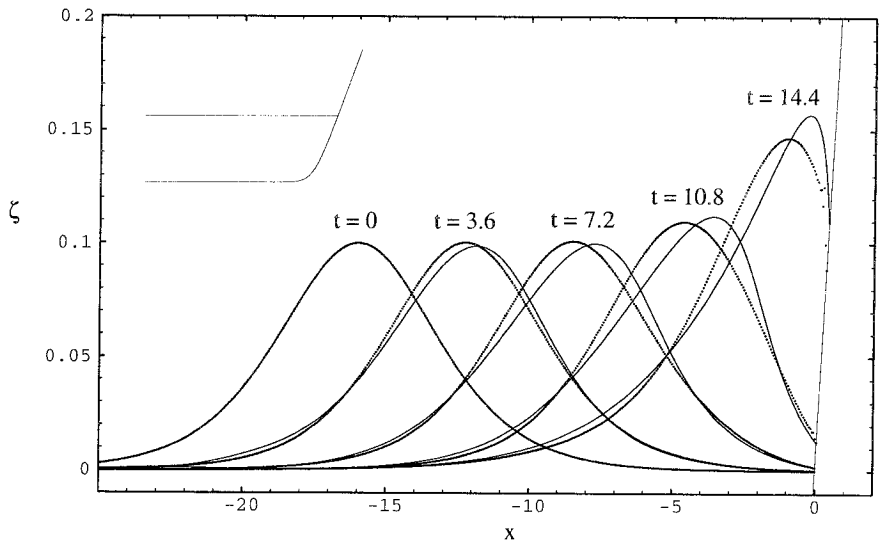

Figure 3.5: Comparison between run-up of a solitary wave predicted by shallow water equations and that predicted by gB model, —— shallow water equation, ... gB model, $\Delta x = 0.05$, $\Delta t = 0.04$.

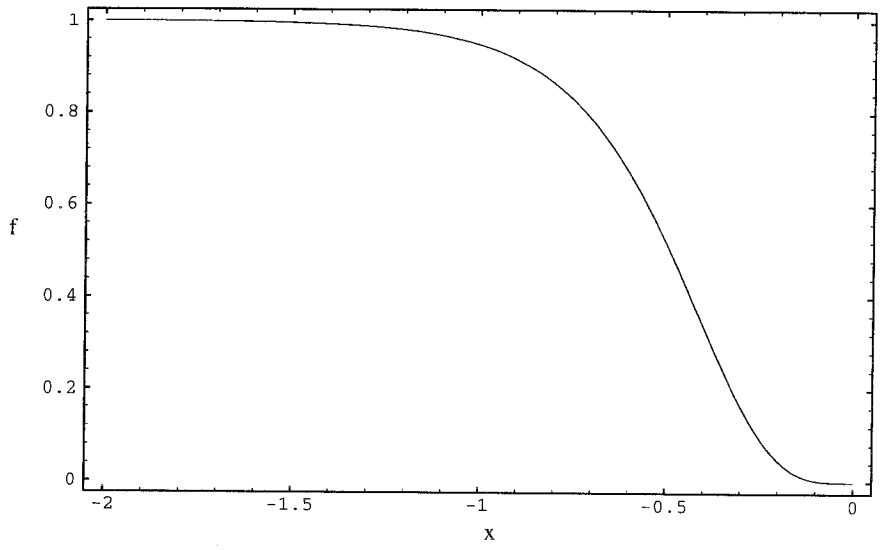

Figure 3.6: Dispersion suppressing factor $f(x)$, for $l = 4$.

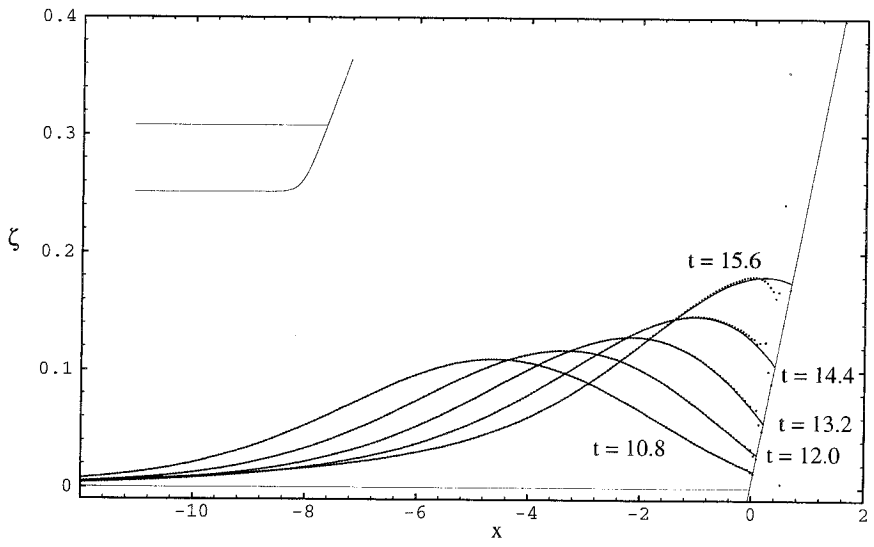

Figure 3.7: Run-up predicted by gB model, —— with dispersion suppressing factor, ... without the factor.

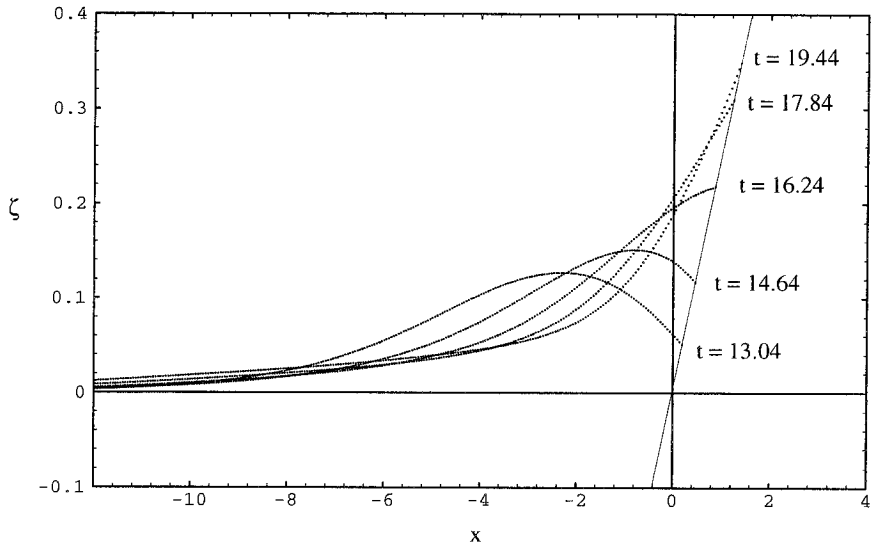

Figure 3.8: Wave elevation of run-up predicted by gB model, maximum run-up is 0.3400, appears at $t = 19.44$.

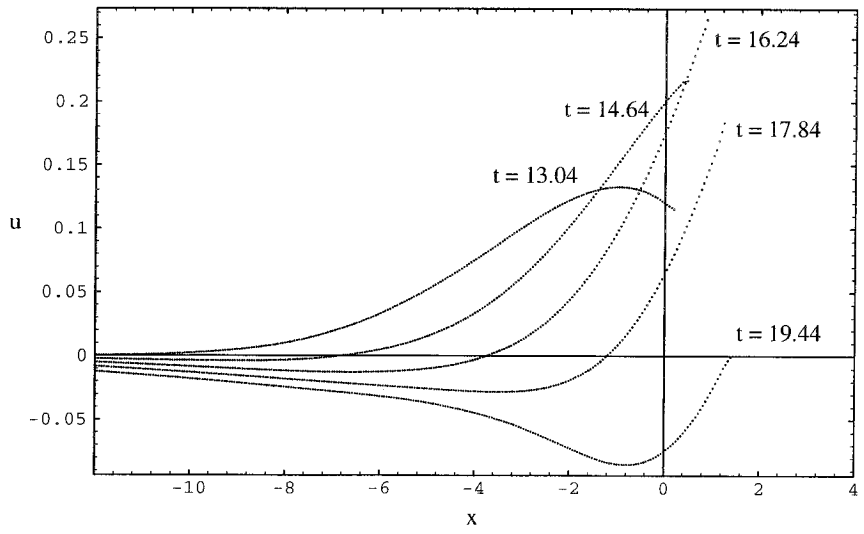

Figure 3.9: Velocity of run-up predicted by gB model.

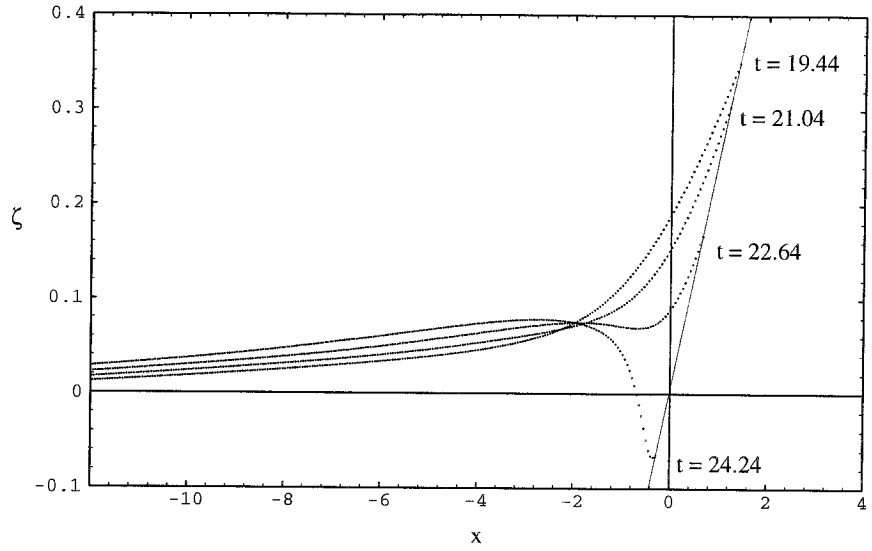

Figure 3.10: Wave elevation of run-down predicted by gB model.

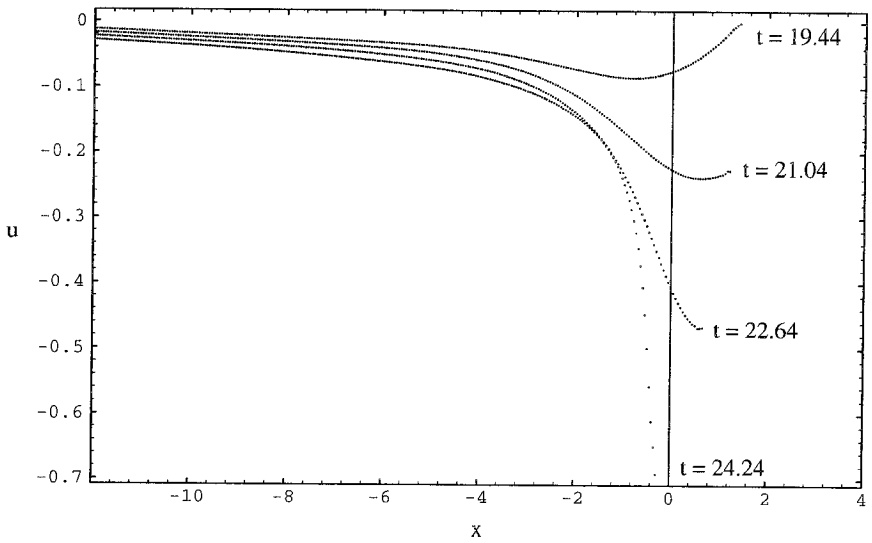

Figure 3.11: Velocity of run-down predicted by gB model.

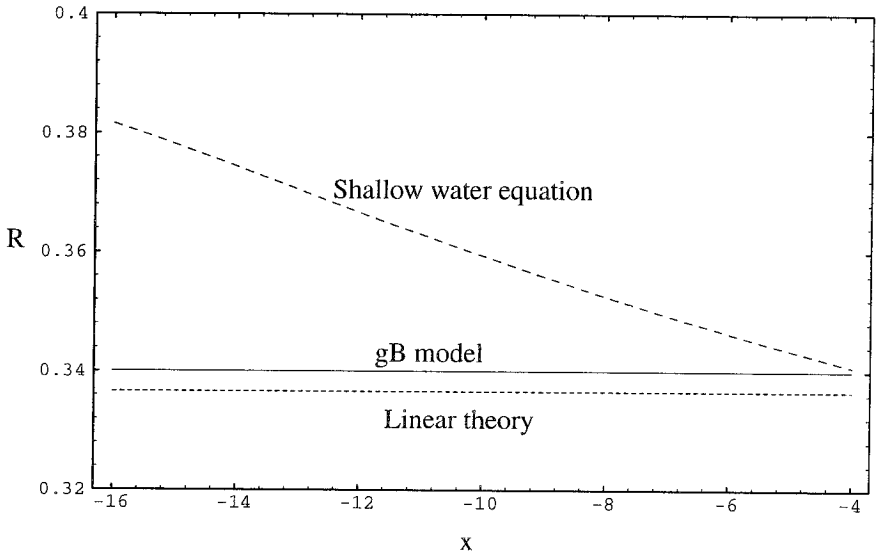

Figure 3.12: Run-up of a solitary wave with $a = 0.1$, centered at different places x, on a plane beach of slope 0.25.

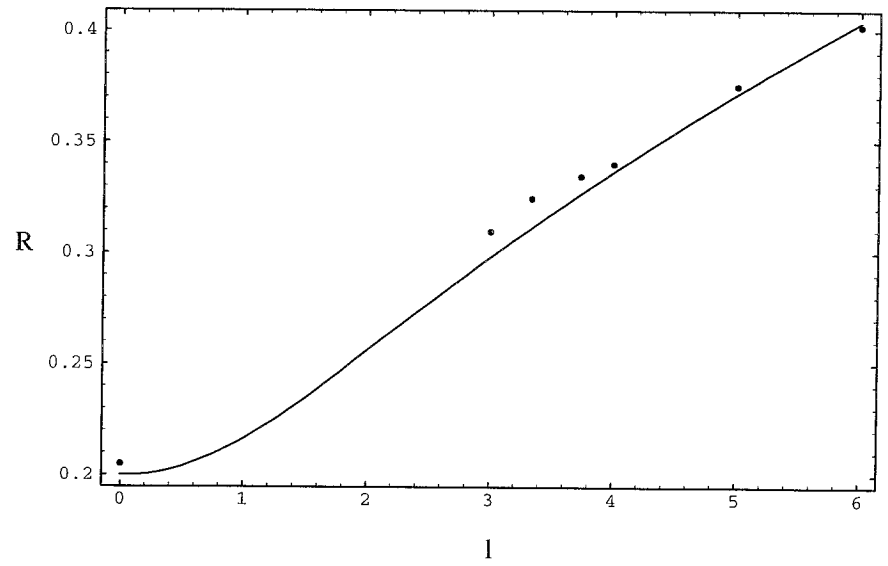

Figure 3.13: Run-up of a solitary wave with amplitude $a = 0.1$ on plane beaches with different slopes α, $1/\alpha = l$, —— linear theory, ... gB model with present scheme.

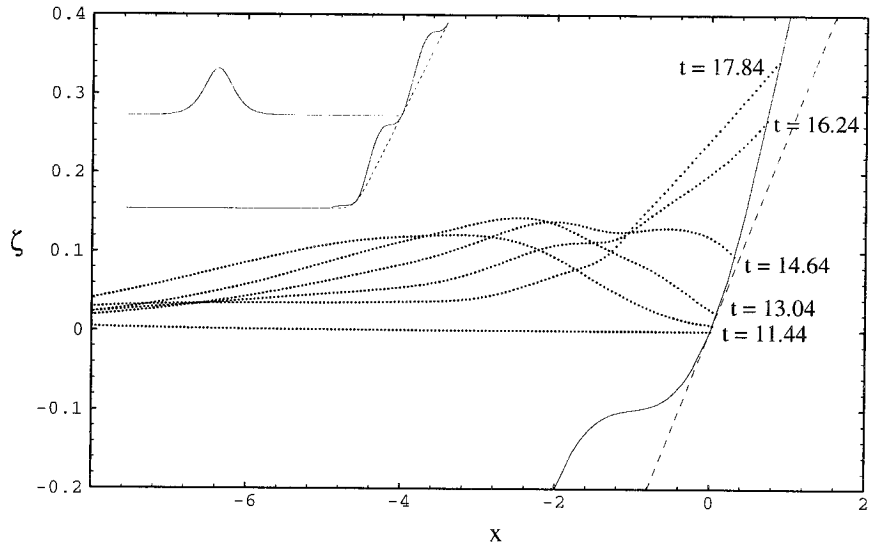

Figure 3.14: Run-up of a solitary wave with $a = 0.1$ on an arbitrary beach $h(x) = 1 - 0.1\log(1.0 + e^{10(1+x/l+0.3\sin^2(\pi x/l))})$, predicted by gB model with present scheme, maximum run-up $R = 0.3408$ appears at $t = 17.84$.

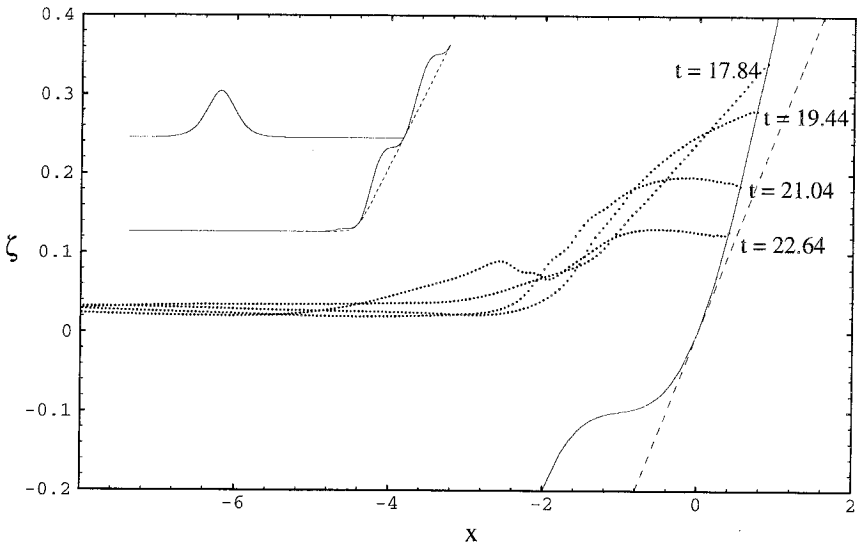

Figure 3.15: Run-down of a solitary wave with $a = 0.1$ on an arbitrary beach $h(x) = 1 - 0.1\log(1.0 + e^{10(1+x/l+0.3\sin^2(\pi x/l))})$, predicted by gB model with present scheme.

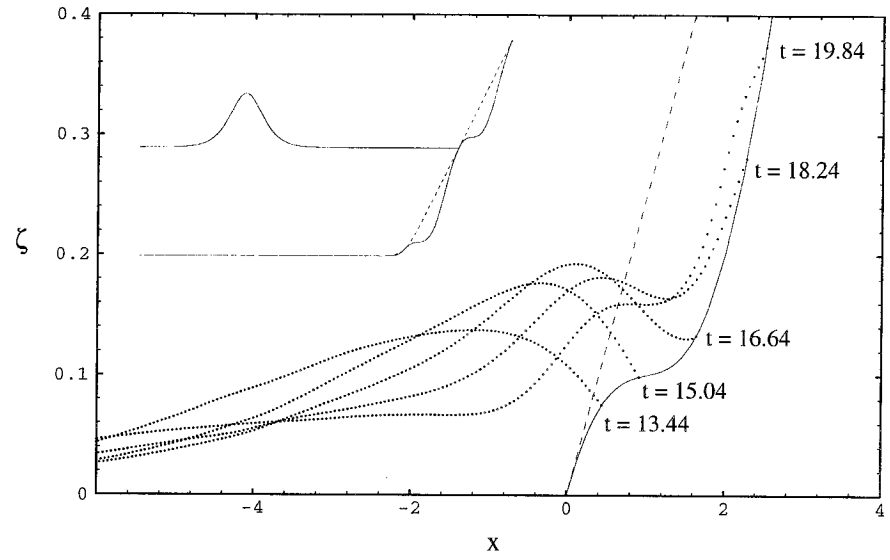

Figure 3.16: Run-up of a solitary wave with $a = 0.1$ on an arbitrary beach $h(x) = 1 - 0.1\log(1.0 + e^{10(1+x/l-0.3\sin^2(\pi x/l))})$, predicted by gB model with present scheme, maximum run-up $R = 0.3735$ appears at $t = 19.84$.

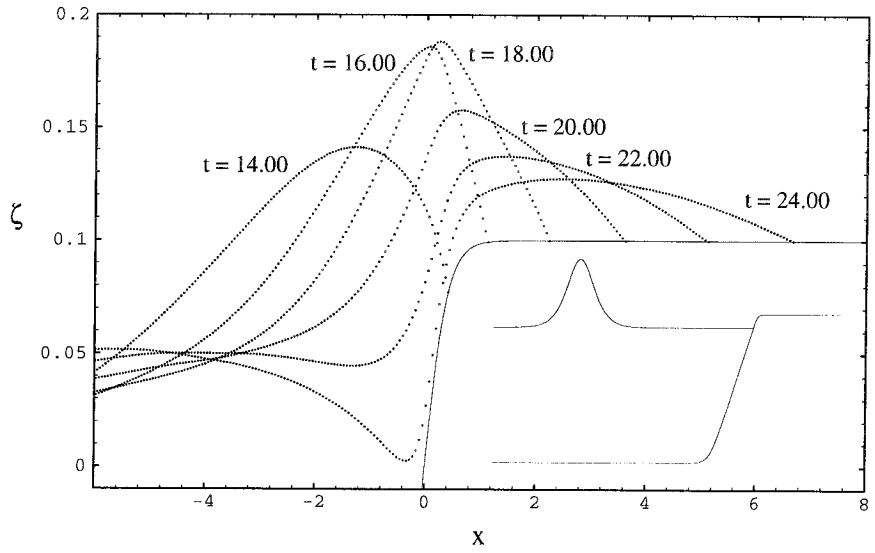

Figure 3.17: Run-up of a solitary wave with $a = 0.1$ on a step beach, predicted by gB model with present scheme.

Chapter 4 Three-dimensional run-up

In Chapter 2 and Chapter 3, we have studied the nonlinear and dispersive effects during normal run-up, or two-dimensional run-up, of ocean waves on beaches. The present treatment of the moving waterline, which we have developed in Chapter 2, is shown to have a very high accuracy by comparison with some exact solutions of the nonlinear shallow water equations.

In this chapter, we shall extend previous scheme for normal run-up to oblique run-up, or three-dimensional run-up. We will study three-dimensional run-ups by using the shallow water equations.

4.1 The governing equations

The shallow water equations for three-dimensional run-up reads

$$\zeta_t + [(h+\zeta)u]_x + [(h+\zeta)v]_y = 0, \tag{4.1}$$

$$u_t + uu_x + vu_y + \zeta_x = 0, \tag{4.2}$$

$$v_t + uv_x + vv_y + \zeta_y = 0. \tag{4.3}$$

Here we have three unknowns, ζ, u and v, and three equations. The system is closed.

The governing equations for waterline are

$$h(X,Y) + \zeta(X,Y,t) = 0, \tag{4.4}$$

$$\frac{dX}{dt} = u(X,Y,t), \tag{4.5}$$

$$\frac{dY}{dt} = v(X,Y,t), \tag{4.6}$$

$$\frac{du}{dt} = -\zeta_x, \tag{4.7}$$

$$\frac{dv}{dt} = -\zeta_y, \tag{4.8}$$

where the first one is the geometrical equation, the second and third are kinematical equations, and the last two are dynamical equations for the waterline. ζ_x and ζ_y can be determined by information inside the flow domain. From these five equations, we can numerically solve the trajectory of waterline $X = X(t)$, $Y = Y(t)$, and the wave elevation at the waterline $\zeta(X, Y, t)$.

Since the domain is changing with time, it is not easy to apply the finite difference scheme to compute the problem for the points inside the domain. To overcome the difficulty, we introduce the waterline transformation

$$x = (1 - X/L)x' + X, \tag{4.9}$$

$$y = y', \tag{4.10}$$

$$t = t', \tag{4.11}$$

where $X = X(y, t)$ is the waterline at time t, and L is the computation domain. This transformation transfers waterline to a fixed boundary $x' = 0$, and keeps the other boundary unchanged at $x' = x = L$. The partial derivatives in the two systems have the following relations:

$$\frac{\partial}{\partial x} = \frac{1}{1 - X/L}\frac{\partial}{\partial x'}, \tag{4.12}$$

$$\frac{\partial}{\partial y} = \frac{\partial}{\partial y'} + \frac{\partial x'}{\partial y}\frac{\partial}{\partial x'} = \frac{\partial}{\partial y'} - \frac{1 - x'/L}{1 - X/L}\frac{\partial X}{\partial y}\frac{\partial}{\partial x'}, \tag{4.13}$$

$$\frac{\partial}{\partial t} = \frac{\partial}{\partial t'} + \frac{\partial x'}{\partial t}\frac{\partial}{\partial x'} = \frac{\partial}{\partial t'} - \frac{1 - x'/L}{1 - X/L}\frac{\partial X}{\partial t}\frac{\partial}{\partial x'}. \tag{4.14}$$

The shallow water equations in (x', y', t') coordinates are as follows (dropping the primes):

$$\zeta_t - c_1 U\zeta_x + c_2[(h + \zeta)u]_x + [(h + \zeta)v]_y - c_1 A[(h + \zeta)v]_x = 0, \tag{4.15}$$

$$u_t - c_1 U u_x + c_2(uu_x + \zeta_x) + vu_y - c_1 Avu_x = 0, \tag{4.16}$$

$$v_t - c_1 U v_x + c_2 uv_x + vv_y + \zeta_y - c_1 A(vv_x + \zeta_x) = 0, \tag{4.17}$$

where $c_1 = (1 - x/L)/(1 - X/L)$, $c_2 = 1/(1 - X/L)$, and $U = \partial X/\partial t$ is the x-component of the waterline speed, and $A = \partial X/\partial y$ is the inverse of the local slope of the waterline. In the (x', y', t') coordinates, the computation domain is always a fixed rectangle.

4.2 Numerical experiments

We compute the propagation of a solitary wave in a channel of uniform or variable depth, and obliquely interacting with a vertical wall. Figure 4.1 shows the bottom topography and the oblique end wall of the channel. In this numerical experiment, the waterline is fixed with time, and X is only a function of y, i.e., $X = X(y)$. Then we do not have to solve the waterline equations.

We use MacCormack's scheme (4.19, 4.20) to do the numerical computation. For a model equation of the form

$$u_t + f_x(u) + g_y(u) = 0, \tag{4.18}$$

we have the following scheme

$$u^*_{i,j} = u^n_{i,j} - \frac{\Delta t}{\Delta x}[f(u^n_{i+1,j}) - f(u^n_{i,j})] - \frac{\Delta t}{\Delta y}[g(u^n_{i,j+1}) - g(u^n_{i,j})], \tag{4.19}$$

$$u^{n+1}_{i,j} = \frac{1}{2}(u^n_{i,j} + u^*_{i,j}) - \frac{\Delta t}{2\Delta x}[f(u^*_{i,j}) - f(u^*_{i-1,j})] - \frac{\Delta t}{2\Delta y}[g(u^*_{i,j}) - g(u^*_{i,j-1})]. \tag{4.20}$$

Following the same idea, we can construct the scheme for equations (4.15 – 4.17).

For the boundary conditions, we prescribe an incoming wave at the open boundary, i.e., the right-hand side of the region of computation in our figures. For the two side walls of the channel, we use

$$v = 0, \qquad \frac{\partial u}{\partial y} = 0, \qquad \frac{\partial \zeta}{\partial y} = 0. \tag{4.21}$$

For the oblique end wall boundary, we invoke

$$u_n = 0, \qquad \frac{\partial u_\tau}{\partial n} = 0, \qquad \frac{\partial \zeta}{\partial n} = 0, \tag{4.22}$$

where τ is the tangential direction along the end wall.

4.2.1 In a channel with uniform depth

We numerically study the wave propagation in a channel with unform depth, i.e.,

$$h(x, y) = 1. \tag{4.23}$$

Our computation domain is a trapezoidal one:

$$0 \leq y \leq 10, \quad 0.5y \leq x \leq 20. \tag{4.24}$$

The wave is located at $x = 10$ initially,

$$\zeta(x, t = 0) = 0.1 \text{ sech}^2(\sqrt{0.3}(x - 10)), \tag{4.25}$$

$$u(x, t = 0) = -0.1 \text{ sech}^2(\sqrt{0.3}(x - 10)), \tag{4.26}$$

$$v(x, t = 0) = 0. \tag{4.27}$$

The wave will propagate from the right to the left.

The evolution of the "solitary wave" is shown in figures 4.2 – 4.7 for $t = 0$, 5, 7.5, 10, 12.5, 15. Three-dimensional feature is very obvious in these figures. The reflected waves will have two different fronts, of which one is the reflected wave from the oblique end wall, the other one is the reflected wave from the side wall, i.e., $y = 0$ in our figures.

4.2.2 In a channel with variable depth

We numerically study the problem of wave propagation in a channel with variable depth,

$$h(x,y) = \begin{cases} 0.5 + 0.1(x - 0.5y) & 0.5y \le x < 5 + 0.5y,\ 0 \le y \le 10 \\ 1 & 5 + 0.5y \le x \le 20,\ 0 \le y \le 10 \end{cases} . \qquad (4.28)$$

We take the same initial condition as in (4.25 – 4.27). The evolution of the "solitary wave" is shown in figures 4.8 – 4.13 for $t = 0,\ 5,\ 7.5,\ 10,\ 12.5,\ 15$. The "solitary wave" now travels slower than that in the former case, because in this case the water is shallower, and consequently the wave velocity is smaller near the end wall.

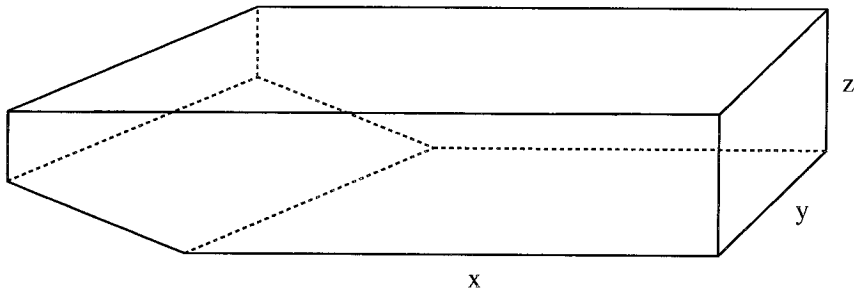

Figure 4.1: Bottom topography and the oblique end wall of the channel.

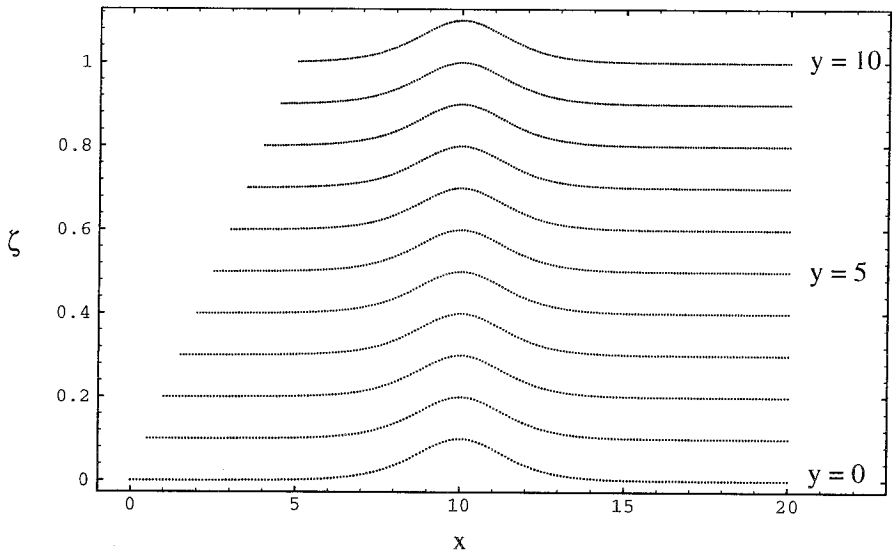

Figure 4.2: Variation of the wave elevation ζ with x and y at $t = 0$; figures 4.2 – 4.7 are for wave propagation in a channel with uniform depth, $h = 1$.

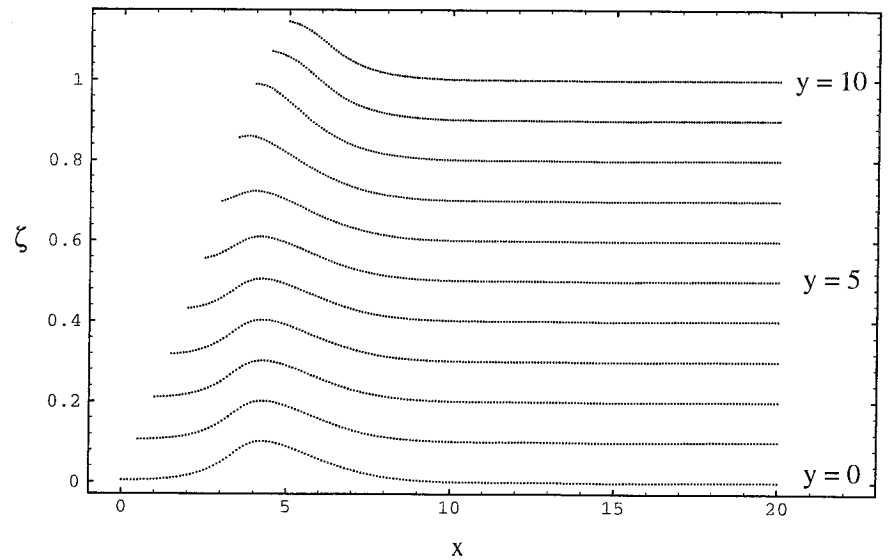

Figure 4.3: Variation of the wave elevation with x and y at $t = 5$.

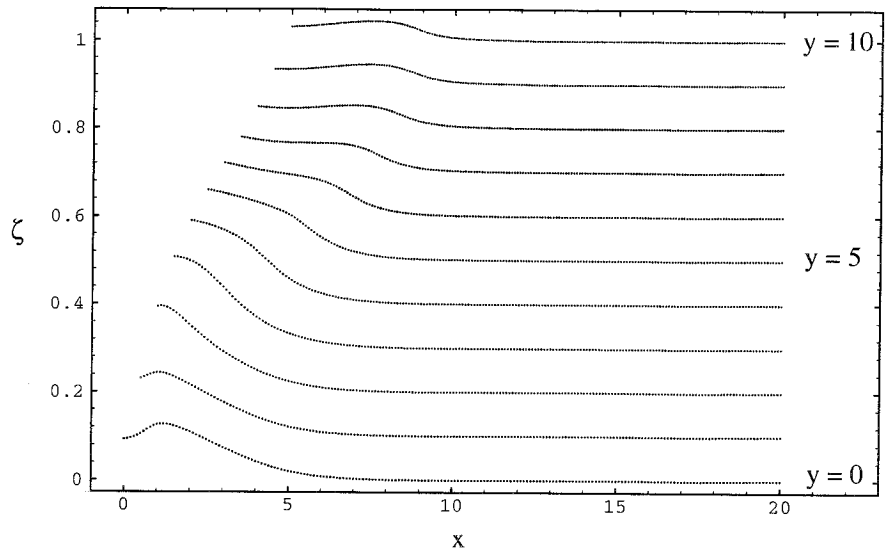

Figure 4.4: Variation of the wave elevation with x and y at $t = 7.5$.

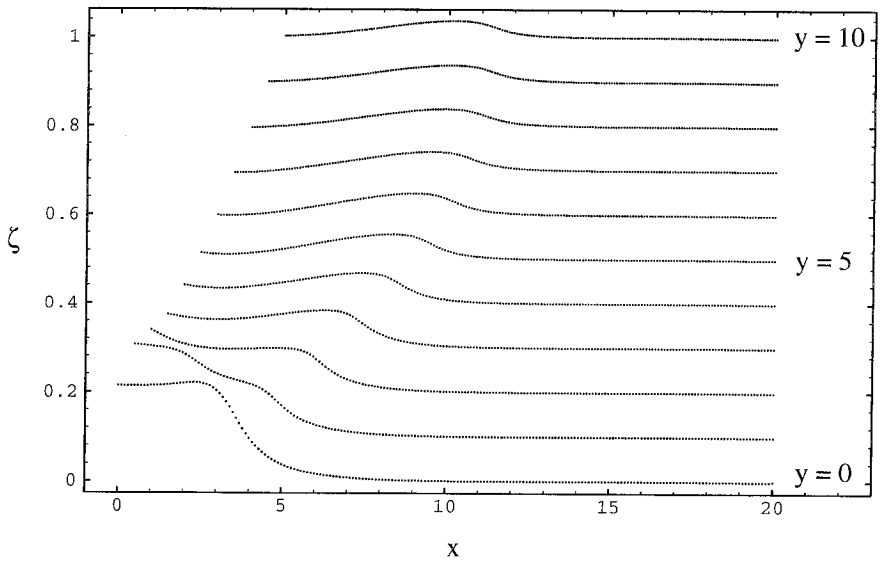

Figure 4.5: Variation of the wave elevation with x and y at $t = 10$.

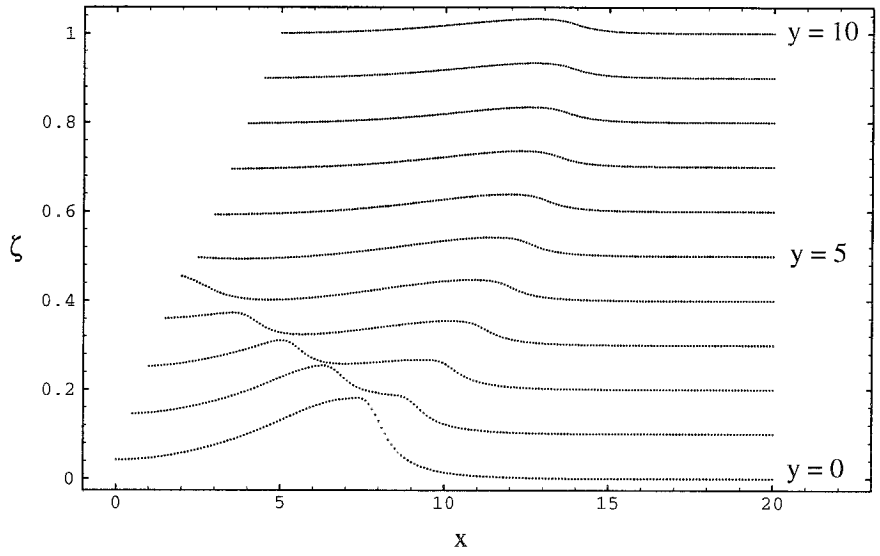

Figure 4.6: Variation of the wave elevation with x and y at $t = 12.5$.

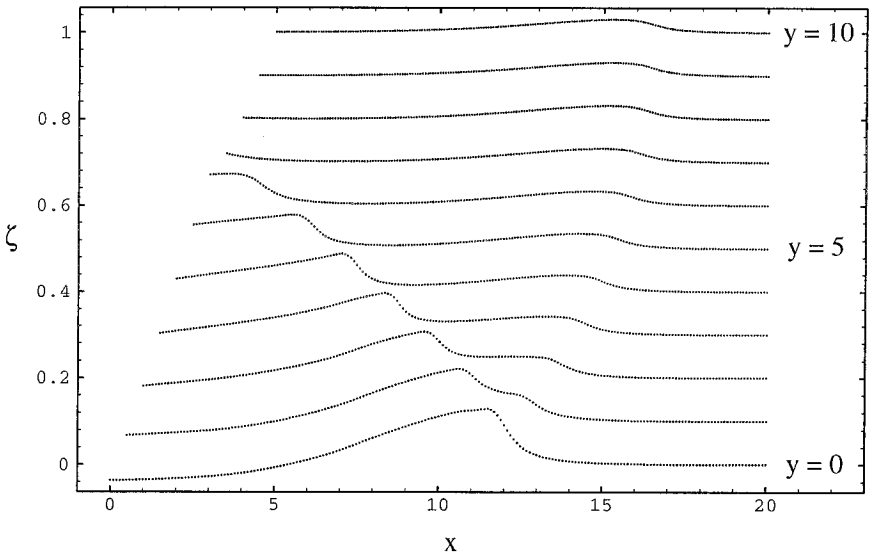

Figure 4.7: Variation of the wave elevation with x and y at $t = 15$.

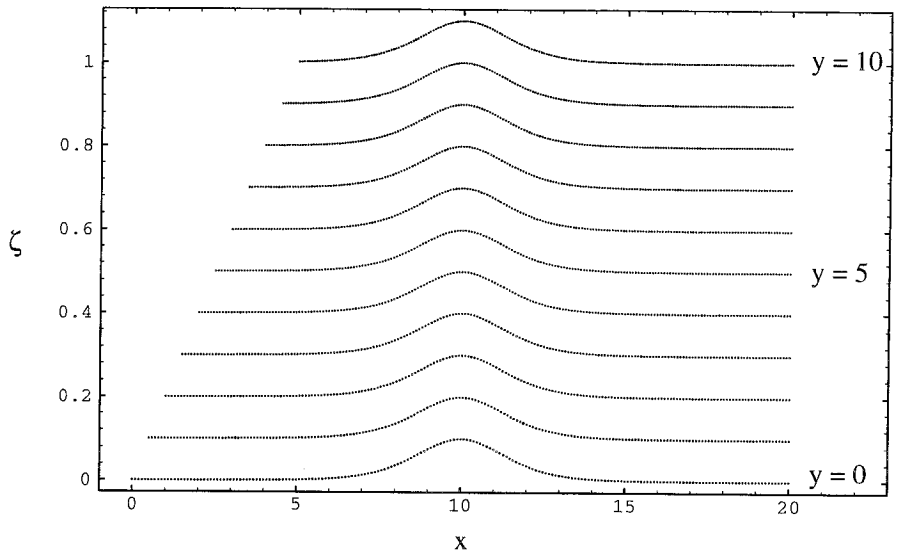

Figure 4.8: Variation of the wave elevation ζ with x and y at $t = 0$; figures 4.8 – 4.13 are for wave propagation in a channel with variable depth, given by (4.28).

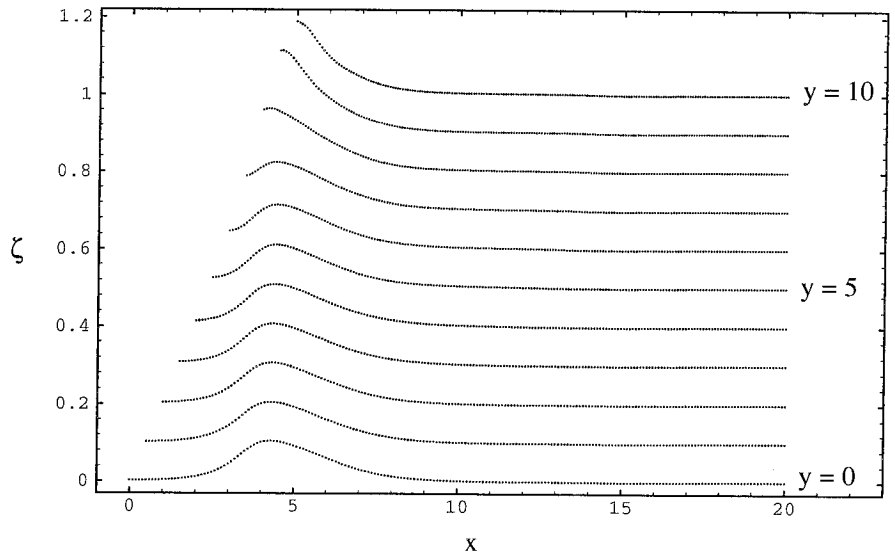

Figure 4.9: Variation of the wave elevation with x and y at $t = 5$.

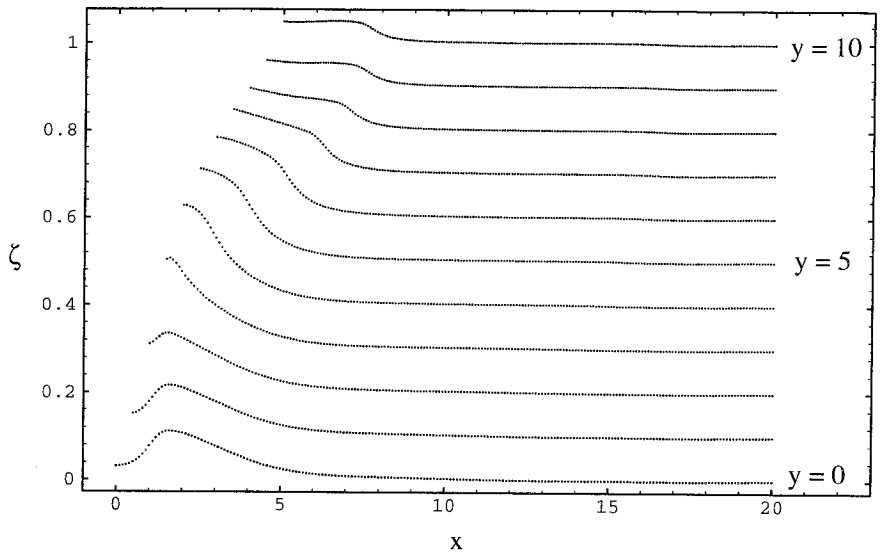

Figure 4.10: Variation of the wave elevation with x and y at $t = 7.5$.

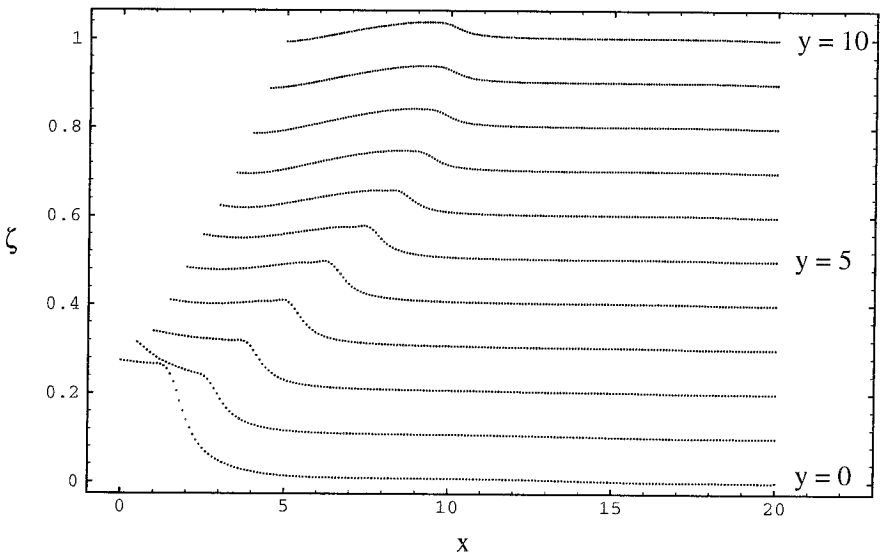

Figure 4.11: Variation of the wave elevation with x and y at $t = 10$.

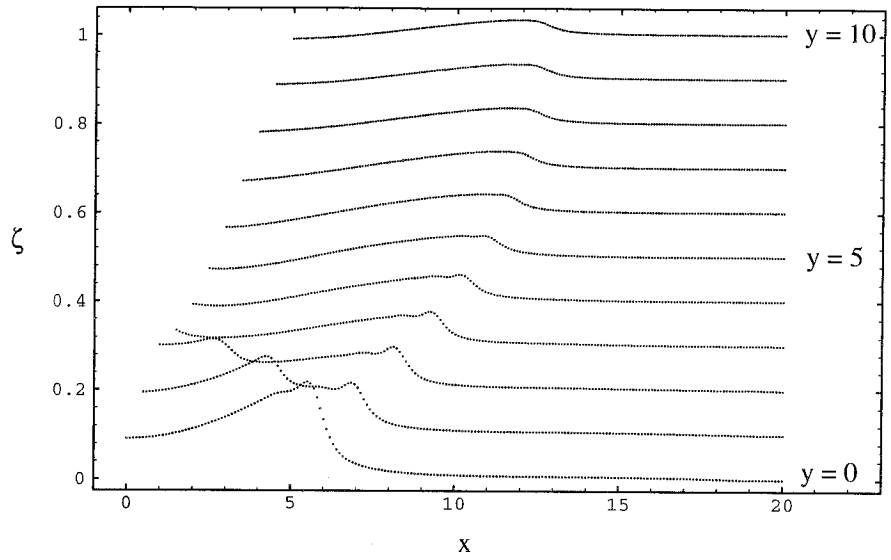

Figure 4.12: Variation of the wave elevation with x and y at $t = 12.5$.

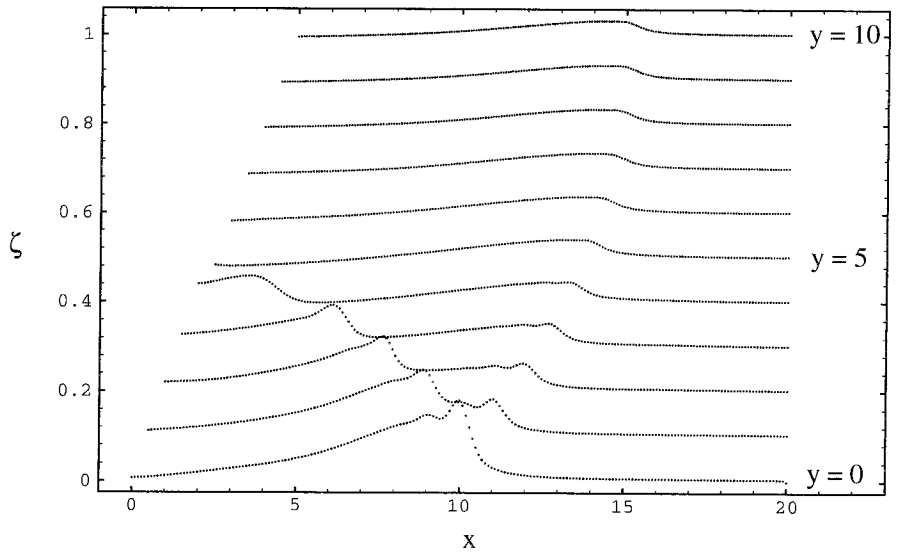

Figure 4.13: Variation of the wave elevation with x and y at $t = 15$.

Chapter 5 Conclusion

5.1 The conclusions from the first four chapters

In summary of the first four Chapters, we may draw the following conclusions:

1. A linear long-wave theory for three-dimensional run-up has been developed in Chapter 1. By using this theory, we can evaluate oblique run-ups of ocean waves, such as sinusoidal waves, solitary waves or other kinds of waves, on a uniform beach with variable downward slope. In general, an oblique run-up is smaller than normal run-up for the same incident wave. Interesting things happen for the grazing incident waves, for which case the prevailing eigenmodes dominate the phenomenon. Nonlinear effects will become very important for grazing incidence. We need more study for this case. We have also developed a theory to evaluate the longshore current induced by obliquely incident nonbreaking waves on beaches. The theory shows that the maximum longshore current appears at the waterline, which is different from the results for longshore current induced by breaking waves (Longuet-Higgins 1970).

2. The exact governing equations for determining a moving inviscid waterline have been ascertained in Chapter 2 based on the local Lagrangian coordinates. A special numerical scheme has been developed for efficient evaluation of these governing equations. The scheme is shown to have a very high accuracy by comparison with some exact solutions of the shallow water equations. The maximum run-up of a solitary wave predicted by the shallow water equations depends on the initial location of the solitary wave and is not unique in value because the wave becomes increasingly more steepened given longer time to travel in the absence of the dispersive effects; it is in general larger than that predicted by the linear long-wave theory in Chapter 1. The farther the initial solitary wave of the KdV form is imposed from the beach, the larger the maximum run-up it will reach. This result disagrees with Synolakis's result, claiming that "the maximum run-up predicted by the linear theory is *identical*

with the maximum run-up predicted by the nonlinear theory" (Synolakis 1987).

3. The dispersive effects are also very important in two-dimensional run-ups in its role of keeping the nonlinear effects balanced at equilibrium, so that the run-ups predicted by the generalized Boussinesq model (Wu 1979) always yield unique values for run-up of a given initial solitary wave, regardless of its initial position. The result for the gB model is slightly larger than wave run-up predicted by linear long-wave theory. The dispersive effects tend to reduce the wave run-up either for linear system or for nonlinear system. This disagrees with Carrier's result, cited by Liu, Synolakis & Yeh (1991), claiming that "For a typical tsunami, G. F. Carrier showed that frequency dispersion is important in the propagation from the source to the coastline, but *unimportant* in the evolution of the leading wave on a sloping beach."

4. A three-dimensional process of wave run-up upon a vertical wall is shown in Chapter 4.

5.2 Further research problems

The following problems are of interest for further research:

1. Numerical study of three-dimensional run-up on non-uniform beaches predicted by the generalized Boussinesq model (Wu 1979). Study of nonlinear and dispersive effects in three-dimensional run-ups.

2. Three-dimensional run-up of grazing incident ocean waves upon a beach. It is a Mach reflection for grazing incident ocean waves upon a vertical wall that was found by Miles (1977). What will it happen for grazing incident ocean waves on a sloping beach?

3. The eigenmode of edge wave predicted by the generalized Boussinesq model. We have predicted the eigenmodes by linear long-wave model in Chapter 1. How do the nonlinear and dispersive effects modify these eigenmodes?

4. The importance of nonlinear dispersion during the wave run-up. To study this problem one needs a higher order nonlinear dispersive wave model (Wu & Zhang

1996).

5. The idea of the treatment of the waterline can be extended to compute the run-up of internal waves on a sea bed (Lin 1996).

Bibliography

[1] Abramowitz, M. & Stegun, L. A. (eds.) 1964 *Handbook of Mathematical Functions.* Nat. Bureau of Standards.

[2] Carrier, G. F. 1966 Gravity waves on water of variable depth. *J. Fluid Mech.* **24**, 641-659.

[3] Carrier, G. F. & Greenspan, H. P. 1958 Water waves of finite amplitude on a sloping beach. *J. Fluid Mech.* **4**, 97-109.

[4] Carrier, G. F. & Noiseux, C. F. 1982 The reflection of obliquely incident tsunamis. *J. Fluid Mech.* **133**, 147-160.

[5] Eckart, C. 1951 Surface waves in water of variable depth. Marine Physical Lab. of Scripps Inst. Ocean. Wave Report 100-99.

[6] Galvin, C. J., Jr., 1967 Longshore current velocity: A review of theory and data. *Reviews of Geophys.*, **5** (3), 287-304.

[7] Hall, J. V. & Watts, J. W. 1953 Laboratory investigation of the vertical rise of solitary waves on impermeable slopes. *Tech. Memo.* 33, Beach Erosion Board, US Army Corps of Engineers. 14pp.

[8] Heitner, K. L. & Housner, G. W. 1970 Numerical model for tsunami run-up. *Proc. ASCE* **WW3**, 701-719.

[9] Hibberd, S. & Peregrine, D. H. 1978 Surf and run-up on a beach: a uniform bore. *J. Fluid Mech.* **95**, 323-345.

[10] Keller, J. B. 1961 Tsunami — water waves produced by earthquake. In *Proc. Tsunami Meetings 10th Pacific Science Congress*, (ed. D. C. Cox) IUGG Monograph, **24** 154-166.

[11] Kim, S. K., Liu, P. L.-F. & Ligget, J.A. 1983 Boundary integral equation solutions for solitary wave generation, propagation and run-up. *Coastal Engng.* **7**, 299-317.

[12] Lin, Duo-min 1996 *Run-up and nonlinear propagation of oceanic internal waves and their interactions.* Ph.D. thesis, California Institute of Technology.

[13] Liu, P. L.-F., Synolakis, C. & Yeh, H. H. 1991 Report on the international workshop on long-wave run-up. *J. Fluid Mech.* **229**, 675-688.

[14] Longuet-Higgins, M. S. & Stewart, R. W. 1962 Radiation stress and mass transport in gravity waves. *J. Fluid Mech.* **13**, 481-504.

[15] Longuet-Higgins, M. S. 1970 Longshore currents generated by obliquely incident sea waves, 1. *J. Geophy. Res.* **75**(33) 6779-6790.

[16] Longuet-Higgins, M. S. 1970 Longshore currents generated by obliquely incident sea waves, 2. *J. Geophy. Res.* **75**(33) 6791-6801.

[17] Mei, C. C. 1983 *The Applied Dynamics of Ocean Surface Wave.* Wiley - Interscience.

[18] Miles, J. W. 1977 Obliquely interacting solitary waves. *J. Fluid Mech.* **79**, 157-169.

[19] Miles, J. W. 1979 On the Korteweg-de Vries equation for a gradually varying channel. *J. Fluid Mech.* **91**, 181-190.

[20] Pedersen, G. & Gjevik, B. 1983 Run-up of solitary waves. *J. Fluid Mech.* **135**, 283-299.

[21] Peregrine, D. H. 1967 Long waves on a beach. *J. Fluid Mech.* **27**, 815-827.

[22] Spielvogel, L. Q. 1976 Single wave run-up on sloping beaches. *J. Fluid Mech.* **74**, 685-694.

[23] Stoker, J. J. 1947 Surface waves in water of variable depth. *Q. Appl. Maths.* **5**, 1-54.

[24] Synolakis, C. E. 1987 The runup of solitary waves. *J. Fluid Mech.* **185**, 523-545.

[25] Teng, M. H. & Wu, T. Y. 1992 Nonlinear water waves in channels of arbitrary shape. *J. Fluid Mech.* **242**, 211-233.

[26] Teng, M. H. & Wu, T. Y. 1994 Evolution of long water waves in variable channels. *J. Fluid Mech.* **266**, 307-317.

[27] Titov, V. V. & Synolakis, C. E. 1995 Modeling of breaking and nonbreaking long-wave evolution and runup using VTCS-2. *J. Wtrwy., Port, Coast. and Oc. Engrg.* ASCE **121**(6), 308-316.

[28] Tuck E. O. & Hwang L.-S. 1972 Long wave generation on a sloping beach. *J. Fluid Mech.* **51**, 449-461.

[29] Whitham, G. B. 1974 *Linear and Nonlinear Waves.* Wiley- Interscience.

[30] Wu, T. Y. 1979 Tsunamis — In *Proc. National Science Foundation Workshop (May 7-9, 1979).* Pasadena: Tetra Tech Inc. 110-149.

[31] Wu, T. Y. 1981 Long waves in ocean and coastal waters. *J. Engng. Mech. Div. ASCE* **107**, 501-522.

[32] Wu, T. Y. 1994 A bidirectional long-wave model. *Meth. Appl. Anal.* **1**(1), 108-117.

[33] Wu, T. Y. & Zhang, J. E. 1996 Mass and energy transfer between unidirectional interacting solitons (to be published).

[34] Wu, T. Y. & Zhang, J. E. 1996 On modeling nonlinear long waves. *SIAM* (to be published).

[35] Zelt, J. A. 1986 Tsunamis: the response of harbours with sloping boundaries to long wave excitation. Rep. No. KH-R-47, W. M. Keck Laboratory of Hydraulics & Water Resources, California Institute of Technology.

[36] Zelt, J. A. & Raichlen, F. 1990 A lagrangian model for wave-induced harbor oscillations. *J. Fluid Mech.* **213**, 203-225.

[37] Zelt, J. A. & Raichlen, F. 1991 Overland-flow from solitary waves. *J. Wtrwy., Port, Coast. and Oc. Engrg.* ASCE **117**(3), 247-263.

[38] Zelt, J. A. 1991 The run-up of nonbreaking and breaking solitary waves. *Coastal Engrg.* **15**(3), 205-246.

Part II

Nonlinear waves in a fluid-filled elastic tube

Chapter 6 Nonlinear waves in a fluid-filled elastic tube

6.1 Introduction

Fluid mechanics is believed by many to hold a key to exposing the basic mechanism underlying some vascular disease. There have been many studies of fluid flow through flexible tubes, motivated by the physiological problems of blood flow through arteries and veins, and air flow through the lungs.

To model flow behavior in large arteries, one often assumes that the fluid is incompressible and inviscid, that the flow is irrotational, and that all disturbances have a long wavelength compared with the tube diameter. A salient feature of most flows described by such long wave models is the steepening of nonlinear waves, i.e., formation of elastic jumps or shocks, which has been pointed out by many authors (e.g., Skalak 1966). Cowley (1982) verified that the elastic balance of the tube can be expressed in terms of a "tube law," and derived conditions between up- and downstream flows of a turbulent elastic jump. Moodie & Swaters (1989) investigated the propagation of both finite amplitude and weakly nonlinear waves in hyperelastic tethered tubes, and computed the time and location of first shock formation in tubes.

For a class of tube whose wall material satisfies the stress-strain law given by the kinetic theory of rubber, Olsen & Shapiro (1967) presented a unidirectional traveling wave solution, in which waves may have arbitrary shape. Due to the nonlinear effects involved, they concluded that "No general solution with waves of both families (bidirectional) has been found except for small amplitude when the linear theory is applicable." This situation has not been much advanced in the intervening years. The primary objective of the present study is to develop a nonlinear bidirectional theory for large-amplitude waves of inviscid incompressible liquid in a long elastic tube with

its wall properties belonging to the class above.

In this study, a mathematical model is developed in §6.2. Then one solitary wave solution is given in §6.3. In §6.4, we give two solutions for head-on collision of two solitary waves, the first being for weakly nonlinear waves (perturbation approximate solution) while the second for fully nonlinear waves (an exact solution). It is shown that the perturbation solution is only the first several terms of Taylor's expansion of the exact solution. The Hamiltonian structure of the evolution system is studied in §6.5. The system is shown to be at least tri-Hamiltonian. It implies the complete integrability of the system. In §6.6 we first show that any initial value imposed on the model will become two solitary waves, separately travelling to the left and to the right. Then we develop an iteration scheme to integrate the initial value problem. Finally, we shall show that nonlinear waves never steepen according to this model, i.e., shock does not form for the system if initial value is continuous.

6.2 The governing equations

We consider the wave motion of a fluid (water) confined in a longitudinal constrained circular elastic latex tube. We assume that the flow is axisymmetric inside the elastic tube whose radius varies along the axis with time in wave motion, and the confined fluid is incompressible and inviscid. And we submerge the tube inside water in order to cancel the gravitational effect. The transversal velocity can be neglected for long waves since it is much smaller than the longitudinal velocity. After integrating the Euler equation over the cross section once, we have the following equations:

$$s_t + (us)_x = 0, \tag{6.1}$$

$$u_t + uu_x + \frac{1}{\rho}p_x = 0, \tag{6.2}$$

where x is the tube axis along the longitudinal direction, $s = s(x,t)$ is the area of the tube cross-section, $u = u(x,t)$ is the velocity averaged over the tube cross-section, ρ is the density of water. $p = p(x,t)$ is the pressure of water in the tube, it is assumed

to be a constant over the cross-section.

For a longitudinally constrained tube made of a specific class of latex, the following relation has been derived from the kinetic theory of rubber (Treloar 1958, Oslen & Shapiro 1967):

$$p = \frac{1}{2}\rho a_0^2 \left(1 - \frac{s_0^2}{s^2}\right), \tag{6.3}$$

where s_0 is the reference cross-sectional area of the tube in equilibrium at rest. Figure 6.1 shows the variation of pressure p with $1 - s_0^2/s^2$, the solidline is from the kinetic theory of rubber, and the dots are our lab data.

The wave speed is

$$a = \sqrt{\frac{s}{\rho}\frac{\partial p}{\partial s}} = a_0 \frac{s_0}{s}.$$

Substituting (6.3) into (6.1) and (6.2), we rescale s by s_0, u by a_0, x by L and t by L/a_0, then the nondimensionalized equations are:

$$s_t + (us)_x = 0, \tag{6.4}$$

$$u_t + uu_x - \left(\frac{1}{2s^2}\right)_x = 0. \tag{6.5}$$

This is the mathematical model for the wave propagation in a fluid-filled elastic tube. We are going to study the solution of the model.

6.3 Unidirectional travelling wave

We now seek a solitary wave solution of equation (6.4) and (6.5) by assuming

$$s = s(x - c\,t), \qquad u = u(x - c\,t),$$

where c is wave speed, which is functional yet to be determined. Substituting these relations into (6.4) and (6.5), integrating once under the regular boundary conditions

at infinity, namely,

$$s = 1, \quad u = 0,$$

we have

$$-cs + us = -c,$$

$$-cu + \frac{1}{2}u^2 - \frac{1}{2s^2} = -\frac{1}{2}.$$

From these two equations it follows that

$$c = \pm 1, \quad u = c\left(1 - \frac{1}{s}\right).$$

This means that we have solitary wave solution of the general form

$$s = 1 + f(\mp t + x), \tag{6.6}$$

$$u = \pm \frac{f(\mp t + x)}{1 + f(\mp t + x)}, \tag{6.7}$$

where $f = f(\mp t + x)$ is an arbitrary function, the upper sign is for right-going wave and the lower sign for left-going wave.

The above solution was first found by Olsen & Shapiro (1967) for unidirectional solitary waves, either right- or left-going. But the problem of interaction between right- and left-going waves remains unsolved.

6.4 Bidirectional waves interaction

6.4.1 Perturbation solution

For weakly nonlinear waves, we can solve the problem of interaction between right-going and left-going waves by using the perturbation scheme:

$$s = 1 + \epsilon s_1 + \epsilon^2 s_2 + \cdots,$$

$$u = \epsilon u_1 + \epsilon^2 u_2 + \cdots,$$

where ϵ is a small parameter, representing the scale of wave amplitude. After substituting these expansions in equation (6.4) and (6.5) and collecting the terms in orders of ϵ, we obtain the leading order equations as

$$s_{1t} + u_{1x} = 0, \tag{6.8}$$

$$u_{1t} + s_{1x} = 0, \tag{6.9}$$

and for the second order equations,

$$s_{2t} + u_{2x} = -(u_1 s_1)_x, \tag{6.10}$$

$$u_{2t} + s_{2x} = \frac{1}{2}(3s_1^2 - u_1^2)_x. \tag{6.11}$$

We introduce new variables ξ_+ and ξ_-:

$$\xi_+ = -t + x, \quad \xi_- = t + x,$$

then

$$\partial_t = \partial_- - \partial_+, \quad \partial_x = \partial_- + \partial_+.$$

The equation for s_1 can be derived from (6.8) and (6.9) to give

$$s_{1tt} - s_{1xx} = -4\partial_-\partial_+ s_1 = 0$$

and likewise for u_1. Hence

$$s_1 = f_+(\xi_+) + f_-(\xi_-), \tag{6.12}$$

$$u_1 = f_+(\xi_+) - f_-(\xi_-). \tag{6.13}$$

The equation for s_2 can be derived from (6.10) and (6.11) to give

$$s_{2tt} - s_{2xx} = -(u_1 s_1)_{xt} - \frac{1}{2}(3s_1^2 - u_1^2)_{xx}.$$

Substituting the expressions for ξ_+, ξ_-, s_1 and u_1 into the above equation yields

$$\partial_-\partial_+ s_2 = (\partial_- + \partial_+)^2(f_+ f_-).$$

Similarly, we obtain equation for u_2:

$$\partial_-\partial_+ u_2 = -(\partial_-^2 - \partial_+^2)(f_+ f_-).$$

We introduce $\phi_\pm$ by $\partial_\pm \phi_\pm = f_\pm$, and integrate the above two equations giving

$$s_2 = \phi_+ \partial_- f_- + \phi_- \partial_+ f_+ + 2 f_+ f_-, \tag{6.14}$$

$$u_2 = -\phi_+ \partial_- f_- + \phi_- \partial_+ f_+. \tag{6.15}$$

Combining (6.12), (6.13), (6.14) and (6.15) yields

$$s = 1 + f_+(x + \phi_-, t) + f_-(x + \phi_+, t) + 2 f_+ f_-, \tag{6.16}$$

$$u = f_+(x + \phi_-, t) - f_-(x + \phi_+, t). \tag{6.17}$$

From these two formulas, we see that ϕ_- and ϕ_+ are the phase shifts for the right and left going waves respectively. For two positive polarized waves in a head-on collision, the phase shifts are backward for both, each by a magnitude of phase shift equal to the area under the curve f of the other wave. Since for this model the solitary wave function $f(\mp t + x)$ can be arbitarily given, the phase shift can therefore be backward, forward and even null. This is quite different from free surface water wave, in which case the phase shift resulting from interactions between two solitary waves on shallow water is always backward after a head-on collision (Wu 1994).

6.4.2 Exact solution

From the above perturbation solution, we can make an Ansatz solution for bidirectional nonlinear wave interaction as follows:

$$s = \frac{(1+f_+)(1+f_-)}{1-f_+f_-}, \tag{6.18}$$

$$u = \frac{f_+ - f_-}{(1+f_+)(1+f_-)}, \tag{6.19}$$

where $$f_+ = f_+(\xi_+), \quad f_- = f_-(\xi_-), \tag{6.20}$$

$$\xi_+ = -t + x + \phi_-(\xi_-), \quad \xi_- = t + x + \phi_+(\xi_+), \tag{6.21}$$

$$\partial_+\phi_+ = f_+, \quad \partial_-\phi_- = f_-. \tag{6.22}$$

Substituting the above equations into the governing equations (6.4) and (6.5), one can easily show this is the exact solution of the problem. The solution is for interacting bidirectional waves of finite amplitude. One can see that the interaction between two solitary waves is clean. All the solitary waves are therefore solitons.

Suppose f_+ and f_- are two solitary waves with the same amplitude a, then the maximum amplitude for cross-sectional area s exactly equals

$$s_m = \frac{1+a}{1-a} = 1 + \frac{2a}{1-a}, \quad (a < 1) \tag{6.23}$$

and the phase shift is exactly equal to

$$\Delta_\pm = \phi_\mp|_{-\infty}^{\infty} = \int_{-\infty}^{\infty} f_\mp \, d\xi_\mp. \tag{6.24}$$

For small wave amplitudes, $|f_\pm| << 1$, expanding (6.18) and (6.19) in Taylor series, one will find that the pertubation solution (6.16) and (6.17) are indeed the first several terms of the series.

Figure 6.2 shows a head-on interaction of two smooth solitary waves $f_+ = f_- = 0.25\ \mathrm{sech}^2 x$. The maximum amplitude for s is $(1 + 0.25)/(1 - 0.25) = 5/3$. Both are positive polarized, so their phase shifts are backward. Figure 6.3 shows another head-on interaction of two smooth solitons $f_+ = -f_- = 0.25\ \mathrm{sech}^2 x$. One is positive

polarized, whereas the other is negative polarized, so the phase shift for the former one is forward, and the phase shift for the latter one is backward. Figure 6.4 shows a head-on interaction of triangle soltions $f_+ = f_- = 0.125(|1-|x||+1-|x|)$. Both are positive polarized, so their phase shifts are backward. Figure 6.5 shows still another head-on interaction of square solitons $f_+ = f_- = 0.125(1+\text{sign}(1-|x|))$.

6.5 Hamiltonian structures of the system

In this section, the Hamiltonian method is used to study evolution equation system (6.4) and (6.5) following Olver (1986). Our system is a special case of the polytropic gas dynamics systems, which has been studied by Olver & Nutku (1988). It has three first order Hamiltonian. The system can be written as

$$U_t = \mathcal{D}_1\ \delta\mathcal{H}_3 = \mathcal{D}_2\ \delta\mathcal{H}_2 = \mathcal{D}_3\ \delta\mathcal{H}_1, \tag{6.25}$$

where $\mathcal{D}_1$, $\mathcal{D}_2$, $\mathcal{D}_3$ are Hamiltonian operators, $\mathcal{H}_1$, $\mathcal{H}_2$, $\mathcal{H}_3$ are Hamiltonian functionals, and $\delta\mathcal{H}_i$, $i=1,2,3$ are the variational derivatives of vector U (see Appendix).

$$U = \begin{pmatrix} u \\ s \end{pmatrix}, \tag{6.26}$$

$$\mathcal{D}_1 = \begin{pmatrix} 0 & \partial \\ \partial & 0 \end{pmatrix}, \quad \mathcal{H}_3 = \int_{-\infty}^{\infty} (-\frac{1}{2}su^2 - \frac{1}{2}s^{-1})\ dx, \tag{6.27}$$

$$\mathcal{D}_2 = \begin{pmatrix} (s^{-3})\partial + \partial(s^{-3}) & (-3u)\partial + \partial u \\ \partial(-3u) + u\partial & s\partial + \partial s \end{pmatrix}, \quad \mathcal{H}_2 = \int_{-\infty}^{\infty} su\ dx, \tag{6.28}$$

$$\mathcal{D}_3 = \begin{pmatrix} (us^{-3})\partial + \partial(us^{-3}) & (-\frac{3}{2}u^2 - \frac{1}{2}s^{-2})\partial + \partial(\frac{1}{2}u^2 - \frac{1}{2}s^{-2}) \\ \partial(-\frac{3}{2}u^2 - \frac{1}{2}s^{-2}) + (\frac{1}{2}u^2 - \frac{1}{2}s^{-2})\partial & (us)\partial + \partial(us) \end{pmatrix},$$

$$\mathcal{H}_1 = \int_{-\infty}^{\infty} -s\ dx. \tag{6.29}$$

The Hamiltonian operators $\mathcal{D}_1$, $\mathcal{D}_2$, $\mathcal{D}_3$ are mutually compatible, leading to three distinct Hamiltonian pairs. One can easily show that $\mathcal{H}_1$, $\mathcal{H}_2$, $\mathcal{H}_3$ are conserved

quantities of the system. Furthermore, by Magris's theorem (Appendix) a conserved quantity $\mathcal{H}_4$ can be calculated from

$$\mathcal{D}_1\ \delta\mathcal{H}_4 = \mathcal{D}_2\ \delta\mathcal{H}_3 = \begin{pmatrix} (\frac{1}{2}u^3 - \frac{3}{2}s^{-2}u)_x \\ (\frac{3}{2}su^2 + \frac{3}{2}s^{-1})_x \end{pmatrix},$$

$$\text{then} \qquad \mathcal{H}_4 = \int_{-\infty}^{\infty} (\frac{1}{2}su^3 + \frac{3}{2}s^{-1}u)\ dx. \tag{6.30}$$

And still another conserved quantity $\mathcal{H}_5$ can be calculated from the equation

$$\mathcal{D}_1\ \delta\mathcal{H}_5 = \mathcal{D}_3\ \delta\mathcal{H}_3, \tag{6.31}$$

and so on. We get infinite number of conservation laws in this way.

Our system is at least tri-Hamiltonian. This suggests that the system is completely integrable.

6.6 Initial value problem

In this section, we are trying to integrate the system (6.4) and (6.5), i.e., to find a solution to the initial value problem.

We make following transformation

$$F = u + \frac{1}{s}, \qquad G = u - \frac{1}{s}. \tag{6.32}$$

Substituting into equation (6.4) and (6.5), after straightforward algebra we have

$$F_t + G\ F_x = 0, \tag{6.33}$$

$$G_t + F\ G_x = 0. \tag{6.34}$$

So the characteristic relations are (figure 6.6):

$$\text{on} \quad \frac{dx}{dt} = G, \qquad F = \text{const.}, \tag{6.35}$$

$$\text{on} \quad \frac{dx}{dt} = F, \qquad G = \text{const.} \tag{6.36}$$

Let us inspect IVP of equation (6.4) and (6.5). Suppose an initial disturbance is at rest except between $x_1 < x < x_2$, so that outside this region $u = 0$ and $s = 1$, i.e., $F = 1$ and $G = -1$. From the characteristic relations, $F = 1$ and $G = -1$ will hold for the region 1, 4 and 5 (see figure 6.6). $G = -1$ will hold for region 2. $F = 1$ will hold for region 3. This means the solution has only left-going waves in region 2, and right-going waves in region 3. There is no wave in region 1, 4 and 5. Region 6 is the interaction region.

This result asserts that any initial disturbance will eventually become a left-going wave train and a right-going wave train, each bearing no wake. And we have obtained a bidirectional wave solution in §6.4.2. So solutions for any IVP of equations (6.4) and (6.5) can be constructed with equations (6.18)–(6.22).

Now we shall develop a scheme to solve the two solitons resulting from arbitrary initial conditions of F and G. From §6.4.2 and equation (6.32), we have the following relations for the initial data:

$$F(x,0) = \frac{1-f_-}{1+f_-}, \quad G(x,0) = \frac{-1+f_+}{1+f_+}, \tag{6.37}$$

$$\text{with} \quad f_+ = f_+(\xi_+), \quad f_- = f_-(\xi_-), \tag{6.38}$$

$$\xi_+ = x + \phi_-(\xi_-), \quad \xi_- = x + \phi_+(\xi_+). \tag{6.39}$$

Then we have

$$f_-(\xi_-) = \frac{1-F(x,0)}{1+F(x,0)}, \tag{6.40}$$

$$f_+(\xi_+) = \frac{1+G(x,0)}{1-G(x,0)}. \tag{6.41}$$

Since the right-hand side of these two equations is given, we can solve $f_+(x)$ and $f_-(x)$ by executing the following iteration scheme:

1. Let $\phi_\pm(x) = 0$, then $\xi_\pm = x$, and equations (6.40) and (6.41) will give $f_\pm(x)$;

then integrating $f_{\pm}(x)$ gives $\phi_{\pm}(x)$ as the first iterate.

2. Substituting $\phi_{\pm}(x)$ into equation (6.39), we can solve (6.39) for $\xi_{\pm} = \xi_{\pm}(x)$.

3. Substituting this $\xi_{\pm} = \xi_{\pm}(x)$ into equations (6.40) and (6.41), we can again solve $f_{\pm}(x)$. Integrating $f_{\pm}(x)$ this time gives $\phi_{\pm}(x)$ as the second iterate.

4. The process could be repeated to completion when a certain criterion is satisfied.

Finally we can solve $f_+(x)$ and $f_-(x)$.

From equations (6.18)—(6.22) and (6.32), one can see that the necessary and sufficient condition for $u(x,t)$ and $s(x,t)$ to be continuous are that f_+ and f_- are continuous or, equivalently, $F(x,0)$ and $G(x,0)$ are continuous, or the initial values $u(x,0)$ and $s(x,0)$ are continuous. This means that shocks will not form if initial values are continuous. Shock exists if and only if it initially exists.

Bibliography

[1] Cowley, S. J. 1982 Elastic jumps on fluid-filled elastic tubes. *J. Fluid Mech.* **116**, 459-473.

[2] Magri, F. 1978 A simple model of the integrable Hamiltonian equation. *J. Math. Phys.* **19**(5), 1156-1162.

[3] Moodie, T. B. & Swaters, G. E. 1989 Nonlinear waves and shock calculations for hyperelastic fluid-filled tubes. *Q. Appl. Math.* **47**(4), 705-722.

[4] Olsen, J. H. & Shapiro, A. H. 1967 Large-amplitude unsteady flow in liquid-filled elastic tubes. *J. Fluid Mech.* **29** , 513-538.

[5] Olver, P. J. 1986 *Applications of Lie Group to Differential Equations*, Springer-Verlag, 433-466.

[6] Olver, P. J. & Nutku, Y. 1988 Hamiltonian structures for systems of hyperbolic conservation laws. *J. Math. Phys.* **29**, 1610-1619.

[7] Treloar, L. R. G. 1958 *The Physics of Rubber Elasticity*, Oxford, 95.

[8] Wu, T. Y. 1994 A bidirectional long wave model. *Methods and Applications of Analysis* **1**(1), 108-117.

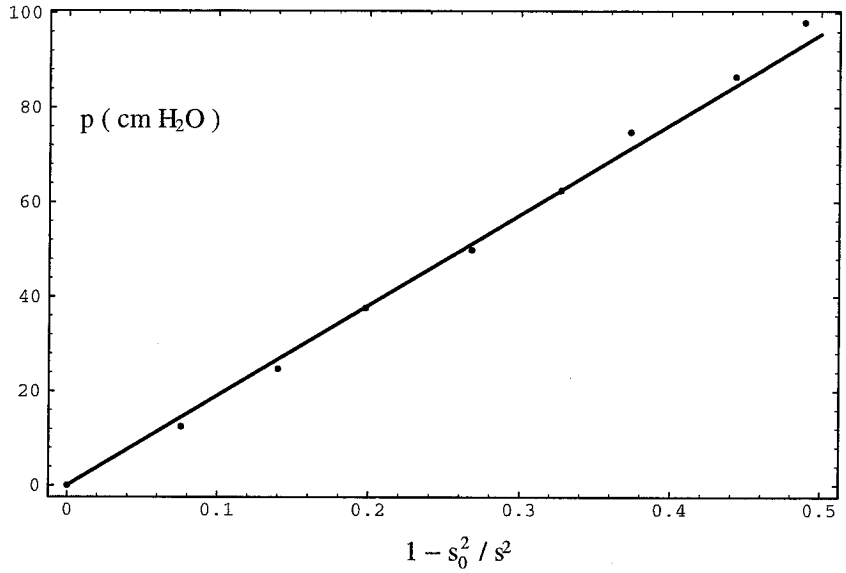

Figure 6.1: Constitutional realtion of the latex elastic tube, pressure p as a function of $1 - s_0^2/s^2$, s being cross-section area. Solid line is from kinetic theory of rubber, and dots are our lab data.

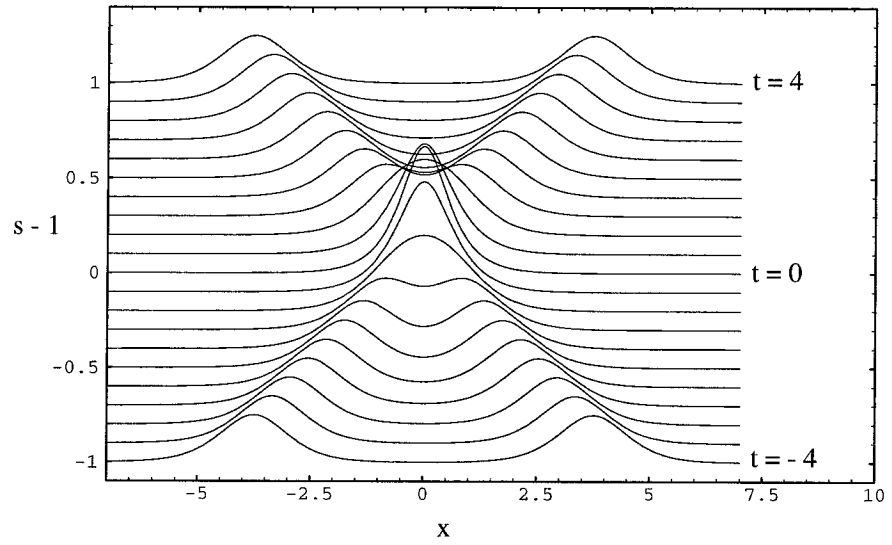

Figure 6.2: Two soliton solution for $f_+ = f_- = 0.25\ \mathrm{sech}^2 x$.

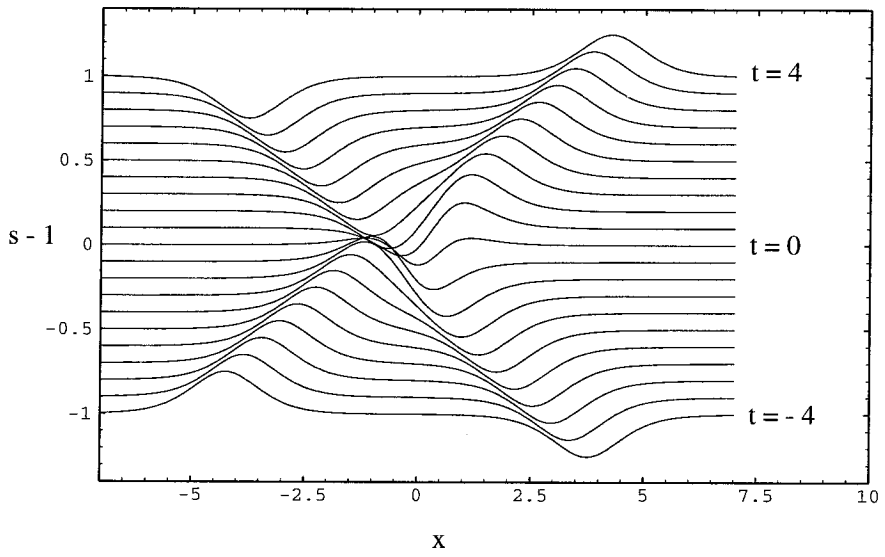

Figure 6.3: Two soliton solution for $f_+ = -f_- = 0.25\ \mathrm{sech}^2 x$.

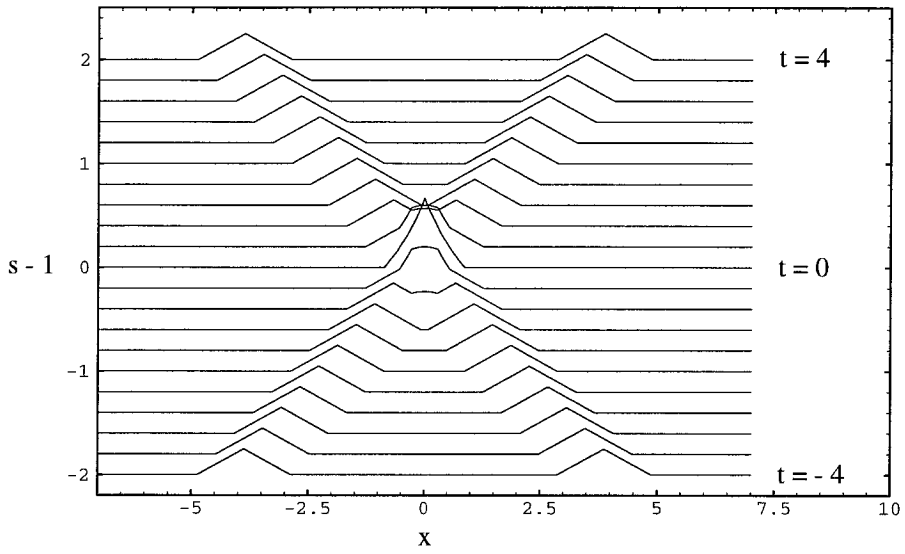

Figure 6.4: Two soliton solution for triangle waves $f_+ = f_- = 0.125(|1-|x||+1-|x|)$.

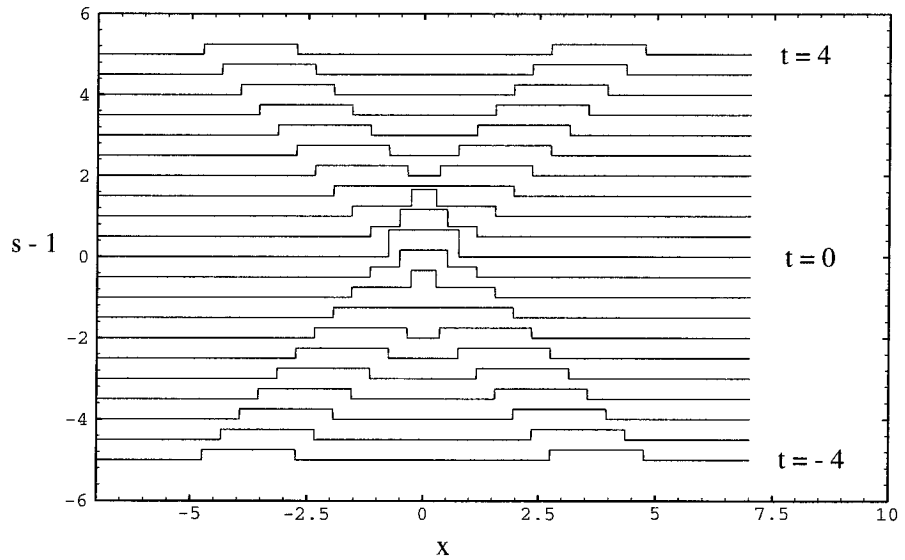

Figure 6.5: Two soliton solution for square waves $f_+ = f_- = 0.125(1+\text{sign}(1-|x|))$.

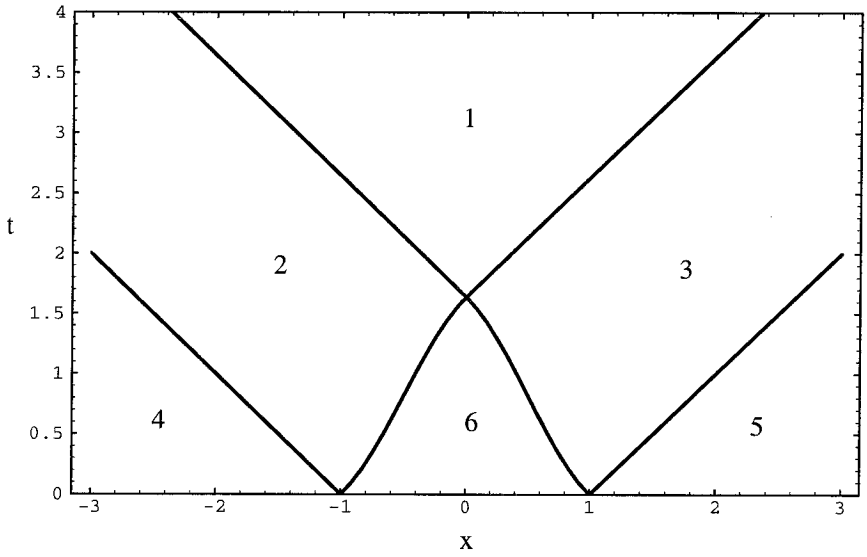

Figure 6.6: Characteristics for the equations.

Appendix A Comparison between results of the present scheme and other's

In Chapter 1, we have obtained the solution for solitary waves running from the ocean of uniform depth to a sloping plane beach by using linear nondispersive theory. On the beach, wave elevation is

$$\zeta(x,t) = \mathrm{Re}\int_0^\infty A_0(k)R_0(\kappa)e^{-ikt+i\Delta_0}J_1(2k\sqrt{lx})dk \quad (0<x<l), \tag{1.72}$$

where $A_0(k)$ is given by (1.66), $R_0(\kappa)$ and $\Delta_0(\kappa)$ by (1.52, 1.53). Then the run-up, i.e., the wave elevation at $x=0$, is

$$R(t) = \mathrm{Re}\int_0^\infty A_0(k)R_0(\kappa)e^{-ikt+i\Delta_0}dk. \tag{A.1}$$

By using an asymptotic expansion method, Synolakis (1987) found an approximate formula for the maximum run-up

$$R = \mathrm{Max}\ R(t) = 2.831\sqrt{l}\ a^{5/4}, \tag{A.2}$$

where $1/l$ is the beach slope and a is the amplitude of the solitary wave. The formula is given a range of validity for

$$a \gg (0.288/l)^2. \tag{A.3}$$

We numerically evaluate the maximum R of equation (A.1) and compare it with formula (A.2) in table A.1 and figure A.1. For $a=0.1$ and $l=1$, Synolakis' approximate formula has an error of about 25%.

We have carried out some numerical computation on the run-up of solitary waves by using generalized Boussinesq model (Wu 1979) with our scheme developed in

Chapter 2 and 3. We compare our numerical results attained from formula (A.2) with experimental results available. The results are shown in table A.2, table A.3, figure A.2 and figure A.3.

For the first case, $l = 19.85$, formula (A.2) is supposedly correct when $a \gg 0.0002$ according to (A.3). The comparison is shown for amplitude a in between 0.0052 and 0.0280. For this mild beach, our numerical results agree with formula (A.2) quite well, the relative difference is less than 5%. Both are larger than experimental results of Synolakis (1987).

For the second case, $l = 1$, formula (A.2) is supposedly correct when $a \gg 0.08$ as claimed by (A.3). We compare for amplitude a in between 0.2 and 0.5. For this steep beach, The relative difference between our numerical results and the formula (A.2) is around 20%. The agreement is poor.

Table A.1: The run-up predicted by linear nondispersive theory, for a solitary wave of amplitude $a/h = 0.1$, running up from an ocean of depth $h = 1$ to a plane beach of slope $\alpha = 1/l$.

Beach length l	Approximate formula (A.2) $R = 2.831\sqrt{l}\ a^{5/4}$	Numerical evaluation of the maximum run-up R by (A.1)
0.0	0.0000	0.2000
1.0	0.1592	0.2163
2.0	0.2251	0.2561
3.0	0.2757	0.2981
4.0	0.3184	0.3366
5.0	0.3560	0.3717
6.0	0.3900	0.4039

Table A.2: Run-up of non-breaking solitary waves predicted by the gB model with present scheme, by an approximate formula and experimental results (Synolakis 1987).

Beach length l	Amplitude a	Formula (A.2) $R = 2.831\sqrt{l}\ a^{5/4}$	Results by gB with present scheme	Laboratory experiments
19.85	0.0052	0.018	0.0187	0.019
19.85	0.0065	0.023	0.0245	0.022
19.85	0.0071	0.026	0.0272	0.026
19.85	0.0080	0.030	0.0315	0.029
19.85	0.0092	0.036	0.0373	0.036
19.85	0.0095	0.037	0.0388	0.041
19.85	0.0097	0.038	0.0398	0.038
19.85	0.0129	0.055	0.0564	0.048
19.85	0.0141	0.061	0.0629	0.052
19.85	0.0144	0.063	0.0646	0.049
19.85	0.0170	0.077	0.0792	0.063
19.85	0.0180	0.083	0.0849	0.074
19.85	0.0190	0.089	0.0908	0.077
19.85	0.0210	0.101	0.1029	0.075
19.85	0.0220	0.107	0.1091	0.098
19.85	0.0230	0.113	0.1155	0.087
19.85	0.0250	0.125	0.1289	0.100
19.85	0.0270	0.138	0.1435	0.108
19.85	0.0280	0.144	0.1514	0.123

Table A.3: The run-up of non-breaking solitary waves predicted by the gB model with present scheme in comparison with the approximate formula of Synolakis (1987).

Beach length l	Amplitude a	Formula (A.2) $R = 2.831\sqrt{l}\ a^{5/4}$	Results by gB with present scheme
1.00	0.200	0.3786	0.4991
1.00	0.210	0.4025	0.5263
1.00	0.220	0.4265	0.5538
1.00	0.230	0.4509	0.5816
1.00	0.240	0.4756	0.6097
1.00	0.250	0.5005	0.6379
1.00	0.260	0.5256	0.6663
1.00	0.270	0.5510	0.6949
1.00	0.280	0.5766	0.7236
1.00	0.290	0.6025	0.7523
1.00	0.300	0.6285	0.7811
1.00	0.310	0.6549	0.8098
1.00	0.320	0.6814	0.8385
1.00	0.330	0.7081	0.8671
1.00	0.340	0.7350	0.8958
1.00	0.350	0.7621	0.9244
1.00	0.360	0.7894	0.9530
1.00	0.370	0.8169	0.9815
1.00	0.380	0.8446	1.0099
1.00	0.390	0.8725	1.0384
1.00	0.400	0.9006	1.0667
1.00	0.410	0.9288	1.0950
1.00	0.420	0.9572	1.1232
1.00	0.430	0.9858	1.1513
1.00	0.440	1.0145	1.1794
1.00	0.450	1.0434	1.2074
1.00	0.460	1.0725	1.2353
1.00	0.470	1.1017	1.2631
1.00	0.480	1.1311	1.2909
1.00	0.490	1.1606	1.3185
1.00	0.500	1.1903	1.3461

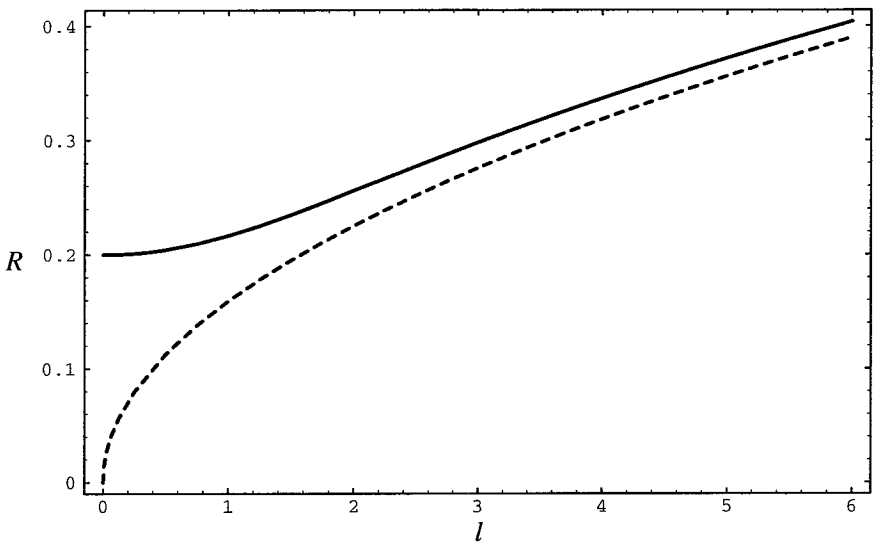

Figure A.1: The Maximum run-up of solitary wave of amplitude $a = 0.1$ as a function of l evaluated by linear nondispersive theory, solid line is our numerical results, dashed line is formula (A.2).

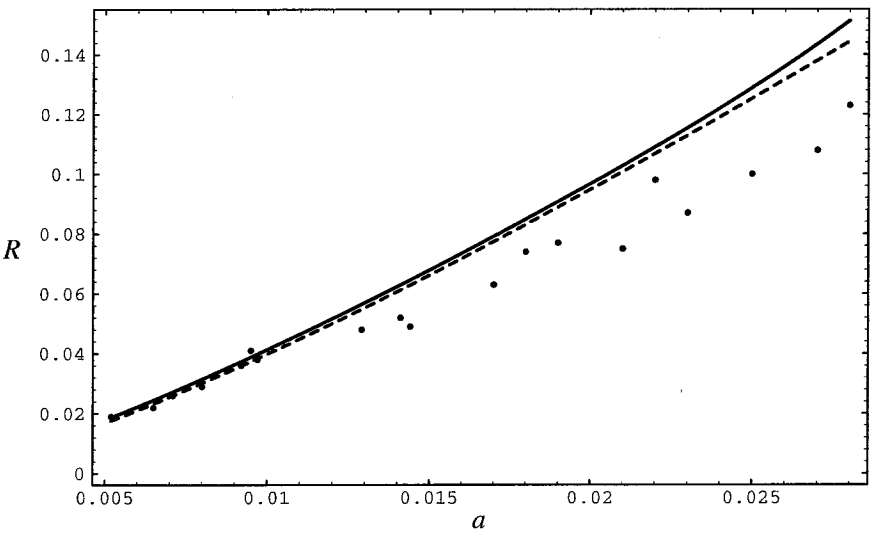

Figure A.2: The maximum run-up of solitary waves running from an ocean with uniform depth up to a plane beach of slope $\alpha = 1/19.85$, as a function of wave amplitude a, solid line is our numerical results, dashed line is formula (A.2), dots are experimental data (Synolakis 1987).

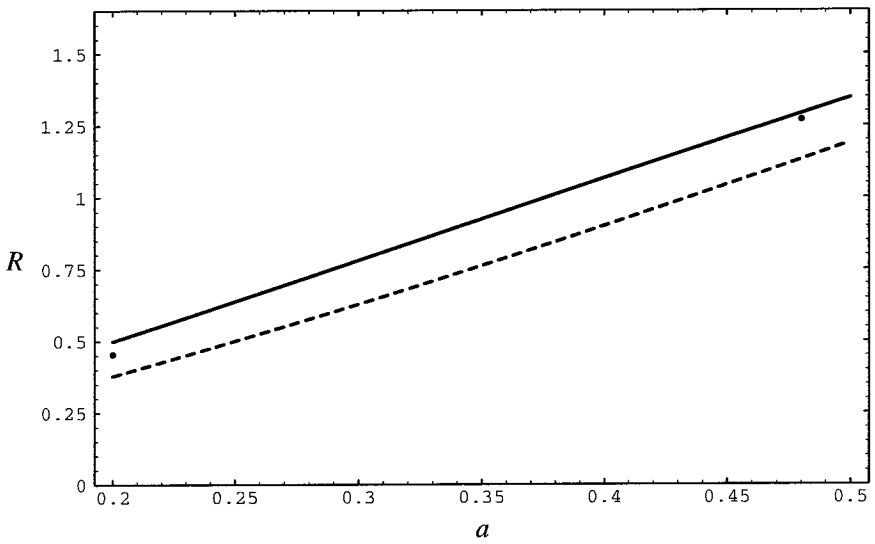

Figure A.3: The maximum run-up of solitary waves running from an ocean with uniform depth up to a plane beach of slope $\alpha = 1$, as a function of wave amplitude a, solid line is our numerical results, dashed line is formula (A.2), dots are experimental data (Hall & Watts 1953).

Appendix B Definition of Hamiltonian for evolution equation and Magri's theorem

Let $M \subset X \times U$ be an open subset of the space of independent and dependent variables $x = (x^1, \cdots, x^p)$ and $u = (u^1, \cdots, u^q)$. The algebra of differential functions $P(x, u^{(n)}) = P[u]$ over M is denoted by $\mathcal{A}$, and its quotient space under the image of the total divergence is the space $\mathcal{F}$ of functionals $\mathcal{P} = \int P dx$.

A system of evolution equations can be written as

$$u_t = K[u] = K(x, u^{(n)}) = \mathcal{D} \cdot \delta\mathcal{H}[u], \quad K \in \mathcal{A}^q, \quad \mathcal{H} \in \mathcal{F}, \tag{A.1}$$

where $\mathcal{D}$ is a differential operator.

Poisson bracket associated with operator $\mathcal{D}$ has the form

$$\{\mathcal{P}, \mathcal{L}\} = \int \delta\mathcal{P} \cdot \mathcal{D}\delta\mathcal{L}\, dx, \tag{A.2}$$

where $\mathcal{P}, \mathcal{L} \in \mathcal{F}$ are functionals.

Definition A.1. A linear operator $\mathcal{D} : \mathcal{A}^q \to \mathcal{A}^q$ is called *Hamiltonian* if its poisson bracket satisfies the conditions of *skew-symmetry*

$$\{\mathcal{P}, \mathcal{L}\} = -\{\mathcal{L}, \mathcal{P}\}, \tag{A.3}$$

and the *Jacobi identity*

$$\{\{\mathcal{P}, \mathcal{L}\}, \mathcal{R}\} + \{\{\mathcal{R}, \mathcal{P}\}, \mathcal{L}\} + \{\{\mathcal{L}, \mathcal{R}\}, \mathcal{P}\} = 0, \tag{A.4}$$

for all functionals $\mathcal{P}, \mathcal{L}, \mathcal{R} \in \mathcal{F}$.

Definition A.2. A pair of skew-adjoint $q \times q$ matrix differential operators $\mathcal{D}$ and $\mathcal{E}$ is said to form a *Hamiltonian pair* if every linear combination $a\mathcal{D} + b\mathcal{E}$, $a, b \in R$, is

a Hamiltonian operator. A system of evolution equations is a *bi-Hamiltonian system* if it can be written in the form

$$u_t = K_1[u] = \mathcal{D} \cdot \delta \mathcal{H}_1 = \mathcal{E} \cdot \delta \mathcal{H}_0, \tag{A.5}$$

where $\mathcal{D}, \mathcal{E}$ form a Hamiltonian pair.

Magri's Theorem: (Magri 1978) Let $(A.5)$ be a bi-Hamiltonian system of evolution equations. Assume that the operator $\mathcal{D}$ of the Hamiltonian pair is nondegenerate. Let $\mathcal{R} = \mathcal{E} \cdot \mathcal{D}^{-1}$ be the corresponding recursion operator, and let $K_0 = \mathcal{D}\delta\mathcal{H}_0$. Assume that for each $n = 1, 2, \cdots$ we can recursively define

$$K_n = \mathcal{R} K_{n-1}, \qquad n \geq 1$$

meaning that for each n, K_{n-1} lies in the image of $\mathcal{D}$. Then there exists a sequence of functionals $\mathcal{H}_0$, $\mathcal{H}_1$, $\mathcal{H}_2, \cdots$, such that

1. for each $n \geq 1$, the evolution equation

$$u_t = K_n[u] = \mathcal{D} \cdot \delta \mathcal{H}_n = \mathcal{E} \cdot \delta \mathcal{H}_{n-1} \tag{A.6}$$

   is a bi-Hamiltonian system;

2. the Hamiltonian functionals $\mathcal{H}_n$ are all in involution with respect to either bracket:

$$\{\mathcal{H}_n, \mathcal{H}_m\}_{\mathcal{D}} = 0 = \{\mathcal{H}_n, \mathcal{H}_m\}_{\mathcal{E}}, \qquad n, m \geq 0, \tag{A.7}$$

   and hence provide an infinite collection of conservation laws for each of the bi-Hamiltonian systems $(A.6)$.

The proof of the theorem can be found in Olver's book (1986).